

PREPARATION AND CHARACTERIZATION OF ORGANOCCLAY-
POLYPROPYLENE NANOCOMPOSITES WITH MALEIC ANHYDRIDE
GRAFTED POLYPROPYLENE COMPATIBILIZER

A THESIS SUBMITTED TO
THE GRADUATE SCHOOL OF NATURAL AND APPLIED SCIENCES
OF
MIDDLE EAST TECHNICAL UNIVERSITY

BY

ŞULE SEDA YILMAZ

IN PARTIAL FULFILLMENT OF THE REQUIREMENTS
FOR
THE DEGREE OF MASTER OF SCIENCE
IN
CHEMICAL ENGINEERING

JUNE 2011

Approval of the thesis:

**PREPARATION AND CHARACTERIZATION OF ORGANOCLAY-
POLYPROPYLENE NANOCOMPOSITES WITH MALEIC ANHYDRIDE GRAFTED
POLYPROPYLENE COMPATIBILIZER**

submitted by **ŞULE SEDA YILMAZ** in partial fulfillment of the requirements for the degree of **Master of Science in Chemical Engineering Department, Middle East Technical University** by,

Prof. Dr. Canan Özgen
Dean, Graduate School of **Natural and Applied Sciences**

Prof. Dr. Deniz Üner
Head of Department, **Chemical Engineering**

Prof. Dr. Ülkü Yilmazer
Supervisor, **Chemical Engineering Dept., METU**

Examining Committee Members:

Prof. Dr. Hayrettin Yücel
Chemical Engineering Dept., METU

Prof. Dr. Ülkü Yilmazer
Chemical Engineering Dept., METU

Prof. Dr. Erdal Bayramlı
Chemistry Dept., METU

Prof. Dr. Necati Özkan
Polymer Science and Technology Dept., METU

Assoc. Prof. Dr. Halil Kalıpçılar
Chemical Engineering Dept., METU

Date: 15.06.2011

I hereby declare that all information in this document has been obtained and presented in accordance with academic rules and ethical conduct. I also declare that, as required by these rules and conduct, I have fully cited and referenced all material and results that are not original to this work.

Name, Last name: Şule Seda YILMAZ

Signature:

ABSTRACT

PREPARATION AND CHARACTERIZATION OF ORGANOCLAY- POLYPROPYLENE NANOCOMPOSITES WITH MALEIC ANHYDRIDE GRAFTED POLYPROPYLENE COMPATIBILIZER

YILMAZ, Şule Seda

M.Sc., Department of Chemical Engineering

Supervisor: Prof. Dr. Ülkü YILMAZER

June 2011, 129 pages

The aim of this study was to improve the mechanical properties “Moplen” EP300L which is a heterophase copolymer. Polymer blends and nanocomposites were prepared by melt compounding method in a twin screw extruder. Nanofil® 5 (N5) and Nanofil® 8(N8) were used as the organoclays, and maleic anhydride grafted polypropylene (M) was used as the compatibilizer. The effects of additive concentrations and types of organoclays on the morphology, mechanical and thermal properties were investigated.

Organoclay loading over 2 wt% prevented the intercalation mechanism resulting in large aggregates of clay, thus the material properties became poor even in the presence of compatibilizer. Compatibilizer addition improved the intercalation ability of the polymer, however a substantial increase in mechanical properties was not obtained up to 6 wt % loading of the compatibilizer.

XRD analysis revealed that intercalated structures were formed with the addition of compatibilizer and organoclay. The nanocomposites that were prepared with N5 type organoclay showed delaminated structures at 6 wt % compatibilizer loading.

Nanofill ® 5 exhibited the highest improvements in mechanical properties, since the degree of organoclay dispersion was better in Nanofill ® 5 containing nanocomposites in comparison to Nanofill ® 8 containing ones. The DSC analysis indicated a insignificant reduction in the melting temperature of the ternary nanocomposites.

Keywords: Polypropylene; Nanocomposite; Organoclay; Compatibilizer; Extrusion

ÖZ

MALEİK ANHİDRİT AŞILANMIŞ POLİPROPİLEN UYUMLAŞTIRICISI İÇEREN ORGANOKİL-POLİPROPİLEN NANOKOMPOZİTLERİN HAZIRLANMASI VE KARAKTERİZASYONU

YILMAZ, Şule Seda

Yüksek Lisans, Kimya Mühendisliği

Tez Yöneticisi: Prof. Dr. Ülkü YILMAZER

Haziran 2011, 129 sayfa

Bu çalışmanın amacı, heterofaz yapılı “Moplen” EP300L polipropilen malzemesinin mekanik özelliklerinin iyileştirilmesidir. Polimer karışımları ve nanokompozitleri, çift vidalı bir ekstruderde eriyik karıştırma metoduyla hazırlanmışlardır. Organik kil olarak Nanofill ® 5 ve Nanofill ® 8, uyumlaştırıcı olarak ise maleik anhidrit aşılantısı polipropilen (M) kullanılmıştır. Katkı maddesi konsantrasyonlarının ve organik kil tiplerinin morfoloji ile, mekanik ve ısı özelliklerine etkileri araştırılmıştır.

Küttelece 2%'den fazla organik kil eklenmesi, büyük kil topaklarının oluşumu sonucu, uyumlaştırıcının var olduğu durumlarda dahi tabakaların aralanma mekanizmasını ve malzeme özelliklerini kötüleştirmiştir. Uyumlaştırıcı eklenmesi polimerin tabakaların arasına girme kabiliyetini iyileştirmiş, ancak mekanik özelliklerde ağırlıkça %6 uyumlaştırıcı derişimine kadar önemli bir artış elde edilmemiştir.

XRD analiz sonuçlarına göre uyumlaştırıcı ve organokil eklenmesi ile polimerin kil tabakaları arasına girdiği ve dağılımı iyi yapılar oluşturduğu görülmüştür. Nanofill ® 5 ile üretilen kompozitlerin %6 uyumlaştırıcı eklenmesi ile matris içinde daha iyi dağıldığı gözlemlenmiştir.

Organik kil dađılım derecesinin Nanofill ® 5 ile üretilen nanokompozitlerde daha iyi olduđu görülmüştür ve dolayısı ile bu malzemelerin mekanik özelliklerindeki artış da Nanofill ® 8 ile üretilen kompozitlerden daha fazladır. DSC analizleri, üçlü kompozitlerin erime sıcaklıklarında çok az bir azalma olduđu gözlemlenmiştir.

Anahtar Kelimeler: Polipropilen; Nanokompozit; Organik Kil; Uyumlaştırıcı; Ekstrüzyon

To my parents and grandparents

ACKNOWLEDGEMENTS

I would like to express my deepest gratitude to my supervisor, Prof. Dr. Ülkü Yılmaz, for his continuous support, guidance, constructive criticism, advice, and insight throughout my thesis study. It was a pleasing honor for me to work with him.

I am grateful to Prof. Dr. Göknur Bayram from Department of Chemical Engineering for letting me use the instruments in her laboratory. Special thanks go to Cengiz Tan from Department of Metallurgical and Materials Engineering for SEM analysis, Mihrican Açıkgöz from Department of Chemical Engineering for DSC analysis, and Necmi Avcı from Department of Metallurgical Engineering for XRD analysis.

I would like to thank my dear friends Sibel Dönmez, Bijen Kadaifçi, Sena Yüzbaşı, Ayşe İrem Balcı, Didem Polat, Edibe Eda Oral, Gamzenur Özsin, and Berk Baltacı for their endless support and for making my graduate study enjoyable and full of friendship.

I sincerely thank to Canan Yeniova and Wissam Abdallah for their help, advice and contributions during my study. Friendly and helpful support of all my friends in the Polymer Laboratory including Sertan Yeşil, Tijen Seyidođlu, Ali Sinan Dike, Fatma Işık, and Fadile Kapaklı are also greatly acknowledged.

I am forever grateful to my parents Mehmet and Nilgün Yılmaz, my brother Yunus Emre Yılmaz, my love M. Asım Ay and all my family for their endless love, encouragement and support trough out my life.

This study was supported by SAN-TEZ 00112.STZ.2007-1.

TABLE OF CONTENT

ABSTRACT	iv
ÖZ	vi
ACKNOWLEDGEMENTS	ix
TABLE OF CONTENTS	x
LIST OF TABLES	xiii
LIST OF FIGURES	xiv
NOMENCLATURE	xx
CHAPTERS	
1. INTRODUCTION	1
2. BACKGROUND	5
2.1 Composite Materials	5
2.1.1 Types of Composites	6
2.1.2 Polymer Matrix Composites	7
2.2 Nanocomposites	7
2.2.1 Polymer Layered Silicate Nanocomposites (PLSN)	8
2.2.1.1 Organically Modified Layered Silicates	8
2.2.2 Nanocomposite Types	10
2.2.3 Nanocomposite Preparation Methods	11
2.2.3.1 In-situ Polymerization Method	11
2.2.3.2 Solution Intercalation	12
2.2.3.3 Sol-Gel Technology	13
2.2.3.4 Melt Intercalation	13
2.3 Polymer Matrix of the Study	14
2.3.1 Polypropylene	14
2.3.1.1 Polymerization, Structure and Tacticity of Polypropylene ..	15
2.4 Polypropylene Nanocomposites	16
2.4.1 Maleic Anhydride (MAH) Functionality	18
2.5 Polymer Processing	19
2.5.1 Extrusion	19

2.5.1.1 Screw Design	20
2.5.1.2 Extruder Types	21
2.5.2 Injection Molding	23
2.6 Characterization of Nanocomposites	24
2.6.1 Mechanical Properties	24
2.6.1.1 Tensile Test	24
2.6.1.2 Impact Test	27
2.6.2 Thermal Analysis	28
2.6.2.1 Differential Scanning Calorimetry (DSC)	28
2.6.3 Morphological Analysis	30
2.6.3.1 X-Ray Diffraction (XRD) Analysis	30
2.6.3.2 Scanning Electron Microscopy (SEM)	32
2.7 Previous Studies	32
3. EXPERIMENTAL	35
3.1 Materials	35
3.1.1 Polymer Matrix	35
3.1.2 Organoclays	36
3.1.2.1 Nanofill ® 8	36
3.1.2.2 Nanofill ® 5	37
3.1.3 Compatibilizers	39
3.2 Preparation of Nanocomposites	40
3.2.1 Injection Molding	46
3.3 Characterization	47
3.3.1 Morphological Testing Procedure and Equipment	47
3.3.1.1 X-Ray Diffraction Analysis	47
3.3.1.2 Scanning Electron Microscopy (SEM) Analysis	47
3.3.2 Mechanical Properties	48
3.3.2.1 Tensile Test	49
3.3.2.2 Impact Test	50
3.3.3 Thermal Analysis	50
3.3.3.1 Differential Scanning Calorimetry (DSC) Analysis	51
4. RESULTS AND DISCUSSION	52
4.1. Morphological Analysis	52
4.1.2 X-RAY Diffraction Analysis	52
4.1.2.1 Effects of Compatibilizer	55

4.1.2.2 Effects of Clay Content	62
4.1.2.3 Effects of Clay Type	66
4.1.3 Scanning Electron Microscopy Analysis (SEM)	71
4.1.3.1 Effects of Clay Content	73
4.1.3.2 Effects of Compatibilizer Content	74
4.1.3.3 Ternary Nanocomposites	76
4.1.3.4 Effects of Clay Type	78
4.2 Mechanical Properties	80
4.2.1 Tensile Tests	80
4.2.1.1 Effects of Compatibilizer	81
4.2.1.2 Effects of Clay Content	85
4.2.1.3 Improved Nanocomposites	89
4.2.1.4 Effects of Clay Type	92
4.2.2 Impact Test	95
4.2.2.1 Effects of Clay Content	95
4.2.2.2 Effects of Compatibilizer Content	97
4.2.2.3 Effects of Clay Type	99
4.3 Differential Scanning Calorimetry (DSC) Analysis	100
5. CONCLUSIONS	105
REFERENCES	107
APPENDICES	115

LIST OF TABLES

TABLES

Table 3.1 Properties of MOPLen EP300L (EP300L) Polymer Matrix	36
Table 3.2 Properties of Nanofill ® 8	37
Table 3.3 Properties of Nanofill ® 5	38
Table 3.4 Characteristics of Bondyram® 1001	39
Table 3.5 Drying conditions	40
Table 3.6 Binary composite compositions prepared in experiments	44
Table 3.7 Ternary composite compositions prepared in experiments	45
Table 3.8 Injection molding parameters	47
Table 3.9 Dimensions of the tensile test specimens	49
Table 3.10 Dimensions of impact test specimens	50
Table 4.1 XRD results of EP300L, N5 and N8	55
Table 4.2 XRD results of binary and ternary nanocomposites with N5	59
Table 4.3 XRD results, effects of clay type with N8	68
Table 4.4 SEM results	72
Table 4.5 DSC results	102
Table A.1 Calculated tensile properties and standard deviations for all compositions	115
Table A.2 Impact strength data and standard deviations for all compositions	118

LIST OF FIGURES

FIGURES

Figure 2.1 Structure of 2:1 layered silicates	9
Figure 2.2 Idealized structures of organically modified silicates	10
Figure 2.3 Nanocomposite types	11
Figure 2.4 In-situ polymerization methods	12
Figure 2.5 Solution intercalation method	13
Figure 2.6 Melt intercalation method	14
Figure 2.7 Polymerization of polypropylene	15
Figure 2.8 Stereochemical configurations of polypropylene	16
Figure 2.9 Structure of maleic anhydride grafted polypropylene and its reaction with hydroxyl groups	18
Figure 2.10 Schematic representation of the intercalation process of MAPP	19
Figure 2.11 A simple extruder scheme and representation of the sections	20
Figure 2.12 The sections of an extruder screw	21
Figure 2.13 Different types of screw configurations for twin-screw extruders	22
Figure 2.14 Screw configurations for twin screw extruders	22
Figure 2.15 Co-rotating twin-screw extruder used in nanocomposite production in this study	23
Figure 2.16 Tensile test machine and dog bone shaped specimen	25
Figure 2.17 Idealized stress-strain curve for a polymer that undergoes ductile failure	26

Figure 2.18 Stress–strain curves at various temperatures (increasing from a to e): (a) low extensibility followed by brittle fracture; (b) localized yielding followed by fracture; (c) necking and cold drawing; (d) homogeneous deformation with indistinct yield; (e) rubber-like behavior	27
Figure 2.19 Charpy and Izod impact tests	28
Figure 2.20 Power compensated differential scanning calorimeter	29
Figure 2.21 Typical DSC curves	30
Figure 2.22 Diffraction of X-Rays	31
Figure 2.23 Schematic diagram representing the main components of a scanning electron microscope	32
Figure 3.1 Chemical structure of Nanofill ® 8	37
Figure 3.2 Chemical structure of Nanofill ® 5	38
Figure 3.3 Chemical structure of maleic anhydride grafted polypropylene	39
Figure 3.4 Thermoprism TSE 16 TC twin-screw extruder	41
Figure 3.5 Schematic diagram of processing parameters; barrel temperature and screw speed	42
Figure 3.6 Flow chart for nanocomposite production and characterization	43
Figure 3.7 Injection molding equipment	46
Figure 3.8 Specimens used in morphological analysis	48
Figure 3.9 Tensile test specimen	49
Figure 3.10 Impact test specimen	50
Figure 4.1 X-Ray Diffraction pattern of EP300L	53
Figure 4.2 XRD pattern of Nanofill ® 5 (N5) in powder form	54
Figure 4.3 XRD pattern of Nanofill ® 8 (N8) in powder form	55
Figure 4.4 XRD pattern of binary composites of N5	56
Figure 4.5 XRD patterns of ternary composites with 2wt%, 3wt%, 4wt%, 6wt% and 8wt% compatibilizer and 1wt% clay loadings	57

Figure 4.6 XRD patterns of ternary composites with 2wt%, 3wt%, 4wt%, 6wt% and 8wt% compatibilizer M and 2wt% clay loadings	61
Figure 4.7 XRD patterns of ternary composites with 2wt%, 3wt%, 4wt%, 6wt% and 8wt% compatibilizer M and 3wt% clay loadings	61
Figure 4.8 XRD patterns of ternary composites with 2wt%, 3wt%, 4wt%, 6wt% and 8wt% compatibilizer M and 4wt% clay loadings	62
Figure 4.9 XRD patterns of ternary composites with 1wt%, 2wt%, 3wt% and 4wt% clay and 2wt% compatibilizer M loadings	63
Figure 4.10 XRD patterns of ternary composites with 1wt%, 2wt%, 3wt% and 4wt% clay and 3wt% compatibilizer M loadings	64
Figure 4.11 XRD patterns of ternary composites with 1wt%, 2wt%, 3wt% and 4wt% clay and 4wt% compatibilizer M loadings	64
Figure 4.12 XRD patterns of ternary composites with 1wt%, 2wt%, 3wt% and 4wt% clay and 6wt% compatibilizer M loadings	65
Figure 4.13 XRD patterns of ternary composites with 1wt%, 2wt%, 3wt% and 4wt% clay and 8wt% compatibilizer M loadings	65
Figure 4.14 XRD patterns of binary composites prepared with Nanofill® 8	67
Figure 4.15 XRD patterns of ternary nanocomposites with different Nanofill® 8 and low compatibilizer loadings	69
Figure 4.16 XRD patterns of ternary nanocomposites with different Nanofill® 8 and high compatibilizer loadings	70
Figure 4.17 SEM micrographs of EP300L extruded once a) x250 b) x3000	73
Figure 4.18 SEM micrographs of binary composites with organoclay N5 a) 1wt% N5 (x250) b) 1wt% N5 (x3000) c) 8 wt% of N5 (x250) d) 8 wt% of N5 (x3000)	74
Figure 4.19 SEM micrographs of binary blends with compatibilizer a) 2wt% M (x250) b) 2 wt% M (x3000) c) 6 wt% of M (x250) d) 6 wt% of M (x3000)	75
Figure 4.20 SEM micrographs of ternary composites a) 6M1N5 (x250) b) 6M1N5 (x3000) c) 6M2N5 (x250) d) 6M2N5 (x3000) e) 6M4N5 (x250) f) 6M4N5 (x3000)	77

Figure 4.21 SEM micrographs of binary composites with organoclay N8 a) 1wt% N8 (x250) b) 1wt% N8 (x3000) c) 8 wt% of N8 (x250) d) 8 wt% of N8 (x3000)	79
Figure 4.22 SEM micrographs of ternary composites with organoclay N8 a) 3M1N8 (x250) b) 3M1N8 (x3000)	80
Figure 4.23 Typical engineering stress-strain curve of EP300L polymer matrix.	81
Figure 4.24 Young's Modulus of binary blends and ternary nanocomposites prepared with compatibilizer M and N5 clay at different loadings	83
Figure 4.25 Tensile stress at yield values of binary blends and ternary nanocomposites prepared with compatibilizer M and N5 clay at different loadings	83
Figure 4.26 Tensile strength values of of binary blends and ternary nanocomposites prepared with compatibilizer M and N5 clay at different loadings	84
Figure 4.27 Elongation at break (%) values of binary blends and ternary nanocomposites prepared with compatibilizer M and N5 clay at different loadings	84
Figure 4.28 Young's Modulus of binary and ternary nanocomposites prepared with compatibilizer M and N5 at different loadings	86
Figure 4.29 Tensile stress at yield values of binary and ternary nanocomposites prepared with compatibilizer M and N5 at different loadings	87
Figure 4.30 Tensile strength values of binary and ternary nanocomposites prepared with compatibilizer M and N5 at different loadings	88
Figure 4.31 Elongation at break (%) values of binary and ternary nanocomposites prepared with compatibilizer M and N5 at different loadings	88
Figure 4.32 Young's Modulus of ternary nanocomposites prepared with 6 wt% compatibilizer M and N5 at different loadings of clay	89
Figure 4.33 Tensile stresses at yield values of ternary nanocomposites prepared with 6 wt% compatibilizer M and N5 at different loadings of clay	90
Figure 4.34 Tensile strength values of ternary nanocomposites prepared with 6 wt% compatibilizer M and N5 at different loadings of clay	90

Figure 4.35 Elongation at break (%) values of ternary nanocomposites prepared with 6 wt% compatibilizer M and N5 at different loadings of clay	91
Figure 4.36 Young's Modulus of binary and ternary nanocomposites prepared with N8 at low content and compatibilizer M at different loadings	93
Figure 4.37 Tensile stress at yield values of binary and ternary nanocomposites prepared with N8 at low content and compatibilizer M at different loadings	93
Figure 4.38 Tensile strength values of binary and ternary nanocomposites prepared with N8 at low content and compatibilizer M at different loadings	94
Figure 4.39 % Elongation at break values of binary and ternary nanocomposites prepared with N8 at low content and compatibilizer M at different loadings	94
Figure 4.40 Impact strength values of binary and ternary nanocomposites prepared with N5 and compatibilizer M at different loadings	96
Figure 4.41 Impact strength values of binary blends and ternary nanocomposites prepared with N5 and compatibilizer M at different loadings	98
Figure 4.42 Impact strength values of binary and ternary nanocomposites prepared with N8 and compatibilizer M at different loadings	100
Figure 4.43 DSC thermogram of EP300L	101
Figure 4.44 DSC thermogram of compatibilizer M	101
Figure B.1 DSC thermogram of binary blend containing 2 wt% M	120
Figure B.2 DSC thermogram of binary blend containing 6 wt% M	121
Figure B.3 DSC thermogram of binary nanocomposite containing 1 wt% Nanofill® 5	121
Figure B.4 DSC thermogram of binary nanocomposite containing 8 wt% Nanofill® 5	122
Figure B.5 DSC thermogram of binary nanocomposite containing 1 wt% Nanofill® 8	122
Figure B.6 DSC thermogram of binary nanocomposite containing 8 wt% Nanofill® 8	123

Figure B.7 DSC thermogram of ternary nanocomposite containing 2 wt% Nanofill [®] 5 and 2 wt% M	123
Figure B.8 DSC thermogram of ternary nanocomposite containing 2 wt% Nanofill [®] 5 and 3 wt% M	124
Figure B.9 DSC thermogram of ternary nanocomposite containing 2 wt% Nanofill [®] 5 and 4 wt% M	124
Figure B.10 DSC thermogram of ternary nanocomposite containing 1 wt% Nanofill [®] 5 and 6 wt% M	125
Figure B.11 DSC thermogram of ternary nanocomposite containing 2 wt% Nanofill [®] 5 and 6 wt% M	125
Figure B.12 DSC thermogram of ternary nanocomposite containing 3 wt% Nanofill [®] 5 and 6 wt% M	126
Figure B.13 DSC thermogram of ternary nanocomposite containing 4 wt% Nanofill [®] 5 and 6 wt% M	126
Figure B.14 DSC thermogram of ternary nanocomposite containing 2 wt% Nanofill [®] 5 and 8 wt% M	127
Figure B.15 DSC thermogram of ternary nanocomposite containing 2 wt% Nanofill [®] 8 and 2 wt% M	127
Figure B.16 DSC thermogram of ternary nanocomposite containing 2 wt% Nanofill [®] 8 and 3 wt% M	128
Figure B.17 DSC thermogram of ternary nanocomposite containing 2 wt% Nanofill [®] 8 and 4 wt% M	128
Figure B.18 DSC thermogram of ternary nanocomposite containing 2 wt% Nanofill [®] 8 and 6 wt% M	129

NOMENCLATURE

\bar{A}	Average area of domains in SEM analysis, μm^2
A_i	Area of a number of domains in SEM analysis, μm^2
A_0	Cross-sectional area of the gauge region, mm^2
d	Interlayer spacing, \AA
d_{av}	Average domain size, nm
\bar{d}	Average domain size, nm
D	Distance between grips of tensile test specimen, mm
D	Diameter of the screws, mm
E	Young's Modulus, MPa
F	Force, N
g	Gauge length of tensile test specimen, mm
ΔH_f	Heat of fusion, J/g
ΔH_f°	Heat of fusion for pure crystalline form of polymer, J/g
L	Length of the Extruder Barrel, mm
L	Total length of impact test specimen, mm
L_0	Initial gauge length, mm
L_0	Overall length of tensile test specimen, mm
ΔL	Change in sample length, mm
n	Degree of diffraction
n	Notch length (v type, 45°), mm
N_i	Number of domains analyzed in SEM analysis
t	Thickness of tensile test specimen, mm
t	Thickness of impact test specimen, mm
T_g	Glass Transition Temperature, $^\circ\text{C}$
T_m	Melting Temperature, $^\circ\text{C}$
T_c	Crystallization Temperature, $^\circ\text{C}$
X_c	Crystallinity, %
w	Unnotched width of impact test specimen, mm
W	Width of narrow section of tensile test specimen, mm

Greek Letters

σ	Stress, MPa
ε	Strain, mm/mm
θ	Diffraction angle, °
λ	Wavelength, nm

Abbreviations

CCC	Carbon-Carbon Matrix Composites
CEC	Cation Exchange Capacity
CMC	Ceramic Matrix Composites
COOH	Carboxyl
CRT	Cathode Ray Tube
DSC	Differential Scanning Calorimetry
EP300L	MOLEN EP300L, Polymer matrix of the study
FTIR	Fourier Transform Infrared Spectroscopy
ISO	International Organization for Standardization
MAH	Maleic Anhydride
MAPP	Maleic Anhydride Grafted Polypropylene
M	Bondyram® 1001 (Maleic Anhydride Modified Polypropylene)
MB	Melt mixing sequence in which organoclay and M are fed into extruder 1 st and added into EP300L in the 2 nd extrusion
MMC	Metal Matrix Composites
MMT	Montmorillonite
N5	Nanofill ® 5
N8	Nanofill ® 8
OH	Hydroxyl
OMLS	Organically Modified Layered Silicate
PLSN	Polymer Layered Silicate Nanocomposites
PMC	Polymer Matrix Composites
PP	Polypropylene
SAXS	Small Angle X-ray Scattering

SEM	Scanning Electron Microscopy
TEM	Transmission Electron Microscopy
XRD	X-Ray Diffraction
WAXS	Wide Angle X-Ray Scattering

CHAPTER 1

INTRODUCTION

Composite materials enable more functional and esthetic structures that have optimum performance which traditional materials do not have. They are preferred and widely used for their design flexibility, outstanding thermal, mechanical, electrical, etc. properties compared to their single phase counterparts [1].

Composites are the combinations of two or more materials which are physically and chemically distinct, arranged or distributed phases with an interface in between that separates them. Reinforcing material is embedded in a matrix material in a controlled manner to obtain the composite. This new material, carrying the identity of each constituent, exhibits unique properties that cannot be achieved by a single component [2, 3].

In composite applications due to their low cost and weight, low heat and pressure requirement and ease of processing advantages, polymer matrices are the most preferred matrix type [3]. Despite these advantages, their low maximum service temperature and high thermal expansion coefficient may lead to dimensional instability and sensitivity to moisture and UV. Also, their mechanical and electrical properties, such as mechanical strength, impact resistance and electrical conductivity, are lower than metallic and ceramic matrices which make the reinforcement utilization with inorganic, synthetic and/or natural compounds a must [4]. Polymer matrices have low density when compared with heavy metallic and ceramic composites whose ductility is rather low, and this is a great advantage for usage [5, 6].

Nanometer scale dispersed fillers in polymer matrices form composites showing improved properties (mechanical, thermal, physical and barrier properties) when compared to conventional polymer composites. These are called polymer matrix nanocomposites [7].

Polymer-clay nanocomposites, which are in the content of this study, are the composites whose reinforcement material is in the form of lamellae and has a high aspect ratio with one to a few nanometer thickness and hundreds to thousands of nanometers in length. Montmorillonite, which is a layered silicate, is especially used as filler in polymer-clay nanocomposites. Montmorillonite (MMT) is a crystalline; 2:1 layered clay mineral. A central alumina sheet is placed between two silica tetrahedral sheets. Usually montmorillonite clays are modified by the substitution reaction of alkyl ammonium ion with surface sodium ions, making the hydrophobic silicate surfaces organophilic to enable insertion of organic materials to the clay layers. Functional group providing alkyl ammonium cations can react with the polymer or initiate polymerization of monomers [7, 8, 9]

Following the studies done by Toyota research group that revealed the significant improvements in thermal and mechanical properties of Nylon-6/MMT nanocomposites, the observations of Vaia et al. [10] on the possible melt intercalation mechanism in the absence of solvent renewed the interest for layered silicates [11, 12].

There are three methods to synthesize nanocomposites: In situ polymerization, solution intercalation and melt intercalation. Melt intercalation method has more advantages among all the three methods, such as compatibility with the current industrial processes, ease of application proper for any type of polymer matrix including polar ones, and solvent free operation type. The state of dispersion and interactions between the filler and polymer matrix are the key parameters affecting the final properties of the nanocomposites prepared by the melt intercalation method.

There are three types of polymer layered silicate nanocomposites that are thermodynamically achievable depending on the strength of interfacial interactions between layered silicates and the matrix; intercalated, intercalated-flocculated, and exfoliated-delaminated. As surface area and interactions between the matrix and

silicate layers enhanced, the degree of dispersion increases by changing the morphology from intercalated structure to exfoliated structure [11]. The degree of dispersion is affected by the polarity of the polymer matrix, compatibilizer type and the organic modifier of the nanoclay [13]. Polypropylene, which is a thermoplastic linear hydrocarbon polymer, is a very appropriate material for room temperature applications due to its convenient physical, mechanical and thermal properties [14]. The bottleneck of using polyolefins such as polypropylene with the direct melt intercalation method is having a low level of dispersion of silicate layers due to its nonpolarity. By using compatibilizer with functional groups, exfoliation is facilitated in addition to the affect of modification of the clay surfaces [15].

The aim of this study was to improve the mechanical properties of polypropylene by using montmorillonite type layered silicate, and compatibilizer having functional groups. The matrix used was; EP300L (EP300L) which is a heterophase copolymer. Nanofil® 5 and Nanofil® 8 were used as the organoclays and maleic anhydride grafted polypropylene (MAPP) was used as the compatibilizer. Throughout the study, the effects of organoclay types, and organoclay and compatibilizer content on the final properties of the nanocomposites were investigated.

During the study, the processing sequence and processing parameter values of the study by Cengiz F. [23] "Preparation and Characterization of Recycled Polypropylene Based Nanocomposites", which was the previously completed study of the SAN-TEZ 00112.STZ.2007-1 project, were used for production and characterization of the polymer matrix. Processing parameters were set to a temperature of 180 °C and screw speed of 350 rpm, and masterbatch method (MB) was applied in order to process nanocomposites with several organoclay contents and increase the interactions between the compatibilizer M and organoclay.

All materials were dried before extrusion and injection molding processes at proper temperatures and durations. Standard test specimens were prepared according to the standard of ISO 527-2 5A for characterization, and specimens were conditioned for specified durations prior to analysis.

Finally, tensile and impact tests were conducted to determine the mechanical properties. Morphological characterization and organoclay dispersion were evaluated

by Scanning Electron Microscopy (SEM) and X-Ray Diffraction (XRD) analysis. Melting and crystallization behavior of the composites were examined by Differential Scanning Calorimetry (DSC) measurements.

CHAPTER 2

BACKGROUND

2.1 Composite Materials

Composites are the combinations of two or more materials, which are physically and chemically distinct, arranged or distributed phases with a distinct interface in between that separates them. This new material, carrying the identity of each constituent, exhibits unique properties that cannot be achieved by a single component [2-3]. Although the composite material may be in homogeneous phase, each constituent of the composite dominates its own distinct structural features remaining their identity in the mixture [16].

Despite the fact that modern composites were started to be used in late 1903s, after the invention of fiber glass reinforced resins, natural composites existed in nature and used by man such as wood, bamboo and bone for hundreds of years. After fiber glass reinforced resins; in 1970s carbon, boron and aramid fibers became popular with new composite systems with metal and ceramic matrices [2]. In recent years, by development of new and improved composite manufacturing processes, unlimited product opportunities with low costs, lead composite materials to be used by many industries like automotive, marine, army, aerospace etc. [3, 5].

Composite materials offer improved strength, stiffness, fatigue and impact resistance, thermal conductivity, corrosion resistance, etc. [2]. These improved properties increased the interest and demand in composite materials due to their design flexibility that provides unlimited selection of characteristics for the invented material [1].

Generally there are two different phases in the structure of composites; matrix and the reinforcement. Matrix is the continuous component in the composite governing

the mechanical properties of the new designed material which can be metallic, ceramic or polymeric. The other phase “reinforcement”, which is mostly stiffer and harder with some exceptions such as phase reinforcement in a brittle polymer matrix, improves the mechanical properties of the matrix [3, 5].

In determining the effectiveness of the reinforcement material, shape and dimension of the reinforcing phase is one of the major parameters. Also, the mechanical properties of composites are a function of the geometry of the reinforcement material [3, 5]. Composites are classified in two ways; according to their matrix and their geometry of reinforcement: flake, particulate and fibers [2]. Flake particles offer high out-of-plane flexural modulus, higher strength, and low cost, since they consist of matrices like mica and glass. Particulate composites' reinforcement particles, which are spherical, platelet, cubic or any regular or irregular geometry, are immersed in the matrices and the load is carried mostly by the matrix phase [2, 3]. In fibrous reinforcement type, the load is mostly carried by fiber phase which has a high aspect ratio, i.e. high particle length to cross-sectional proportion [3]. The interaction of matrix and reinforcement at phase boundaries, which is called as interface or interphase, is one of the parameters affecting the behavior of a composite besides the matrix and reinforcement properties. Throughout this thick interface, which is often considered as a separate phase and bonds the two constituent, material parameters such as density, concentration, elastic modulus etc. can vary. If load is effectively transmitted from one component to another through the interface, the performance of the composite will be improved. Effective load transmission is possible with optimum interfacial interaction. Wettability, bonding and surface roughness are the parameters affecting interfacial interaction [5].

2.1.1 Types of Composites

There are three types of composites according to their matrix types; metal matrix composites (MMC), ceramic matrix composites (CMC), carbon-carbon matrix composites (CCC), and polymer matrix composites (PMC).

In MMC, the matrix is a metal which is ductile, naturally strong and tough. Metal matrix composites may be utilized at higher service temperatures than their matrix material with the reinforcement. Reinforcement improves specific stiffness and

strength, abrasion resistance, creep resistance, dimensional stability and thermal conductivity. Although MMCs have some advantages over other composites like high operating temperatures and non-flammability, their high cost make their usage limited [6].

Since ceramic materials are widely used at high temperature applications due to their high strength and stiffness, CMCs are also applicable for high temperatures and severe stresses. Fibers are incorporated with CMCs to improve failure strain [2].

When both the reinforcement and the matrix is carbon, these composites are called carbon-carbon composites. In these types of composites, carbon fiber reinforcement is embedded in a carbon matrix. They have high tensile modulus, high tensile strength and low creep at very high temperatures up to 3315°C, and they are 20 times stronger and 30% lighter than carbon structured graphite. However, their susceptibility to oxidation and high cost are their major disadvantages [2].

2.1.2 Polymer Matrix Composites

Polymeric materials are the most commonly used matrix materials since they are easily processed at low temperatures and pressures. However, their mechanical properties need to be improved for industrial applications [3]. Matrix material can be thermoplastic, thermoset or rubber according to their response to temperature. PMCs are made by addition of inorganic/organic additives in certain geometries such as fibers, flakes and particulates [4].

2.2 Nanocomposites

Composites, in which one of the component's phases, at least in one dimension, is less than 100 nm, are called nanocomposites [17]. At nanometer scale, the properties of the materials differ from that of the bulk phase [2]. With these materials, it is possible to achieve multifunctional behavior for any specific property of the material which is more than the sum of the individual components [17]. Researches in this area showed that with only a small amount of nanofiller addition outstanding

mechanical properties are achievable due to large surface area to volume ratio of nanoadditives [18].

Depending on how many dimensions of the dispersed particles are in the nanometer range, nanocomposites are divided into three classes. If all three dimensions are in the nanometer size, isodimensional particle structure exists. Secondly, when two dimensions of the particles are in nanometer level and the third one is larger, elongated structures are formed. Lastly, if one dimension is in the nanometer scale and nanofiller are present in the form of sheets of one to a few nanometer thick, and hundreds to thousands nanometers long, they are called polymer-layered crystal nanocomposites [19].

2.2.1 Polymer Layered Silicate Nanocomposites (PLSN)

Polymer layered silicate nanocomposites are hybrids between the polymer matrix phase and the inorganic phase [20]. With the increase in interest in PLSNs regarding the significant enhancements of thermal and mechanical properties and the possibility of melt mixing polymer with layered silicates without using solvents, today, almost all types of polymer matrices are being studied for the development of these promising organic-inorganic mixtures [11].

2.2.1.1 Organically Modified Layered Silicates

Layered silicate is a member of the 2:1 phyllosilicates family. Their crystal lattice structure is shown in Figure 2.1. Layer thickness of the structure is approximately 1 nm and lateral dimensions may range from Å level to several microns. The layers are organized in parallel to form stacks with their interspace distances which are named as *interlayer* or *gallery*. Interlayers are the regular Van der Waals gaps between the layers. Isomorphic substitution within the layers generates negative charges which are counterbalanced by alkaline earth cations occupied in the interlayer, like Al^{3+} replaced by Mg^{2+} or by Fe^{2+} , or Mg^{2+} replaced by Li^+ [19]. Thus, they have cation exchange capacity (CEC) to characterize the surface charge which is generally expressed as meq/100g, and their layer morphology is considered as hydrophobic colloids of the constant-charge type.

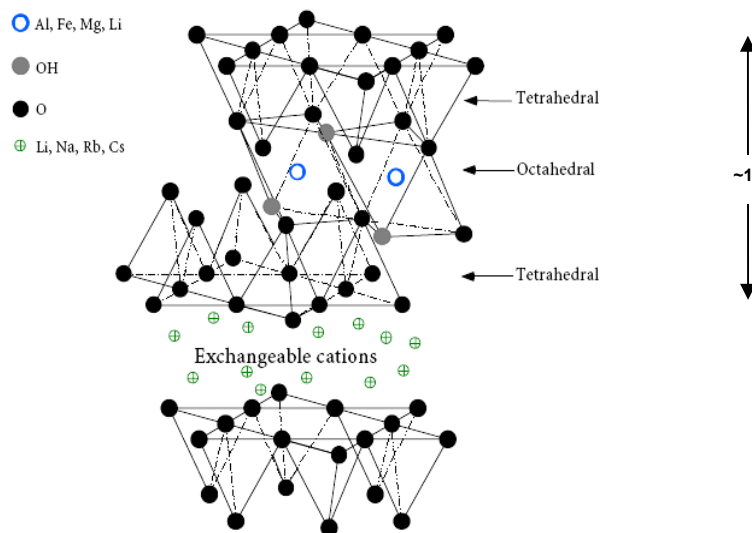


Figure 2.1 Structure of 2:1 layered silicates [21].

In order to overcome the incompatibility of the layered silicates with most organic structured polymers with hydrophilic structure, layered silicates are organically modified. This modification makes intercalation mechanism for many polymers possible. Modification is done by replacement of the cations, which are present in the galleries, with organic cations. The most used ions for modification of the surface of the layers are alkyl ammonium ions. By the effect of these salts, the negative charge is located on the surface of the silicate and the cationic head of the alkyl ammonium is attached to the wall of the interlayer. Its aliphatic tail renders the hydrophilic silicate surface organophilic. These cations also increase the distance between the layers and reduce the surface energy of the filler. In addition, they provide functional groups which can react with the polymer to improve the strength of the interface between the inorganic component and the polymer. Figure 2.2 represents the ideal structure of the organically modified layered silicates, i.e. organoclays.

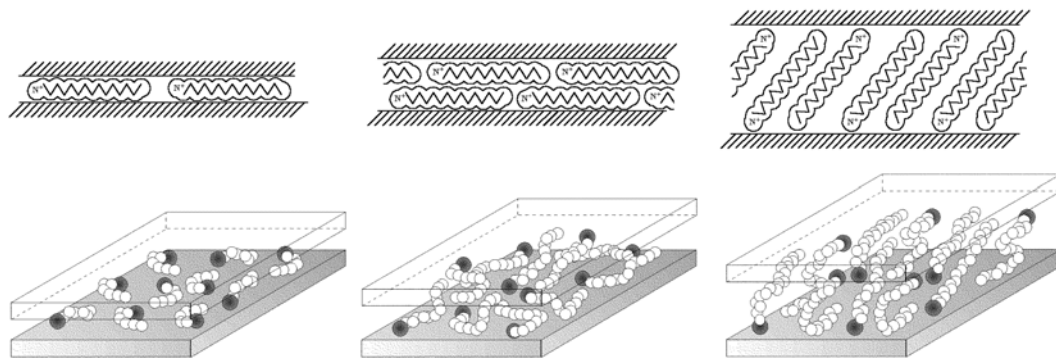


Figure 2.2 Idealized structures of organically modified silicates [21].

2.2.2 Nanocomposite Types

Depending of the nature of the components used, achievable types of the nanocomposites are divided into four; microcomposites (in which polymer and organoclays are phase separated, i.e. remain immiscible, by the absence of intercalation), intercalated nanocomposites, intercalated-flocculated nanocomposites and exfoliated-delaminated nanocomposites. Figure 2.3 shows the types of nanocomposites. Better dispersion of the layered silicates, which have remarkably high aspect ratio (e.g. 10-1000) throughout the polymer matrix, would increase the surface area for polymer filler interaction which promotes enhancements in material properties [11].

Polymer chains are inserted into the gallery space between parallel individual clay layers in a well order in *intercalated* structures [22]. The difference between the intercalated and the *flocculated* nanocomposites is the flocculation of the silicate layers due to hydroxylated edge–edge interactions. On the other hand a complete and uniform dispersion of the silicates in the polymer matrix, forms *exfoliated* or *delaminated* structures maximizing the polymer-clay interactions and making the entire surface of layers available for polymer. Then, this structure provides the most significant improvements in mechanical and physical properties [3].

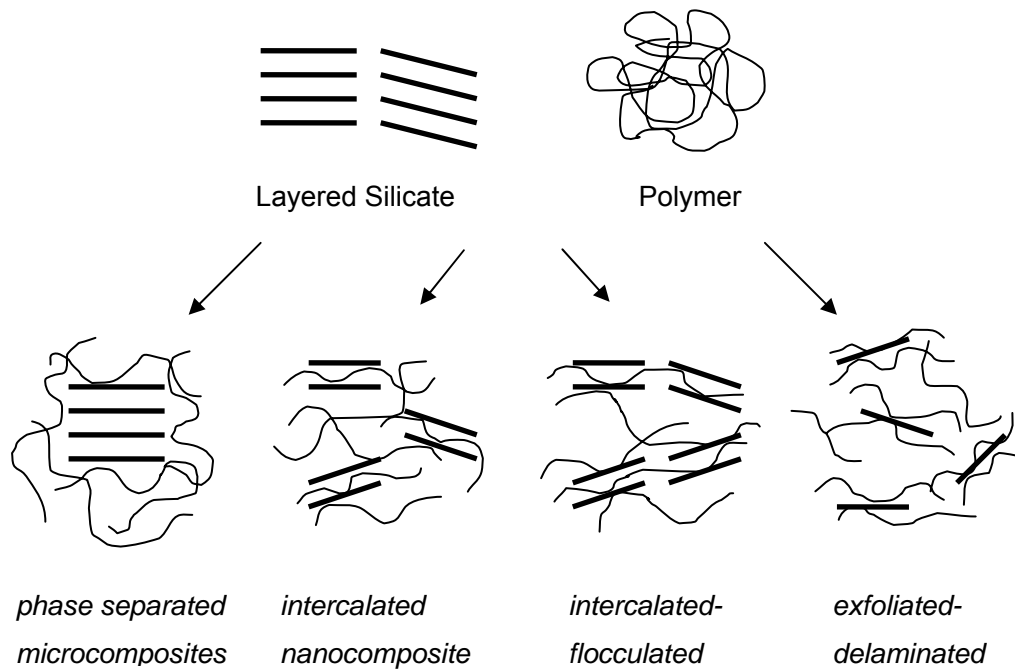


Figure 2.3 Nanocomposite types [23].

2.2.3 Nanocomposite Preparation Methods

Intercalation of polymer in layered silicates is a successful method in synthesis of polymer layered silicate nanocomposites. Preparation methods can be investigated under four main categories: in-situ polymerization, solution intercalation, sol-gel technology and melt intercalation, according to the selected materials and processing techniques [11, 20].

2.2.3.1 In-situ Polymerization Method

In-situ polymerization method has been used for the synthesis of stereospecific polymers, which are constituted from the monomers entrapped in interlayer spacing [20]. In this technique, the layered silicate is within a liquid monomer or a monomer solution, and the polymer formation takes place between the intercalated sheets of the layered silicate. The polymerization process can be initiated by heat or radiation,

by diffusion of a suitable initiator or by an organic initiator or catalyst residing inside the interlayer [19].

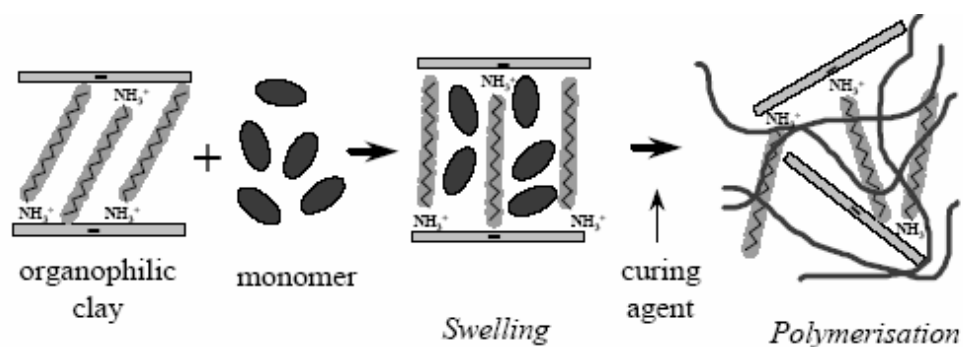


Figure 2.4 In-situ polymerization method [24].

2.2.3.2 Solution Intercalation

Since the forces stacking the layers together are weak, layered silicates are dispersed into single layers in a proper solvent such as water, chloroform or toluene. The solvated polymer and swelled layered silicates are then mixed. The solvated polymer chains diffuse within the silicate layers. After the solvent is removed by evaporation or precipitation of the mixture, the polymer is adsorbed onto the delaminated sheets. The sheets are reassembled by sandwiching the polymer to form an ordered multilayer structure [11, 19]. The intercalation process is represented in Figure 2.5. The advantage of this method is to synthesize intercalated nanocomposites with low or no polarity. But the use of large quantities of solvent makes the process difficult in industrial applications [25].

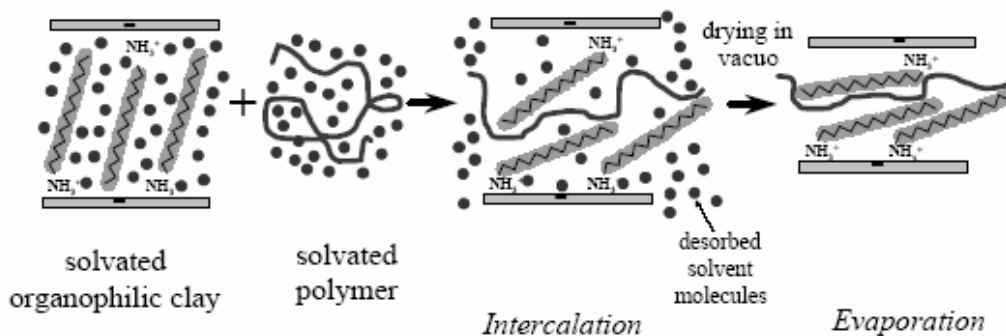


Figure 2.5 Solution intercalation method [24].

2.2.3.3 Sol-Gel Technology

Hydrothermal treatment of a gel is implemented in Sol-Gel technology. The gel containing organics and organometallics including polymer is crystallized by heat. For the crystallization of the clay, silica sol, magnesium hydroxide sol and lithium fluoride are used. High dispersion of the silicate layers is achieved by this method and this method does not require onium ions [20].

2.2.3.4 Melt Intercalation

In this method, polymer chains diffuse into the space between the clay and the galleries above the softening point. The dispersion of the clay particles starts when the hydrodynamic separating forces applied by the matrix fluid exceed the cohesive forces. The degree of dispersion depends on the matrix viscosity, average shear rate and the residence time in the mixing process [26]. To increase the interlayer spacing, using organically modified clays is a usual application. Another reason for this application is to extenuate the incompatibility between the polymer and the layered silicate because of the polarity [20].

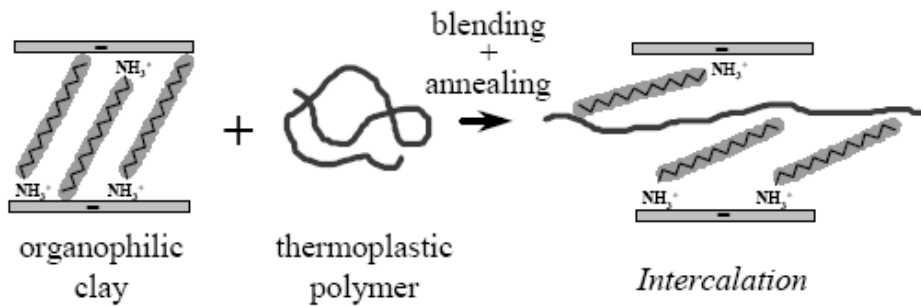


Figure 2.6 Melt intercalation method [24].

Selection of the organically modified layered silicate (OMLS) is one of the most important parts of the process, since by addition of the organoclay the layer separation is increased and the interaction at the interlayer surface should be optimized. The structure of the polar groups of a polymer may help or lead to intercalation but in the presence of a polar polymer the functional group in the OMLS may cause undesired interactions [11].

Since there is no need for a solvent, melt intercalation technique is economically and environmentally favorable over solution polymerization and in-situ polymerization. Another advantage of this technique is the compatibility with the industrial processes. The polymers which are not suitable for solution intercalation or in-situ polymerization can be processed by melt intercalation [11].

2.3 Polymer Matrix of the Study

2.3.1 Polypropylene

Polypropylene (PP) is a thermoplastic polymer of propylene monomer, which was first produced by G. Natta and his coworkers in 1954 after the development of K. Ziegler catalyst [14, 27].

Polypropylene is used in a wide variety of applications including packaging, textiles, plastic parts, laboratory equipments, automotive components, etc. Since propylene monomer is a petroleum byproduct, the ease of availability and low cost makes it favorable. Moreover, the ability to process by different techniques due to its physical properties increases the demand, i.e. in 2007; the global market for polypropylene had a volume of 45.1 million tons [14, 28]. Low density, high melting point, resistance to many chemical solvents, acids and basis and the bending resistance are the main characteristics of polypropylene [29].

2.3.1.1 Polymerization, Structure and Tacticity of Polypropylene

Polypropylene is a simple vinyl polymer such that the methyl groups are attached to the second carbon atom on the backbone chain in different arrangements which determine the tacticity (regularity) of the chain. In other words, the symmetry or the orientation of each methyl group relative to the methyl group of the neighboring monomer has a strong effect on the main characteristic of the propylene polymerization [28].

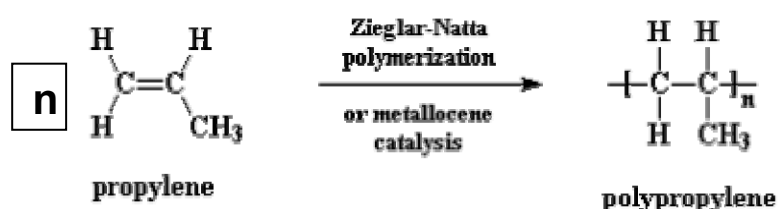


Figure 2.7 Polymerization of polypropylene [30].

Depending on the catalyst, isotactic arrangement occurs when the methyl groups of the monomers are on the same side of the backbone chain or syndiotactic arrangement occurs when the position of the methyl groups alternate. Atactic polypropylene chain exhibits no regularity in orientation of the methyl groups where both isotactic and syndiotactic has as shown in Figure 2.8 [14, 27].

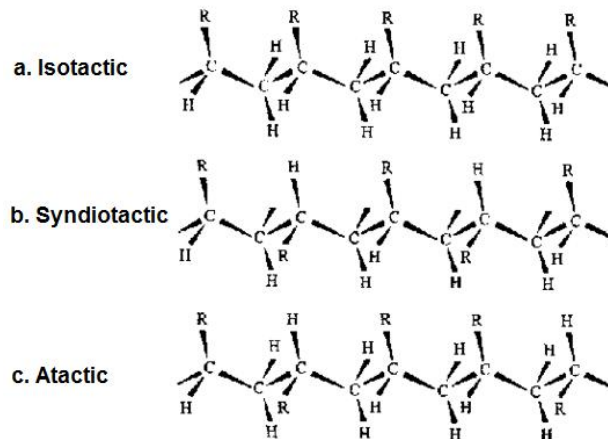


Figure 2.8 Stereochemical configurations of polypropylene [27]

As mentioned before, the structure of the chain determines the tacticity and the properties of the polymer. Isotactic PP has an intermediate level of crystallinity due to the helical chain, high melting point and low density because of the space created by the methyl groups. Syndiotactic PP is less crystalline than isotactic PP and has a lower melting point. Atactic PP is a viscous liquid and has a little use which is generally with other polymers. So, high tacticity or high isotactic content PP is favorable and is used commercially due to the advantages of processing, especially by injection molding and extrusion, low cost, low density, and resistance to temperature, fatigue, chemicals and cracking [14].

2.4 Polypropylene Nanocomposites

Besides the many advantages and attractive properties of PP as mentioned above, PP has some disadvantages such as; low service temperature and low toughness. In order to improve the mechanical properties conventional fillers such as talc, mica and silicate nanolayers are used. The loading rate and dispersion of the filler is very critical for the process conditions and the resultant product [31, 32].

The required loading for talc and mica is relatively high in order to improve stiffness, and it results in an increase in weight and rough surface. Silicate nanolayers are used to enhance stiffness and scratch resistance at much lower loading since they have high aspect ratio [33]. The nanoscale structure maximizes the interactions between the fillers and the PP molecules if they are well dispersed. However, the dispersion of the silicate layers is very difficult at nanometer level since PP has no polar group in its chain and is one of the most hydrophobic polymers, whereas, nanofillers have polar hydroxyl groups in their structure and are naturally hydrophilic [34, 35]. In order to solve this problem clay surface is modified with organic cations as previously mentioned and clays become chemically compatible with the polymer matrix.

The miscibility and linkage between the polypropylene and the layered silicates can also be improved by using compatibilizers having functional groups such as maleic anhydride (MAH) or acrylic acid grafted onto a polymer matrix [36, 37]. Since the dispersion and the resultant PP properties depend on the compatibilizer content, choosing the compatibilizer is very critical. The polarity of the compatibilizer should be high enough to have a stronger interaction between the compatibilizer and the clay surface than the interaction between the clay surface and the surfactant in order to obtain delamination of the silicates. The compatibilizer must also be miscible with PP. The content of the functional groups should be optimized due to the effect of the functional groups on the miscibility with the polypropylene [38]. In polypropylene preparation, one of the most used compatibilizers is maleic anhydride grafted polypropylene (MAPP) which is also used in this study. Presence of the functional group, which is MAH in this case, is capable of forming hydrogen bonding with the clay while providing compatibility with the matrix through its polypropylene backbone.

There are some studies done in order to investigate the effect of MAPP to organoclay ratio on the morphology and the performance of the PP based nanocomposites [15, 39] and to observe degree of functionality and effect of maleic anhydride content of MAPP on the nanocomposite structure [40, 41].

In this study, a heterophasic polypropylene copolymer is used in production of the nanocomposites. With introduction of the organoclay into the blend, well dispersed silicate layers create a barrier effect and avoid agglomeration of the immiscible

domains and the mechanical properties and toughness are positively affected [33, 42]. Addition of the compatibilizer can stabilize the blend morphology by reducing the interfacial tension, hindering and coarsening by forming a protecting layer as in the case of organoclays [43, 44].

2.4.1 Maleic Anhydride (MAH) Functionality

Maleic anhydride is used to increase the adhesion onto polar substrates. Reaction occurs between the hydroxyl groups generated from the hydrolysis of the maleic anhydride and the oxygen group of the layered silicates [45, 46]. The polar character of the MAH group causes an affinity for the organoclay surface and the functionality imparts compatibility between the reinforcing phase and the polymer matrix [15].

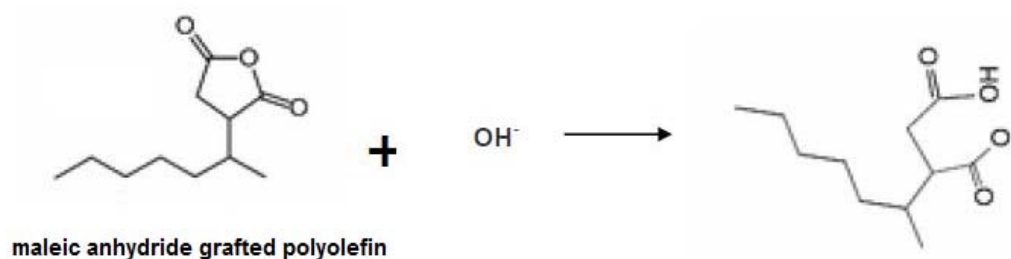


Figure 2.9 Structure of maleic anhydride grafted polypropylene and its reaction with hydroxyl groups [47].

The main driving force for intercalation is originated from the strong hydrogen bonding between the maleic anhydride group, more specifically the carboxyl (COOH) or hydroxyl (OH) groups generated from the hydrolysis of the maleic anhydride group, and the oxygen group of the silicates as represented in Figure 2.9.

The intercalation of the silicate layers into the PP matrix is obtained by this mechanism as represented in Figure 2.10. The strong hydrogen bonding between the maleic anhydride group and the oxygen group of the silicates is the driving force of intercalation mechanism [45, 46]. The polarity of the MAPP also allows the polypropylene macromolecules enter the galleries.

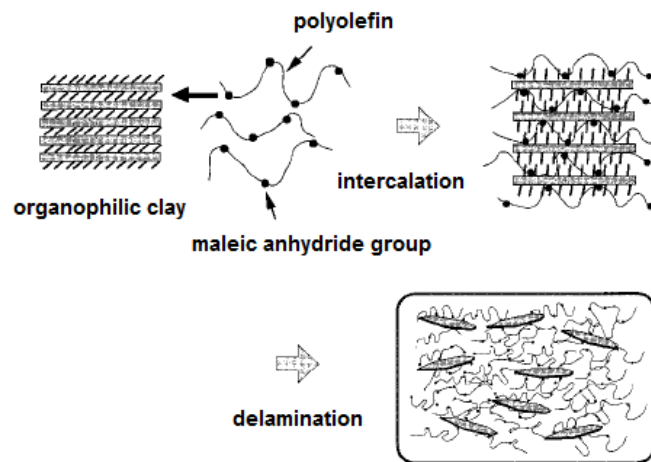


Figure 2.10 Schematic representation of the intercalation process of MAPP [48].

2.5 Polymer Processing

Polymer processing is simply, getting the shaped valuable product from polymeric materials as well as stabilizing the polymer morphology. There are a number of industrial applications such as extrusion and injection molding.

2.5.1 Extrusion

An extruder is used for extrusion to pump the molten material, by means of pressure created by the rotation of the screw, through the die which is the discharge of the extruder. The pressure required for the operation depends on the type of the material, flow rate and the die section. Generally, the polymer is fed to the hopper as granules or powder and conveyed along the screw. The product is a solid polymer

which is tempered in the extruder. Extrusion process is used to produce significant quantities of products continuously. A representative drawing of an extruder is shown in Figure 2.11 [49].

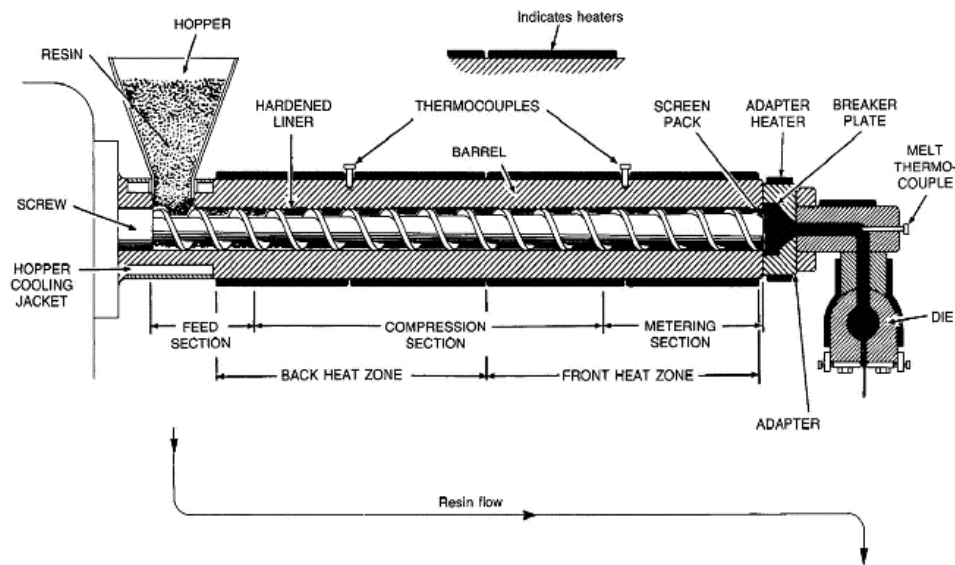


Figure 2.11 A simple extruder scheme and representation of the sections [50].

2.5.1.1 Screw Design

The screw in an extruder is designed in three sections as feed, compression and metering, see Figure 2.12. The function of the feed section is to preheat the solid polymer and convey it to the next section as melt. The energy needed to melt the resin is supplied from the walls of the barrels and the friction of the rotating screw. In the compression section, which has a variable depth, the molten polymer is squeezed to have homogeneity and better heat transfer with reduced thickness. The depth is decreased in this section with increasing root diameter since the screw flight is constant along the screw. In metering zone, the depth is constant, but less than as it is in the feed zone, in order to have a constant temperature and pressure to the die

section. The stability and the quality mostly depend on the design of the screw, thus a screw designed for a specific process is used preferably for that purpose only [50].

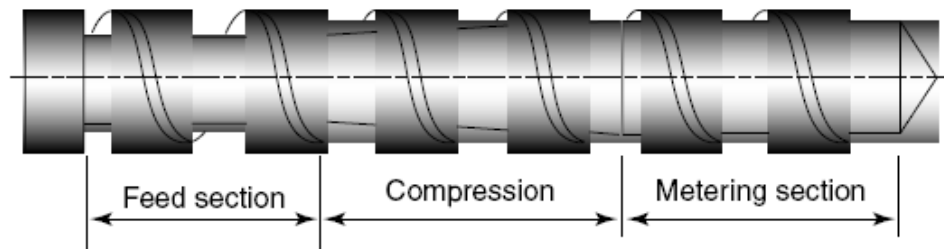


Figure 2.12 The sections of an extruder screw [28].

2.5.1.2 Extruder Types

Most of the extruders designed and used are single screw type which is the one described above. There are also twin-screw extruders, which perform the same process as single screws do, have some additional advantages and properties due to effects of the mechanism of two screws, co-rotating or counter-rotating depending on the design, see Figure 2.13 [51].

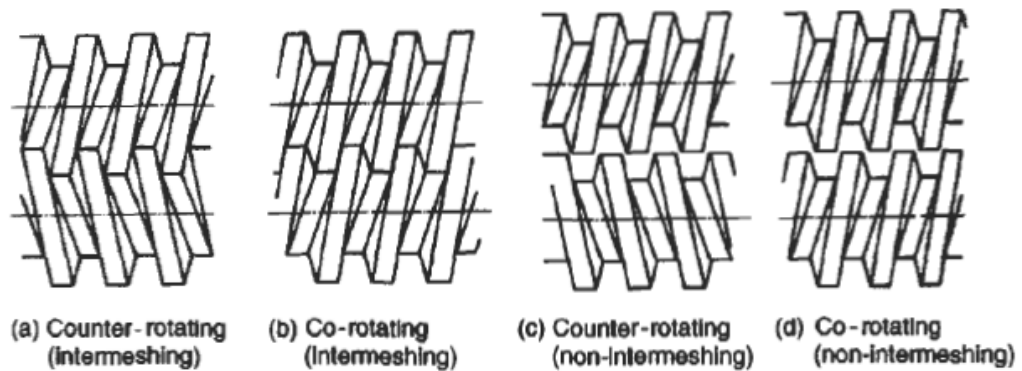


Figure 2.13 Different types of screw configurations for twin-screw extruders [52]

As seen from the figure, the non-intermeshing screws have space between the flights of the screws used generally for the reactive extruders. The intermeshing screws are conjugated to transfer the polymer from one to the other to improve mixing effect during conveyance [50]. Figure 2.14 shows the screw configurations for twin screw extruders.

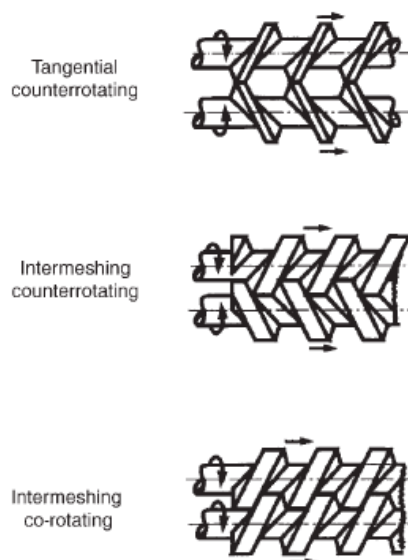


Figure 2.14 Screw configurations for twin screw extruders [53].

Co-rotating twin-screw extruders are generally preferred to produce nanocomposites. The extrusion process parameters such as, feed rate, screw speed, temperature and pressure of the die are monitored and controlled with the control panel on the cabinet. Figure 2.15 the co-rotating twin-screw extruder used in nanocomposite production during this study.

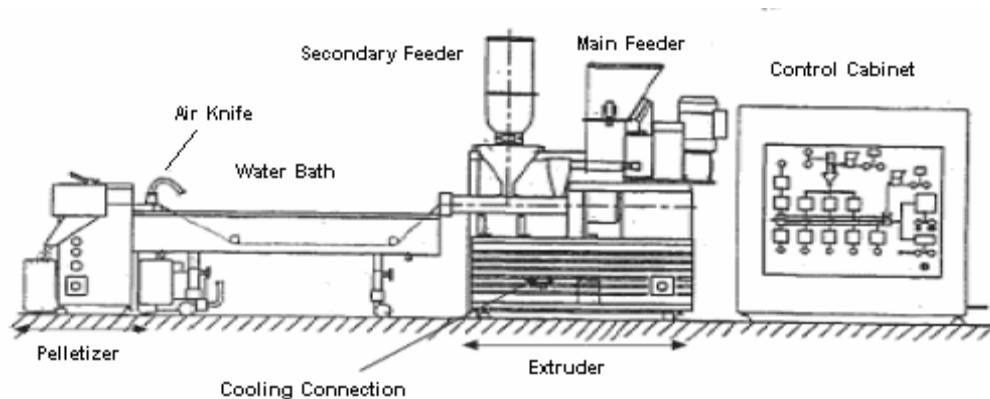


Figure 2.15 Co-rotating twin-screw extruder used in nanocomposite production in this study [47].

2.5.2 Injection Molding

Injection molding is a common process for especially thermoplastics which is simply described in four stages; melting, injecting into the mold, cooling the mold and removing the part from the mold. Injection molding is a batch process, whereas extrusion is continuous. Cycle time, temperature and pressure, which are the main process parameters, are controlled with very complex control systems. The injection molding machines and the molds are very expensive due to the control system and the pressure needed for injection [54].

Melting and the injection are carried by a screw through a nozzle like extrusion, cooling and the final shape is obtained in the mold. Decreasing the cycle time is

preferred due to economical reasons. The temperature of the melt, and the temperature and the shape of the mold determine the cycle time. The temperature of the melt is directly related to the polymer properties. In order to decrease the cycle time mold temperature is kept as low as possible, however, crystallization on the surface may occur which is generally not desired. Injection is done as fast as possible to decrease the cycle time and not to have pre-crystallization in the mold, especially if the parts are complicated [55].

2.6 Characterization of Nanocomposites

In order to evaluate the properties of nanocomposites, different test methods are carried out, such as; tensile and impact tests for mechanical properties, differential scanning calorimetry (DSC) for thermal properties, X-ray diffraction (XRD) analysis and scanning electron microscopy (SEM) for morphological properties.

2.6.1 Mechanical Properties

The structure of the polymer, determined by the bonds in the chain and the interactions between the chains, determines the mechanical behavior of a polymer under applied forces such as tension, shear, torsion, compression and bending. The results of these tests are very important for the applications of a polymer [28].

2.6.1.1 Tensile Test

Tensile test is done to predict how the material will react under forces in opposite direction until it fails. During the test the elongation of the sample is recorded against the force applied. The shape of the sample is like a dog bone to ensure that the rupture takes place in the middle and it is called the gage section. The grips used for holding the sample are shown in Figure 2.16 [56].

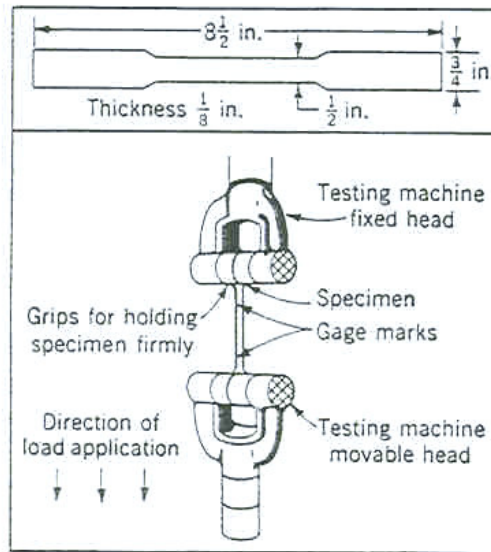


Figure 2.16 Tensile test machine and dog bone shaped specimen [57].

The specimen is clamped by holders and pulled by the movable head with increasing tensile load while the strain or elongation rate is constant during the test. According to the mechanical properties of the material, the test results may vary with the ambient temperature, thus it is better to do quality control tests at the temperature of use [28].

The strength of the material and the modulus of elasticity are determined from the stress-strain curve plotted during the test. Engineering stress and strain are calculated with the equations, respectively;

$$\sigma = F / A_0 \quad [2.1]$$

$$\epsilon = \Delta L / L_0 \quad [2.2]$$

where, σ is the engineering stress (MPa), F is the load at any time as a function of elongation (N), A_0 is the original cross sectional area of the gage section (mm^2), ϵ is the engineering strain, ΔL is the change in length (mm) and L_0 is the initial gage length (mm) [56].

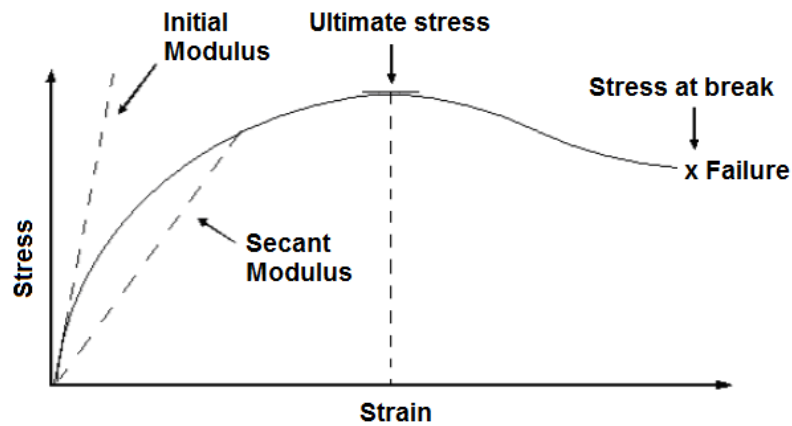


Figure 2.17 Idealized stress-strain curve for a polymer that undergoes ductile failure [58].

The ratio of stress to strain where the load is proportional to the strain is the modulus of elasticity (E) or Young's Modulus which is the deformation resistance of the material expressed in MPa. The area under the curve represents the toughness and is the work for deformation in units of energy per unit volume. The deformation is called elastic, if it is recoverable after removing the load, thus the elastic region of the curve extends up to a specific load. With a high modulus (σ / ϵ), the material is hard since the elastic region of the curve is very narrow due to the slope of the curve [57]. Typical behaviors of polymers under load are shown in Figure 2.18.

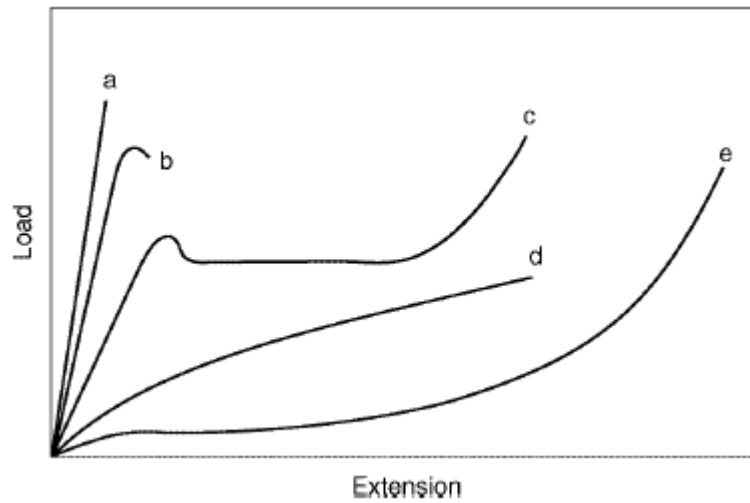


Figure 2.18 Stress–strain curves at various temperatures (increasing from a to e): (a) low extensibility followed by brittle fracture; (b) localized yielding followed by fracture; (c) necking and cold drawing; (d) homogeneous deformation with indistinct yield; (e) rubber-like behavior [28].

2.6.1.2 Impact Test

Impact test is another method of evaluating the toughness. The energy required to fracture the sample is the impact resistance of a material. The test is performed with the machines designed to apply high loads, in two types; Izod or Charpy, according to the geometry of the support as shown in Figure 2.19 [28].

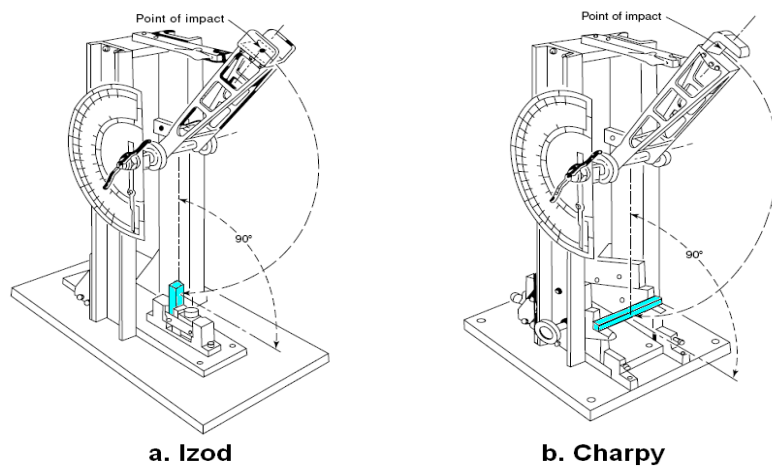


Figure 2.19 Charpy and Izod impact tests [28].

The specimen is often notched for both tests to promote fracture and have a standard weak point to break. The main difference of the tests is the support point of the specimen. Results are generally reported in J/m^2 or kJ/m^2 .

2.6.2 Thermal Analysis

In order to determine the thermal properties of nanocomposites, thermal analysis such as differential scanning calorimetry (DSC), differential thermal analysis (DTA), thermogravimetry (TG), thermomechanical analysis (TMA), dynamic mechanical analysis (DMA) methods are applied. In this study, DSC analysis was applied to determine crystallinity and the melting temperature of the polymer.

2.6.2.1 Differential Scanning Calorimetry (DSC)

Differential Scanning Calorimetry, DSC, analysis is to measure the required heat to increase the temperature of a small amount of sample and a reference which are kept at the same temperature, at the same time as shown in Figure 2.20 [59]. At the point of phase transformation such as thermal transition the sample and the reference is kept at the same and constant temperature by giving more heat or giving

less heat by the power supply. More or less heat during thermal transition is directed by the process if it is endothermic or exothermic. The temperature and the power are recorded and plotted throughout the experiment to have a DSC curve [60].

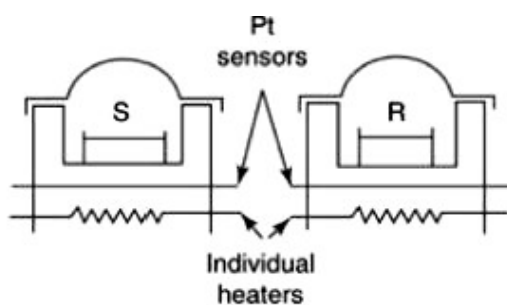


Figure 2.20 Power compensated differential scanning calorimeter [28].

With the DSC curve as shown in Figure 2.21 (T_g), melting temperature (T_m), crystallization temperature (T_c) and heat of fusion of polymers which is the area under the curve (ΔH_f) are determined. If the heat of fusion of 100 % crystalline polymer is known, then the % crystallinity of the sample is obtained by using the measured heat of fusion [59].

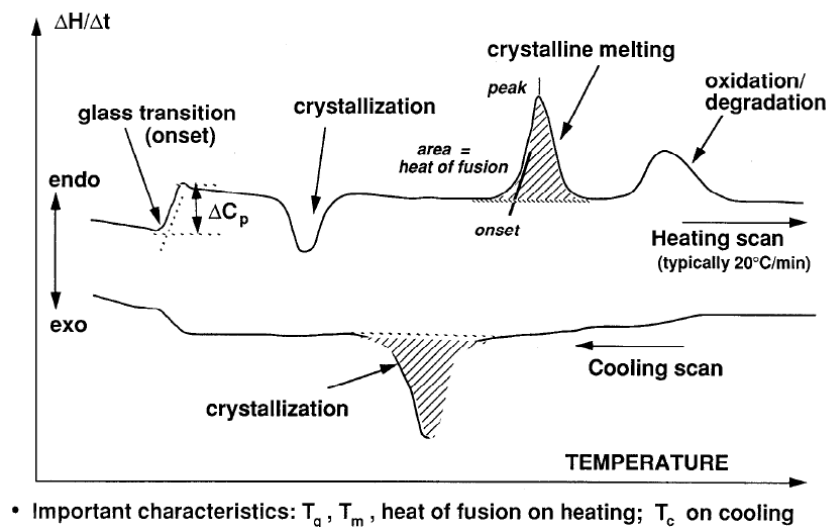


Figure 2.21 Typical DSC curves [59].

Since the molecular motions increase during transition the heat capacity of the material also increases. So, T_g is detected from shift on the endothermic side of the curve, as well as T_m which is the sudden phase change, is detected by a peak on the curve [61].

2.6.3 Morphological Analysis

2.6.3.1 X-Ray Diffraction (XRD) Analysis

X-Ray Diffraction, XRD, analysis is applied to the crystalline substances since 1912 to obtain information about the crystallographic structure, physical properties, and chemical composition of the materials. There are two types of X-ray scattering; wide angle X-Ray scattering (diffraction) (WAXS) and small angle X-ray scattering (SAXS). The crystallinity is analyzed by WAXS and structural analysis is done by SAXS [57].

X-Rays having very short wavelengths are diffracted by the crystalline phases. The wavelength of the x-rays for the polymer studies are typically 0.1 – 0.2 nm. The waves are scattered from the structure at an angle depending on the structure and

the length within the structure. If the structures are regular or periodic so are the angles, then the scattering is called diffraction [62].

The regular reflection of x-rays from parallel planes according to Bragg's law is recorded by the diffractometer. The manipulated intensity of the diffracted beams versus angular position in terms of 2θ is plotted [63]. The spacing between the planes is calculated with Bragg's equation;

$$n\lambda = 2d \sin\theta \quad [2.3]$$

where, λ is the wavelength of the radiation, d is the distance between the parallel planes in the crystal, θ is the angle between the x-ray beam and the plane, and n is the order of diffraction [64].

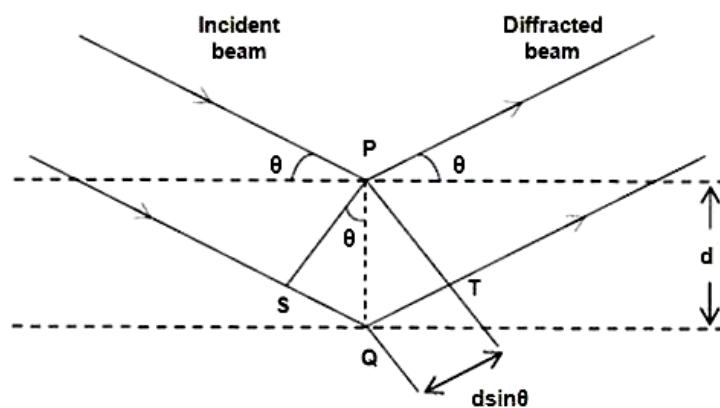


Figure 2.22 Diffraction of X-Rays [6].

With peaks in the XRD plots, d -spacing can be determined. Increase in d -spacing will lead to shift to lower angles of the clay peak which represents intercalated structure, whereas no peak will be observed in exfoliated systems.

2.6.3.2 Scanning Electron Microscopy (SEM)

Scanning electron microscopy, SEM, is a qualitative analysis for the surface and surface morphology in 3D images with magnification up to 50000 times. The synchronized scanning of electron beams on the sample, which is generally coated with a thin layer of gold or silver to have conductivity, and the cathode ray tube (CRT) gives the three dimensional images on screen as shown in Figure 2.23. The magnification is adjusted first and the image is adjusted with the CRT according to detected scattered electrons [65].

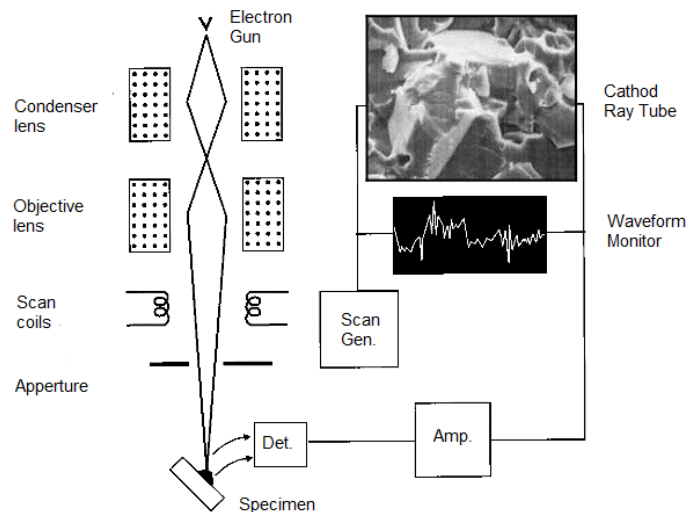


Figure 2.23 Schematic diagram representing the main components of a scanning electron microscope [65].

2.7 Previous Studies

Deshmane et al. [66] studied the effects of same clay loadings on the properties of the nanocomposites with polypropylene and polyethylene. 4 % clay loading improved the impact strength of polypropylene based nanocomposites, whereas the behavior polyethylene based nanocomposites was the opposite. Tensile properties of both

were improved but the improvement for polypropylene was higher. The different results for PP and PE caused by the different interactions of the polymers with clay, resulting in different structural characteristics, such as crystallization and glass transition temperature, increased intergallery spacing and decreased spherulite size.

Zhang et al. [67] used a twin screw extruder to prepare PP-MMT nanocomposites with MAPP compatibilizer. XRD and TEM analysis were performed during the study. At low clay content, high dispersion of the silicate layers and highly improved impact properties were observed, while tensile properties were the same compared to conventionally filled PP nanocomposites.

Thon-That et al. [68] prepared three different types of organoclay nanocomposites in a twin screw extruder. Two grades of MAPP and two different methods of processes were investigated. The presence of coupling agent improved the degree of intercalation. Organoclay, having high thermal stability, and MAPP coupling agent with high molecular weight, enhanced tensile and impact properties. Mixing procedures did not alter the results significantly.

Kim et al. [15] investigated the structures and properties of melt blended nanocomposites composed of thermoplastic polyolefin, organoclay and MAPP with respect to MAPP to organoclay ratio. As MAPP to organoclay ratio was increased tensile properties were enhanced. Increasing clay stacks, at fixed ratio of MAPP, resulted in improvement of percolation networks caused by physical interaction of clay particles.

Lertwimolnum et al. [69] prepared nanocomposites in a twin screw extruder with MAPP compatibilizer to investigate the effects of the compatibilizer and processing conditions on nanoclay dispersion. With MAPP degree of dispersion was improved and clay aggregates were smaller for increased loading of MAPP. It was observed that increasing shear stress and mixing time, and decreasing mixing temperature enhanced exfoliation and increases the yield stress.

Modesti et al. [35] reported the mechanical properties of polypropylene based nanocomposites with MAPP compatibilizer and organoclay in which the process conditions were changed. The process conditions at low temperature and high screw

speed enhanced tensile properties. Excluding the effect of the process conditions, addition of compatibilizer and organoclay already improved tensile properties, and exfoliation of clay platelets was only achieved only when MAPP compatibilizer was present.

In the following study of Modesti et al. [70], thermal properties of melt blended nanocomposites were reported. The process condition had significant effect only on the mechanical properties. Thermal stability, crystallinity and flammability behavior were affected mainly by the composition of the nanocomposites, and improvement was observed with MMT and MAPP.

Deenadayalan et al. [107] studied the effect of the compatibilizers such as, MAPP and maleic anhydride grafted polyethylene (MAPE), on the mechanical properties of PP nanocomposites. MAPP improved the modulus and strength due to the well dispersion of clay particles but decreased the ductility, whereas the use of MAPE resulted in opposite results.

Zhu et al. [71] investigated the effects of mixing procedures and screw configurations and reported the effects on dispersion. Pre-mixing of clay and MAPP was compared with the concurrent processing of the components. Since residence time was increased, pre-mixing has shown better exfoliation of nanocomposites.

In the previous study in this SAN-TEZ 00112.STZ.2007-1 project which is completed by Filiz Cengiz [23], in order to improve the mechanical properties of a recycled grade of polypropylene, the effects of additive concentrations, types of organoclays and compatibilizers, processing conditions, and the compatibilizer to organoclay ratio, on the morphology and mechanical, thermal and flow properties were investigated. Cloisite® 15A, Cloisite® 25A and Cloisite® 30B were used as organoclays, and ethylene-methyl acrylate-glycidyl methacrylate and maleic anhydride grafted polypropylene were used as compatibilizers in the production of the nanocomposites by melt compounding method. Mechanical properties were improved significantly at low temperatures and high screw speeds. More effective dispersion of organoclay and improved tensile properties were obtained as the MAPP to clay ratio was increased.

CHAPTER 3

EXPERIMENTAL

3.1 Materials

3.1.1 Polymer Matrix

The polymer matrix used in the study was a heterophasic copolymer “MOPLEN EP300L” and it was purchased from LyondellBasell Company, Holland at 25 kg polyethylene bags. For simplicity MOPLEN EP300L is abbreviated as EP300L in the thesis and the material properties are shown in Table 3.1.

Table 3.1 Properties of MOPLen EP300L (EP300L) Polymer matrix

Characteristics	Unit	Value	Test Method
Physical Properties			
Density	g/cm ³	0.905	ISO 1183
Melt Flow Index (230°C; 2,16 kg)	g/10 min	6	ISO 1133
Mechanical Properties			
Young's Modulus (at 23°C)	MPa	1434	ISO 527 (15 mm/min)
Notched Charpy Impact Strength (at 23°C)	kJ/m ²	11.9	ISO179
Ball Indentation Hardness	MPa	53	ISO 2039-1
Thermal Properties			
Distortion temperature under load (load=0.45 MPa)	°C	77	ISO 75B-1,-2
Vicat softening temperature(50 N)	°C	151	ISO 306

3.1.2 Organoclays

In this study, two types of layered silicates were used; Nanofil® 8 and Nanofil® 5. They were purchased from Southern Clay Products, Texas, USA and used as reinforcing agents. They are natural off-white montmorillonites produced by a cation exchange reaction with different organic modifiers. The tallow (long alkyl chain) structures in both type of the clays are constituted of primarily 18 carbon chains (~65 %) and the rest of the components are chains with 16 carbons (~30 %) and 14 carbons (~5 %).

3.1.2.1 Nanofill ® 8

Nanofill ® 8 (N8) is an organically modified, nanodispersible layered silicate based on a natural bentonite, and the surface treatment of the clay is a dimethyl, di(hydrogenated tallow)alkyl quaternary ammonium salt. According to information supplied by the production company, the clay has high hydrophobicity. The chemical

structure of the modifier is shown in Figure 3.1 and the properties are shown in Table 3.2.

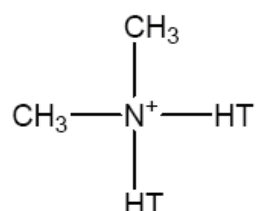


Figure 3.1 Chemical structure of Nanofill ® 8.

Table 3.2 Properties of Nanofill ® 8 [72].

Properties	Unit	Value
Modifier Content	meq/100g clay	125
Interlayer spacing	nm	3.5
Moisture Content	%	1.6
Weight Loss on Ignition	%	43
Bulk Density	g/l	270
Typical Dry Particle Sizes		
50%	μ, by volume	5

3.1.2.2 Nanofill ® 5

Nanofill ® 5(N5) is an organically modified, nanodispersible layered silicate based on a natural bentonite, and the surface treatment of the clay is a dimethyl, di(hydrogenated tallow) alkyl quaternary ammonium salt. According to information

supplied by the production company, this clay has a lower hydrophobicity than Nanofill ® 8. The chemical structure of the modifier is shown in Figure 3.2 and the properties are shown in Table 3.3. The main differences between the two organoclays are the modifier content and d-spacing. Nanofill ® 8 has a higher modifier content and d-spacing than Nanofill ® 5.

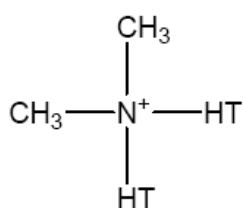


Figure 3.2 Chemical structure of Nanofill ® 5.

Table 3.3 Properties of Nanofill ® 5 [72].

Properties	Unit	Value
Modifier Content	meq/100g clay	93
Interlayer spacing	nm	2.8
Moisture Content	%	1.3
Weight Loss on Ignition	%	38
Bulk Density	g/l	270
Typical Dry Particle Sizes		
50%	μ, by volume	8

3.1.3 Compatibilizers

In this study, Bondyram® 1001, a Maleic Anhydride Modified Polypropylene (M) was used as compatibilizing agent. It was purchased from EMAŞ Plastik, Bursa, Turkey. The polar character of the anhydride causes an affinity for the silicate surface of the clays. Chemical structure of Bondyram® 1001 is shown in Figure 3.3 and material properties are given in Table 3.4.

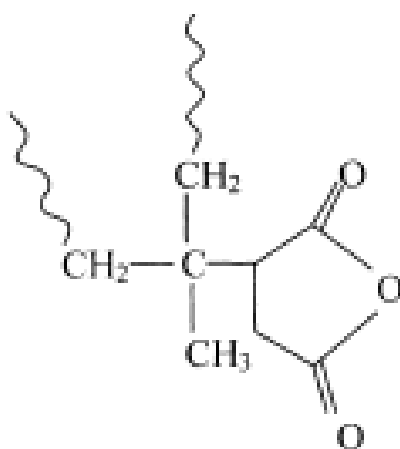


Figure 3.3 Chemical structure of maleic anhydride grafted polypropylene.

Table 3.4 Characteristics of Bondyram® 1001 [73].

Properties	Unit	Value	Test Method
Melt Index (190°C, 2.16Kg)	g/10 min	100	ASTM D-1238
Maleic Anhydride content	%	1	FTIR
Young's Modulus	MPa	991	ISO 527
Tensile Strength	MPa	32	ISO 527
Elongation at Break	%	506	ISO 527
Density	g/cm ³	0.90	ASTM D-792
Melting temperature	°C	160	DSC

3.2 Preparation of Nanocomposites

Nanocomposites having different compositions of polypropylene matrix, clay and compatibilizer were prepared by melt compounding method by extrusion, and then were injection molded for analysis. The very first step of the production process was drying of all the materials. The materials were dried at proper temperatures and under vacuum conditions before beginning the production of the nanocomposites. The drying temperatures are shown in Table 3.5.

Table 3.5 Drying conditions.

Materials	Drying Temperature (°C)	Duration (h)
Before 1st Extrusion		
Organoclays	80	12-16
Compatibilizer	40	12-16
Before 2nd Extrusion		
Polypropylene Matrix	100	4
Organoclay+ Compatibilizer (Masterbatch)	40	4
Before Injection Molding		
Products	100	12-16

Melt compounding method was conducted with a co-rotating, fully intermeshing twin screw extruder; Thermoprism TSE 16 TC (D=16 mm, L=384 mm). Thermoprism TSE 16 TC has maximum 12 Nm torque capability and 500 rpm maximum screw speed. Barrel temperatures were set to 180 °C during the study by using the temperature controllers on the control panel of the extruder. Figure 3.4 shows the extruder used in the experiments during the study.



Figure 3.4 Thermoprism TSE 16 TC twin-screw extruder.

During extrusion, polymer matrix and compatibilizer were fed from the main feeder; and clays were fed from the side feeder. Total feeding rate of the materials was set to 25 g/min and kept constant during the study. Materials were melt and mixed at 180 °C and 350 rpm screw speed in the extruder. The processing parameters are shown in Figure 3.5. The molten product was cooled by passing through a water bath, and the wet product was dried by an air knife after the water bath, and then the product was pelletized.

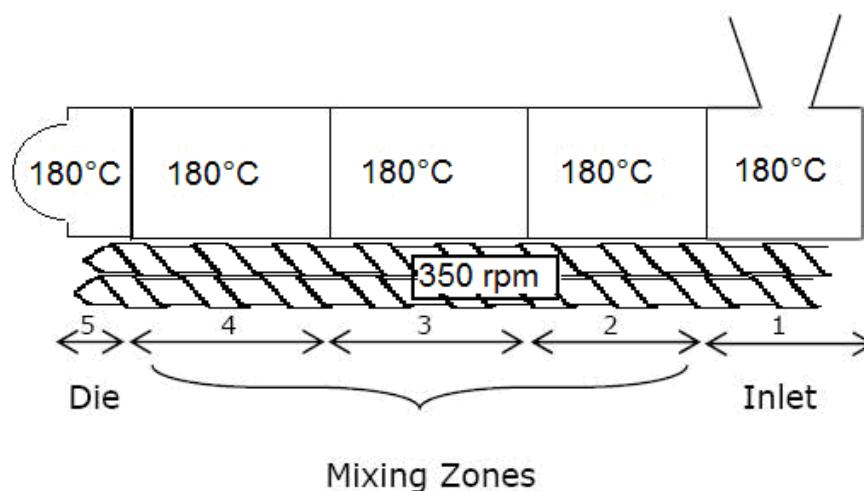


Figure 3.5 Schematic diagram of processing parameters; barrel temperature and screw speed.

In the previous study of Cengiz F. [23]; experiments were done under several processing conditions. When the screw speed was increased to 350 rpm and the barrel temperature was 180 °C, i.e. with low temperature and high screw speed, improvements on nanocomposite mechanical properties were maximized. High screw speed decreases the residence time, and with low temperature the diffusive effect decreases and the melt viscosity increases. On the other hand, the shear stress exerted on the polymer and silicate layer during the extrusion, reaches a level that compensates the effects of low temperature [23]. It is stated in the literature that, in order to obtain exfoliated structures, the shear stress should be sufficient to overcome the electrostatic forces between silicate layers. It is also reported that low temperature profile, high screw speed and high polymer viscosity are recommended for enhanced mixing properties [35, 74, 75]. Experimental steps of the preparation of ternary nanocomposites are shown schematically in Figure 3.6. In order to investigate the effects of adding compatibilizer or organoclay as a third component, binary blends of polypropylene-compatibilizer polypropylene -organoclay were also prepared.

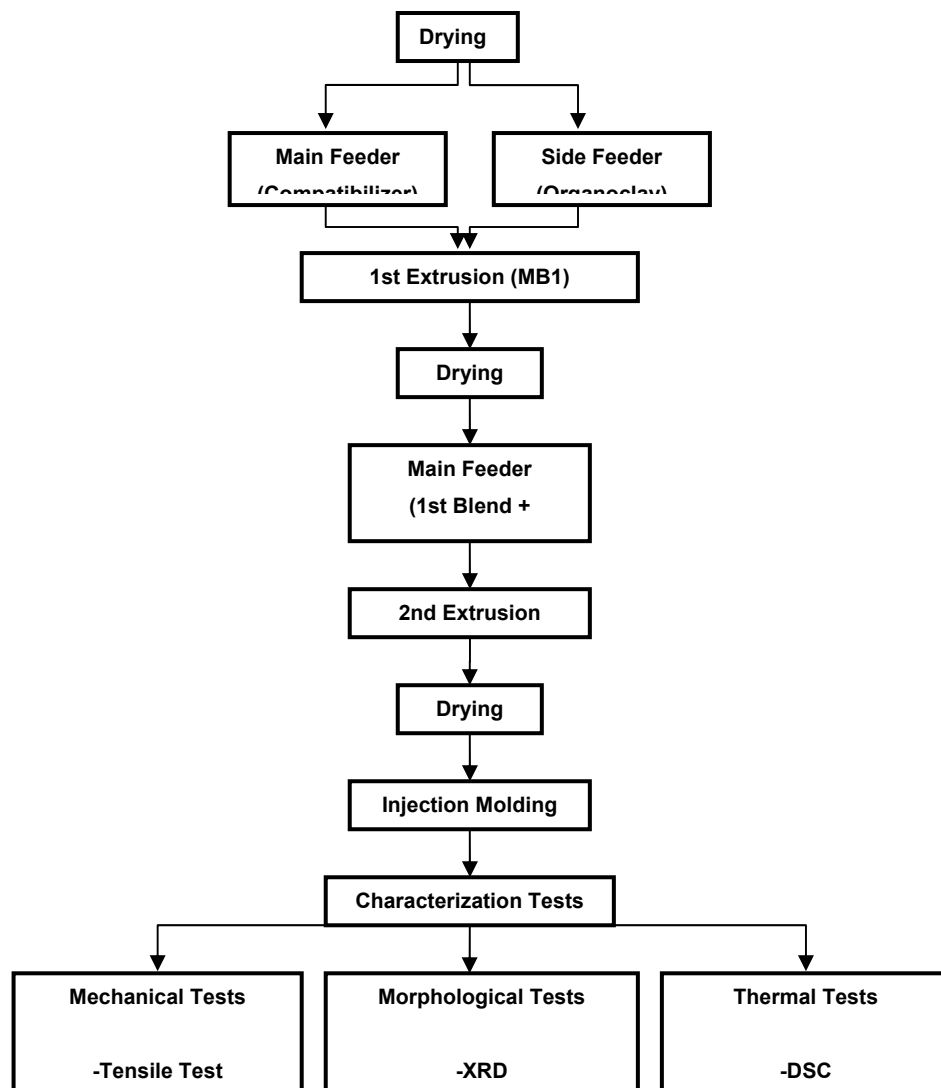


Figure 3.6 Flow chart for nanocomposite production and characterization.

The aim of extruding organoclay and compatibilizer simultaneously in the first extrusion is to increase the reaction between the clay and the compatibilizer and provide expansion in interlayer spacings of organoclay particulates in order to obtain enhanced polymer intercalation in the second extrusion.

In the first extrusion of organoclay and compatibilizer (MB1); the organoclay was fed to the extruder from the side feeder and the compatibilizer was fed from the main feeder. In the second extrusion; after the drying step, polypropylene and first mixture that resulted from were dry blended and fed to the extruder from the main feeder to obtain ternary nanocomposites. Nanocomposite compositions prepared in this study are given in Table 3.6 and Table 3.7.

Table 3.6 Binary composite compositions prepared in experiments.

Binary composites		
EP300L + 2 % Compatibilizer (M)	EP300L + % 2 M (2M)	
EP300L + 6 % Compatibilizer (M)	EP300L + % 6 M (6M)	
	Nanofil 5 (N5)	Nanofil 8 (N8)
EP300L + 1 % Organoclay	EP300L + 1% N5 (1N5)	EP300L + 1% N8 (1N8)
EP300L + 8 % Organoclay	EP300L + 8% N5 (8N5)	EP300L + 8% N8 (8N8)

Table 3.7 Ternary composite compositions prepared in experiments.

Ternary Nanocomposites		
	Nanofil 5 (N5)	Nanofil 8 (N8)
EP300L + 8 % Compatibilizer (M) + Organoclay	EP300L+8% M+1%N5 (8M1N5)	-
	EP300L+8% M+2% N5 (8M2N5)	-
	EP300L+8% M+3% N5 (8M3N5)	-
	EP300L+8% M+4% N5 (8M4N5)	-
EP300L + 6 % Compatibilizer (M) + Organoclay	EP300L+6% M+1% N5 (6M1N5)	EP300L+6% M+1% N8 (6M1N8)
	EP300L+6% M+2% N5 (6M2N5)	EP300L+6% M+2% N8 (6M2N8)
	EP300L+6% M+3% N5 (6M3N5)	-
	EP300L+6% M+4% N5 (6M4N5)	-
EP300L + 4 % Compatibilizer (M) + Organoclay	EP300L+4% M+1% N5 (4M1N5)	EP300L+4% M+1% N8 (4M1N8)
	EP300L+4% M+2% N5 (4M2N5)	EP300L+4% M+2% N8 (4M2N8)
	EP300L+4% M+3% N5 (4M3N5)	-
	EP300L+4% M+4% N5 (4M4N5)	-
EP300L + 3 % Compatibilizer (M) + Organoclay	EP300L+3% M+1% N5 (3M1N5)	EP300L+2% M+1% N8 (3M1N8)
	EP300L+3% M+2% N5 (3M2N5)	EP300L+2% M+2% N8 (3M2N8)
	EP300L+3% M+3% N5 (3M3N5)	-
	EP300L+3% M+4% N5 (3M4N5)	-
EP300L + 2 % Compatibilizer (M) + Organoclay	EP300L+2% M+1% N5 (2M1N5)	EP300L+1% M+1% N8 (2M1N8)
	EP300L+2% M+2% N5 (2M2N5)	EP300L+1% M+2% N8 (2M2N8)
	EP300L+2% M+3% N5 (2M3N5)	-
	EP300L+2% M+4% N5 (2M4N5)	-

3.2.1 Injection Molding

The nanocomposite samples for analysis were made by injection molding with DSM Xplore (laboratory scale of 10 cc) micro injection molding equipment, as shown in Figure 3.7. The melt and mold temperatures were set to 220°C and 30°C respectively for all the experiments. Hold time for melting of the polymer was 3 minutes and 30 seconds, including the feeding time of 10 seconds. Molding cycle of the injection machine had three steps; filling step (pressure: 10 bar, duration: 5 seconds), packing in order to offset shrinkage (15 bar, 10 seconds), cooling step (no pressure, 10 seconds). After cooling step, specimens were taken out at 30 °C temperature. Specimens were conditioned at room temperature for 24 hours before conducting the characterization tests. Molding parameters are shown in Table 3.8.



Figure 3.7 Injection molding equipment.

Table 3.8 Injection molding parameters.

Molding Parameters	
Nozzle temperature	220 °C
Mold temperature	30 °C
Hold time	3.5 min
Injection pressure	15 bar

3.3 Characterization

3.3.1 Morphological Testing Procedure and Equipment

In order to determine the basal spacings of the organoclay layers and dispersion of the clay particles in the polymer matrix; X-ray Diffraction (XRD) analyses were done. Also, in order to see the surface morphologies, failure mechanisms and phase structures of the composites, Scanning electron Microscopy (SEM) photographs were taken from the fracture surface of the specimens in impact tests. Specimens used in morphological tests are shown in Figure 3.8.

3.3.1.1 X-Ray Diffraction Analysis

The samples were analyzed by Rigaku D/Max-2200/PC X-Ray diffractometer with monochromatic Cu K α radiation source ($\lambda = 1.5418$) at 40 kV and 40 mA. Diffraction angle 2θ was scanned from 1° to 8° at a scan rate of $1^\circ/\text{min}$ with a step size of 0.01° . Peak positions were used to calculate the d-spacings of organoclay layers by using Bragg's Law. Molded, dog bone shaped tensile bars were used in XRD analysis.

3.3.1.2 Scanning Electron Microscopy (SEM) Analysis

SEM micrographs were taken with a JEOL JSM-6400 low voltage scanning electron microscope after gold coating of the samples. Average domain was calculated by Image J program.

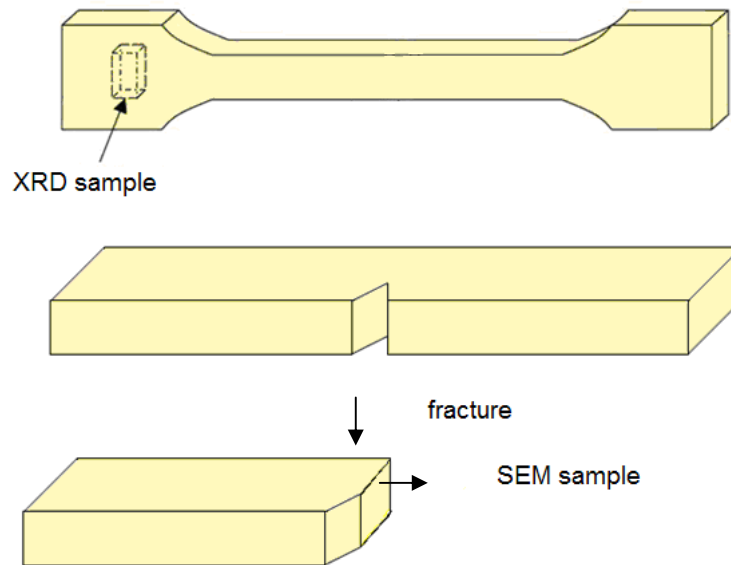


Figure 3.8 Specimens used in morphological analysis.

3.3.2 Mechanical Properties

In this study, mechanical tests were done to determine the tensile strength, tensile stress at yield, Young's Modulus, elongation at break (%) and impact strength. Effects of clay type and composition on composite performance could easily be detected by mechanical testing. The tensile test results show the stiffness of the materials, while impact test gives information about the impact toughness. The improvements of the mechanical properties of the materials are expected to be a reflection of the degree of dispersion of the organoclays and compatibility of the compatibilizer with the polymer matrix.

All mechanical tests were conducted at $23^{\circ}\text{C} \pm 2^{\circ}\text{C}$, and at least five specimens were tested for each set of experiment. After injection molding, specimens were left for 24 h in desiccators for slow cooling and completion of crystallization. Tensile test specimens were molded according to ISO 527-5A and impact test specimens were molded according to ISO 179 standards. Test results reported are the average results of five specimens. The standard deviations for each set are also shown on the figures.

3.3.2.1 Tensile Test

Tensile tests were performed by Lloyd 30K universal testing machine according to ISO 527 [76]. The dimensions of the specimens are shown in Figure 3.9 and tabulated in Table 3.9. The strain rate applied was 0.5 min^{-1} (Crosshead speed: 15 mm/min, gauge length of the specimen: 30 mm). At the end of the test, stress-strain curve of the sample was obtained and the tensile stress, tensile strength, elongation at break (%) and Young's Modulus values were calculated from the stress-strain curve.

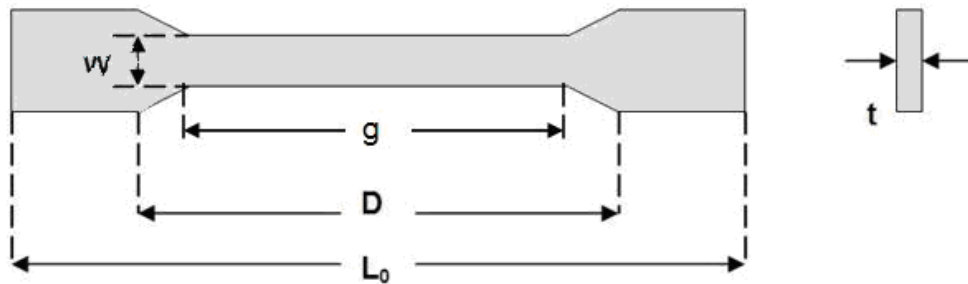


Figure 3.9 Tensile test specimen.

Table 3.9 Dimensions of the tensile test specimens.

Symbol	Definition	Value (mm)
W	Width of narrow section	4
D	Distance between grips	50
L₀	Overall length	75
g	Gauge Length	30
t	Thickness	>2

3.3.2.2 Impact Test

Charpy impact tests were performed by a pendulum Ceast Resil Impactor to one side notched specimens according to the ISO 179 standards [77] at room temperature. The dimensions of the specimens are shown in Figure 3.10 and tabulated in Table 3.10.

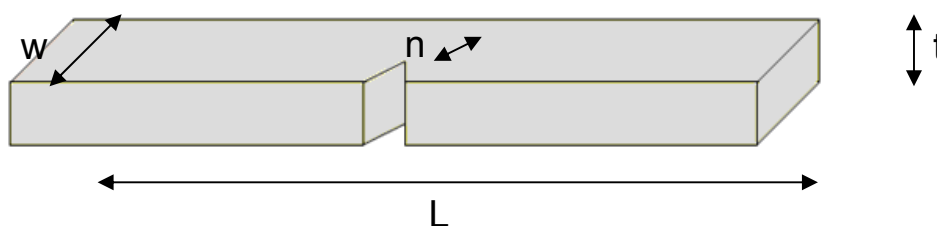


Figure 3.10 Impact test specimen.

Table 3.10 Dimensions of impact test specimens.

Symbol	Definition	Value (mm)
L	Total length	80
w	Unnotched width	10
n	Notch length (v type, 45°)	2
t	Thickness	4

3.3.3 Thermal Analysis

In order to determine the melting and crystallinity behaviors of the nanocomposites, Differential scanning calorimetry (DSC) analyses were done.

3.3.3.1 Differential Scanning Calorimetry (DSC) Analysis

In order to evaluate the deviations in melting point (T_m) and percent crystallinity value due to the addition of organoclay and compatibilizer, Differential scanning calorimetry (DSC) measurements were carried out under nitrogen atmosphere with DSC-60 Shimadzu differential scanning calorimeter. Samples weighing 3-4 mg were cut from the middle of the molded dog bone specimens. Samples were placed in aluminum pans and heated from room temperature to 250 °C at a rate of 5 °C/min.

Percent crystallinity values were calculated using the heat of fusion and the weight fraction of the polymer matrix of the specimen and the heat of fusion of 100 % crystalline polypropylene for EP300L polymer matrix. The proportion of the heat of fusion (ΔH_f) values of the specimens divided by the weight fraction of EP300L (w) in the nanocomposite and the heat of fusion of the pure crystalline form of the PP (ΔH_f^0) gives the percent crystallinity. Heat of fusion value of 100% crystalline PP was taken as 209 J/g [78].

CHAPTER 4

RESULTS AND DISCUSSION

4.1. Morphological Analysis

In order to examine the morphological structure of nanocomposites XRD and SEM analyses were done.

4.1.2 X-RAY Diffraction Analysis

X-ray diffraction is a simple, useful and widely used characterization technique for determination of clay dispersibility. By monitoring the reflections from the silicate layers in the clay, regarding to their periodic arrangement and repetitive multilayer structure, intercalation of the clay can be examined [19, 21].

Intensity versus 2θ values graphs were obtained after XRD analysis, and interlayer spacings were calculated by using Bragg's Law. Intercalation of the polymer chains is indicated by the shift of the diffraction peak towards lower angles in the XRD graphs (a shift to left in the graph) [19]. On the other hand, the disappearance of the d_1 peak indicates exfoliated structure in nanocomposites due to disordered silicate layers [19, 22, and 79]. As the amount of intercalated clay decreases, the intensity of the peak decreases; implying breakdown of the platelet agglomerates or partial exfoliation. There is also a possibility of intermediate structures which may have the characteristics of both intercalated and exfoliated morphologies. If in the XRD analysis the intensity is decreased and the diffraction peak is broadened, then in this case the structure is partially exfoliated or delaminated [19].

Figure 4.1 shows the X-Ray Diffraction pattern of the polymer matrix used (EP300L) and d-spacing values are given in Table 4.1. As it seen from the pattern, there is no diffraction peak observed in 1-8 2θ ($^{\circ}$) range.

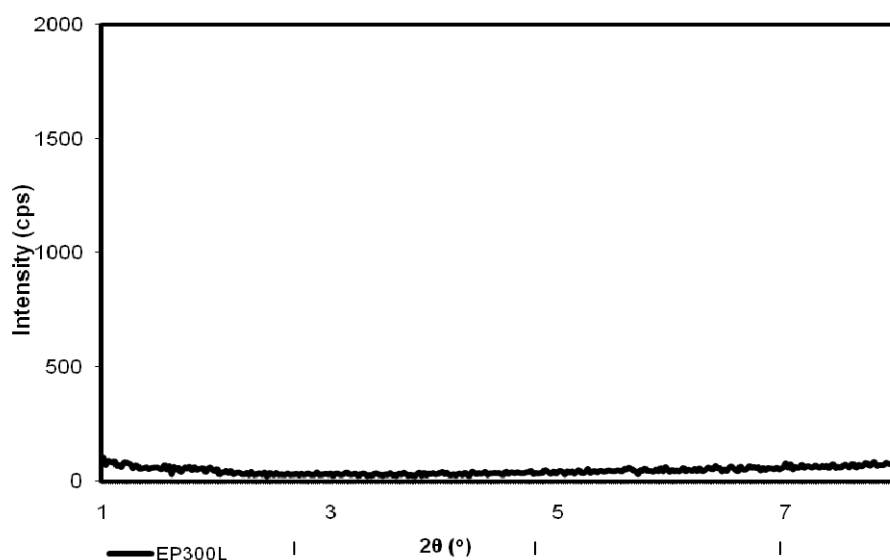


Figure 4.1 X-Ray Diffraction pattern of EP300L

XRD of organoclays Nanofil[®] 5(N5) and Nanofil[®] 8(N8) in powder form are shown in Figures 4.2 - 4.3 and Table 4.1. N5 has two diffraction peaks and N8 has three diffraction peaks which are consistent with the data provided by their producer. The first basal reflections exists at $2\theta=2.79^{\circ}$ ($d_1=31.6 \text{ \AA}$) for N5 and $2\theta=2.59^{\circ}$ ($d_1=34.1 \text{ \AA}$) for N8; representing the characteristic peaks of the organoclay silicate layers. The intercalation and exfoliation of the nanocomposites were determined by analyzing the changes in these characteristic diffraction peaks.

If d_2 is twice d_1 , it may have resulted from secondary reflections. Also appearance of a second peak may result from the existence of another silicate layer or as a consequence of the presence of unmodified natural MMT due to improper modification [80-82]. In Nanofil[®] 5 d_2 is due to unmodified MMT, since the main peak in natural(unmodified) MMT is observed at approximately 12 \AA .

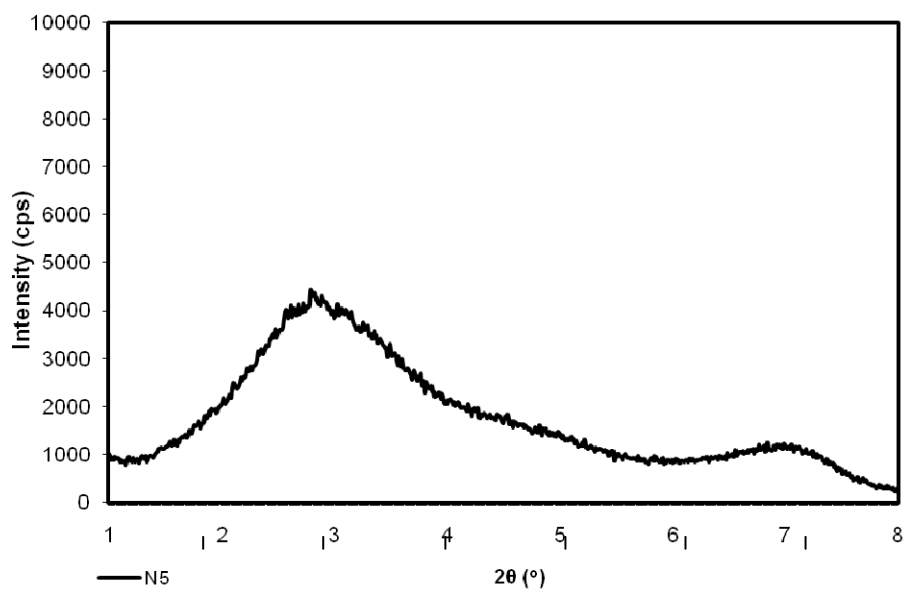


Figure 4.2 XRD pattern of Nanofill © 5 (N5) in powder form.

In N8 organoclay, the second peak may have resulted from some inorganic cations of the smectite clay that are not fully replaced by organic ions after modification in the clay. The third peak in N8 is due to unmodified MMT clay layers, since it occurs at 12 Å.

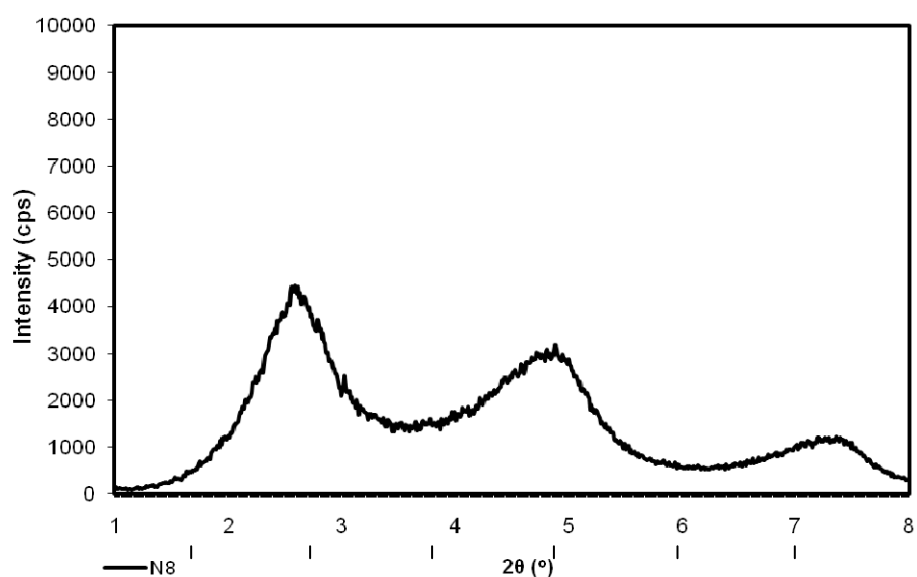


Figure 4.3 XRD pattern of Nanofill ® 8 (N8) in powder form.

Table 4.1 XRD results of EP300L, N5 and N8.

Sample	Peak-I		Peak-II		Peak-III	
	2θ (°)	d ₁ (Å)	2θ (°)	d ₂ (Å)	2θ (°)	d ₃ (Å)
Polymer Matrix						
EP300L	-	-	-	-	-	-
Organoclay						
N5	2.8	31.6	6.8	12.9	-	-
N8	2.6	34.1	4.9	18.1	7.36	12.0

4.1.2.1 Effects of Compatibilizer

Polypropylene is a non polar and highly hydrophobic polymer that makes diffusion of polypropylene macromolecules between silicate layers difficult due to thermodynamic restrictions [34, 67]. In order to promote intercalation between MMT and polypropylene, usually compatibilizers are added and high shear and dispersive

forces are applied during compounding [40, 41]. In this study Bondyram® 1001(Maleic Anhydride Modified Polypropylene (M)) was added in different compositions as the compatibilizer.

In order to determine the effects of the compatibilizer, binary composites of EP300L and Nanofill ® 5, having 1wt% and 8wt% clay loading, were analyzed. Figure 4.4 shows the XRD diagrams of the binary composites. The basal spacing d_1 of the composites were increased from 31.6 Å to 32.93 Å and 33.05 Å respectively. The degree of intercalation was not significant. But these results, which are obtained in the absence of the compatibilizer, indicate that although the polymer and clay are incompatible, presence of sufficient shear and adequate residence time, resulted in some intercalation of the polymer at these clay loadings [83]. The second peak would be due to the intercalation of the unmodified silicate layers that had d_1 12.9 Å before compounding.

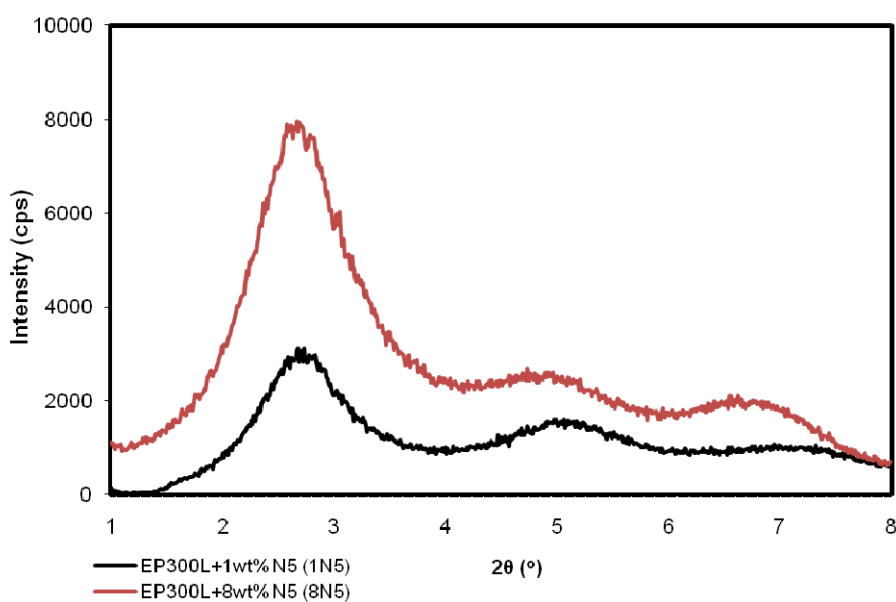


Figure 4.4 XRD patterns of binary composites of N5.

Figure 4.5 shows the effects of different compatibilizer loadings in 1 wt % N5 organoclay loaded nanocomposites. All the XRD data are also summarized in Table 4.2. Adding Bondyram® 1001 (Maleic Anhydride Modified Polypropylene) (M) as a compatibilizer increased d_1 values up to 35.87 Å at 3 wt % compatibilizer loading, when compared with 1 wt% N5 loaded binary composite (with no compatibilizer). There were significant reductions in the intensity of peak amplitudes at 3 and 6 wt% compatibilizer loadings. When binary composite and ternary composite observations are considered together, the results indicate that M acted as a compatibilizer and resulted in the intercalation of polymer chains inside the organoclay interlayer, and there are partially delaminated layers of Nanofill ® 5 in the polymer matrix.

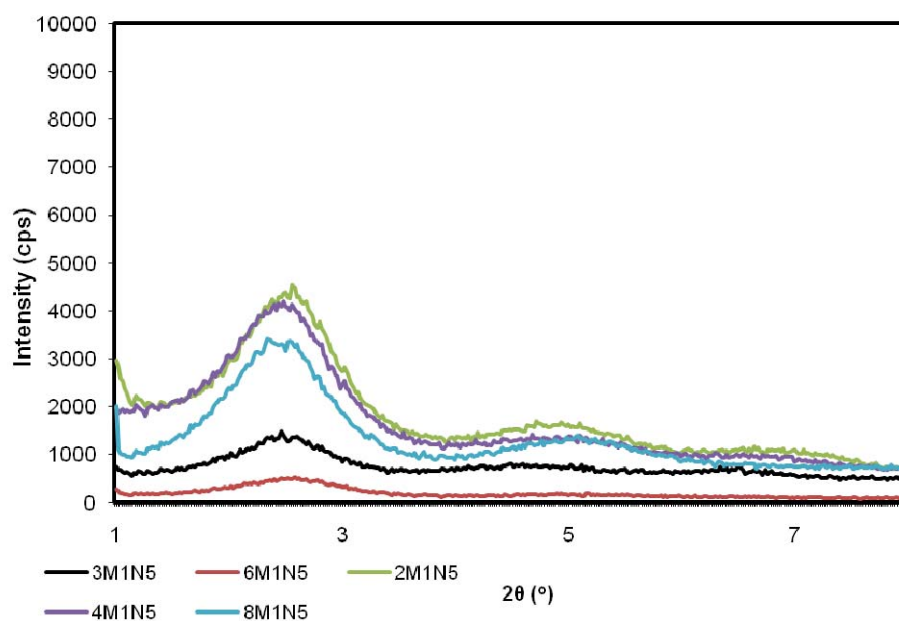


Figure 4.5 XRD patterns of ternary composites with 2wt%, 3wt%, 4wt%, 6wt% and 8wt% compatibilizer M and 1wt% clay loadings.

Since the d-spacing value of the 8wt% compatibilizer loaded nanocomposite was lower than those of 2wt%, 3wt%, 4wt% and 6 wt% compatibilizer loaded composites, increasing the weight fraction of the compatibilizer more than 6 wt% did not

significantly contribute to further expansion of the galleries. Polypropylene has no polar groups in its structure, but on the other hand, even if the hydrophilic clay surfaces are modified with long alkyl groups, they may remain polar, and non polar polyolefins cannot enter the clay galleries without the compatibilizing agent. The balance between the polarities of the organoclay surface and the polymer matrix can be accomplished by an interaction between the polar group of the compatibilizer and the oxygen group of the silicates. So, resulting polarity could be the reason of compatibilization effect [84].

Table 4.2 XRD results of binary and ternary nanocomposites with N5.

Sample	Peak-I		Peak-II		Peak-III	
	2 θ (°)	d ₁ (Å)	2 θ (°)	d ₂ (Å)	2 θ (°)	d ₃ (Å)
N5	2.8	31.6	-	-	6.8	12.9
1N5	2.68	32.93	4.99	17.69	6.95	12.70
8N5	2.67	33.05	4.74	18.62	6.80	12.98
2M1N5	2.56	34.47	4.72	18.70	6.64	13.30
3M1N5	2.46	35.87	4.50	19.61	6.52	13.54
4M1N5	2.48	35.58	4.68	18.86	6.30	14.01
6M1N5	2.58	34.20	5.16	17.11	6.42	13.75
8M1N5	2.59	34.07	5.16	17.11	-	-
2M2N5	2.56	34.47	4.76	18.54	7.36	12.00
3M2N5	2.56	34.47	3.94	22.40	6.56	13.46
4M2N5	2.64	35.89	4.68	18.86	6.56	13.46
6M2N5	2.53	34.88	4.80	18.39	6.68	13.22
8M2N5	2.55	34.61	4.88	18.09	-	-
2M3N5	2.56	34.47	4.48	19.70	6.62	13.34
3M3N5	2.56	34.47	3.06	28.84	6.50	13.58
4M3N5	2.58	34.20	4.64	19.02	6.96	13.69
6M3N5	2.60	33.94	4.90	18.01	6.64	13.30
8M3N5	2.61	33.81	4.90	18.01	-	-
2M4N5	2.60	33.94	4.64	19.02	6.72	13.14
3M4N5	2.68	32.93	3.52	25.07	6.60	13.38
4M4N5	2.60	33.94	4.42	19.97	6.58	13.42
6M4N5	2.78	31.74	5.12	17.24	6.66	13.26
8M4N5	2.80	31.52	5.13	17.21	6.84	12.91

In the presence of M, the driving force for intercalation is the strong hydrogen bonding between MAH (or carboxyl group in the case of the hydrolysis of MAH group) and the oxygen groups of the silicates on the organoclay surface [11, 46]. Owing to compounding compatibilizer M and organoclay first in the MB method, the interactions between silicate layers were initially weakened, and hence the polymer chains were more easily intercalated into the clay galleries under strong shear field [39]. Compatibilizer M has both polar MAH group and nonpolar polypropylene moiety combined in its structure bridging the gap between MMT and polymer [85]. Moreover, the polar character of the anhydride in the M has caused an affinity for the silicate surface [15]. So, as the proportion of maleic anhydride was increased, a stronger affinity would be formed on the silicates layers and separate them more easily during compounding. Since there was no phase separation observed, matrix and filler interaction was also promoted by the miscibility of EP300L in the M structure. Figures 4.6 to 4.8 show the X-Ray Diffraction patterns of the ternary composites. The corresponding d-spacings are given in Table 4.2.

According to the Table 4.2 and Figures 4.6 to 4.8, shifting of the second peak of the organoclay to lower angles was observed. This change was more remarkable with increasing compatibilizer addition. This shift may have resulted from the intercalation of the polymer chains between the unmodified silicate layers owing to the compatibilization effect and breakage of large clay agglomerates into small tactoids under applied shear at low temperature and high screw speed.

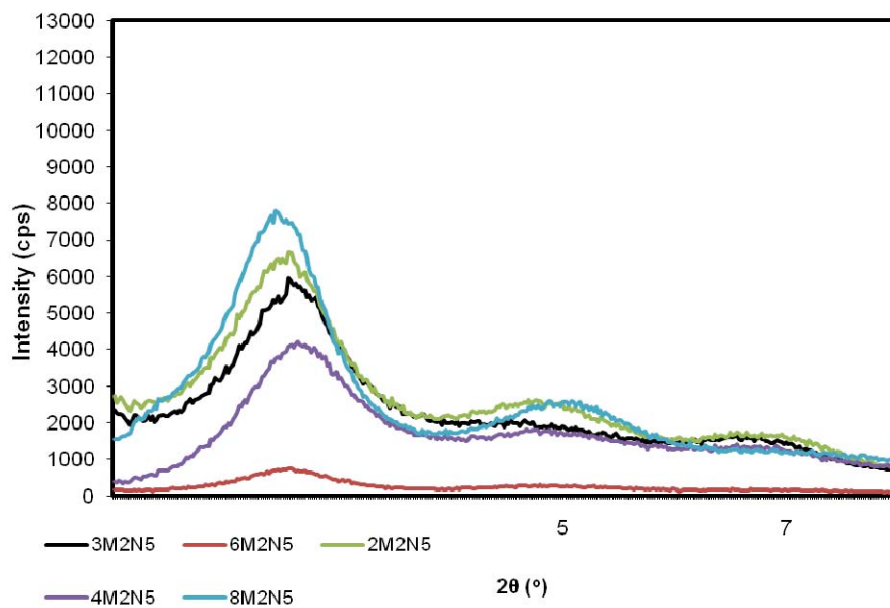


Figure 4.6 XRD patterns of ternary composites with 2wt%, 3wt%, 4wt%, 6wt% and 8wt% compatibilizer M and 2wt% clay loadings.

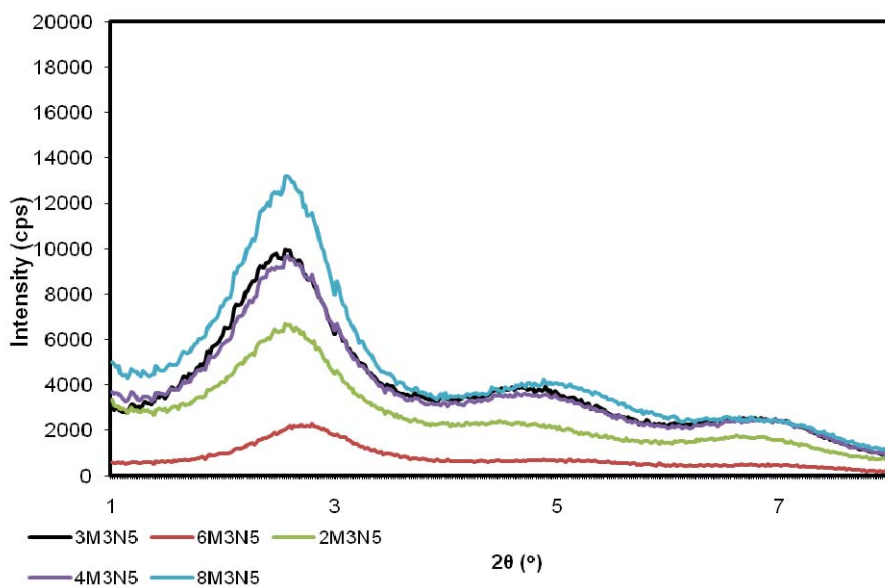


Figure 4.7 XRD patterns of ternary composites with 2wt%, 3wt%, 4wt%, 6wt% and 8wt% compatibilizer M and 3wt% clay loadings.

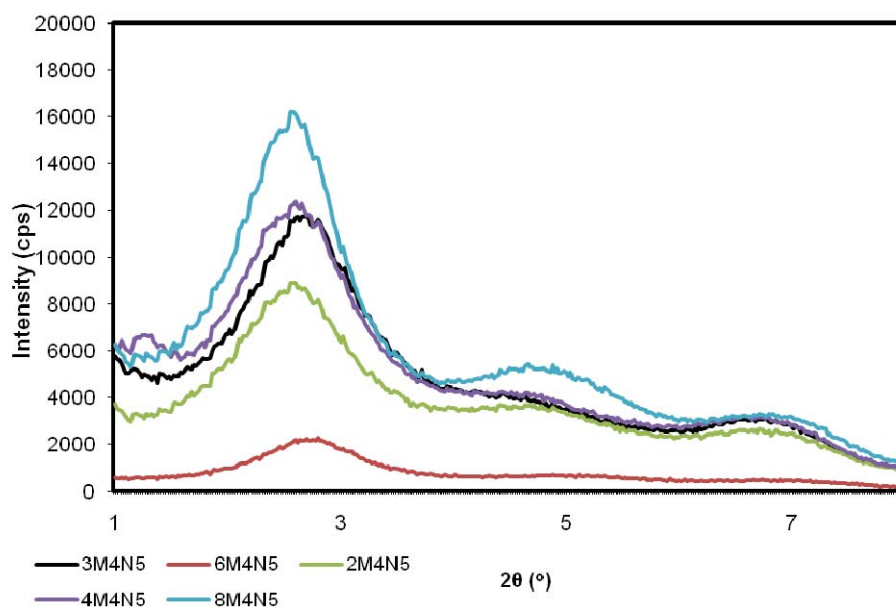


Figure 4.8 XRD patterns of ternary composites with 2wt%, 3wt%, 4wt%, 6wt% and 8wt% compatibilizer M and 4wt% clay loadings.

Moreover, it was also observed in Figures 4.5 to 4.8 that, 6 wt% compatibilizer loaded nanocomposites have XRD patterns with lower intensity and broadened peaks. This reduction was more significant for the nanocomposites prepared with lower organoclay loadings (1wt% and 2wt%, Figures 4.5 and 4.6 respectively) indicating the formation of a delaminated structure.

4.1.2.2 Effects of Clay Content

Figures 4.9 to 4.13 show the X-Ray Diffraction patterns of ternary composites prepared with Nanofil® 5 (N5) from 1wt% to 4 wt% and compatibilizer with 2wt%, 3wt%, 4wt%, 6wt% and 8wt% compositions, i.e. the previous data are shown with respect to clay content at fixed compatibilizer loading. These data are already shown in Table 4.2. When the clay content was higher than 2wt%, diffraction peaks shifted to higher angles with increasing peak intensity, in the binary mixtures of polypropylene and Nanofil® 5.

Following the surface treatment of organoclays attractions between the particles are rendered and the interlayer galleries are expanded, but there are other factors affecting the polymer intercalation mechanism such as chemical compatibility, polarity and dispersive forces, etc. [34]. Nanofil® 5 does not have any functional groups in its modified structure, so dispersive forces, which are applied during compounding, are more effective in delamination of the organoclay. The shear stress applied by the matrix polymer could not overcome the cohesive forces between the clay platelets when the clay loading was higher than a certain concentration (2 wt% for this study). In this case, silicate layers only break down to large agglomerates [74].

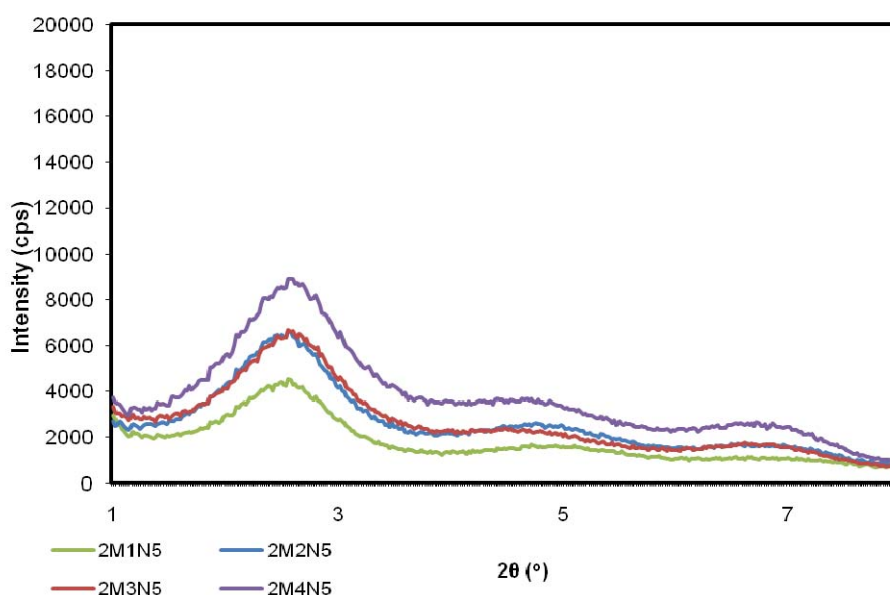


Figure 4.9 XRD patterns of ternary composites with 1wt%, 2wt%, 3wt% and 4wt% clay and 2wt% compatibilizer loadings.

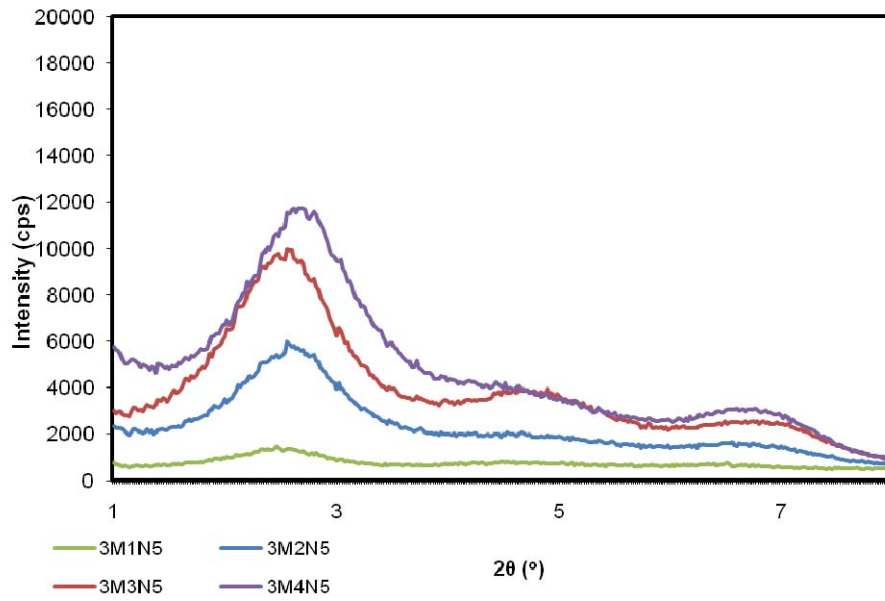


Figure 4.10 XRD patterns of ternary composites with 1 wt%, 2 wt%, 3 wt% and 4 wt% clay and 3wt% compatibilizer loadings.

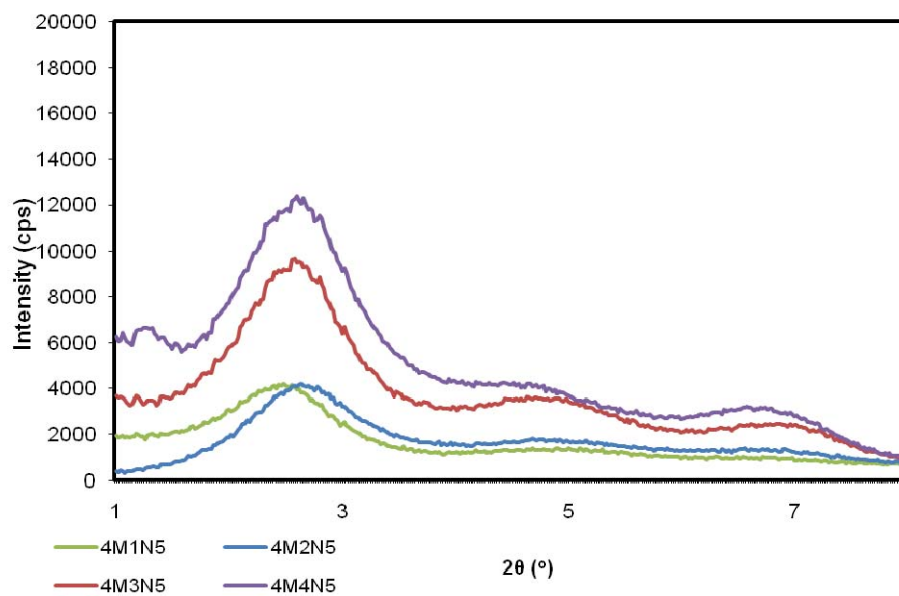


Figure 4.11 XRD patterns of ternary composites with 1 wt%, 2 wt%, 3 wt% and 4 wt% clay and 4wt% compatibilizer loadings.

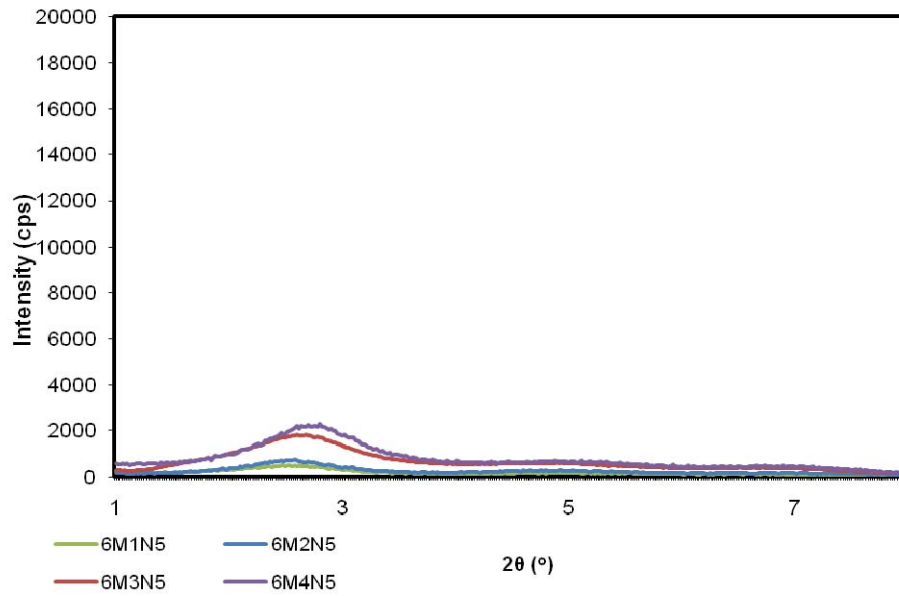


Figure 4.12 XRD patterns of ternary composites with 1 wt%, 2 wt%, 3 wt% and 4 wt% clay and 6wt% compatibilizer loadings.

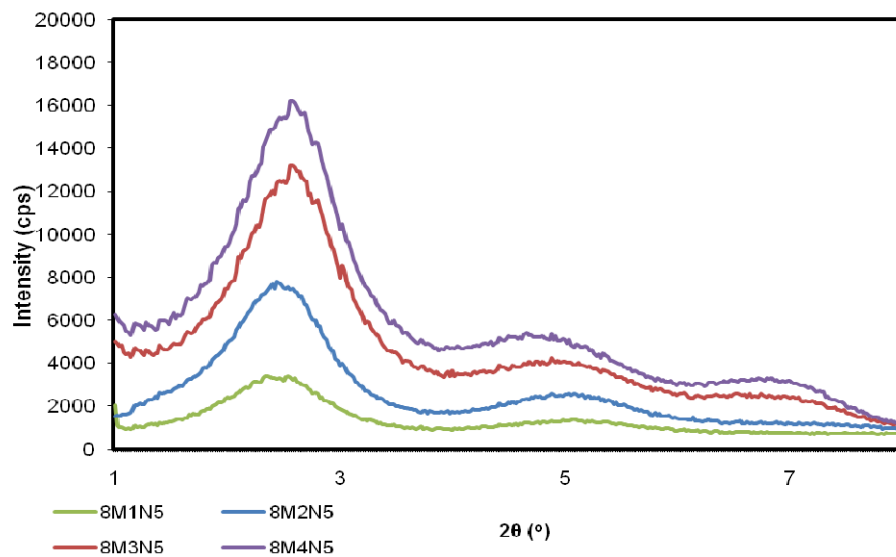


Figure 4.13 XRD patterns of ternary composites with 1 wt%, 2 wt%, 3 wt% and 4 wt% clay and 8wt% compatibilizer loadings.

The decrease in d-spacing values of the composites having more than 2 wt% clay loading observed in Figures 4.9 to 4.13, could be also a consequence of collapsed clay sheet due to displacement of ammonium compounds during thermal and mechanical treatment [86].

The most significant reduction in intensity and broadening of the peaks with increase in the basal spacing was observed in 6 wt% compatibilizer loaded composites indicating intercalated-delaminated structure formation. The positive effect of compatibilization was also observed in these nanocomposites even with high clay loadings (3 wt% and 4 wt %) but still with poor intercalation. As a result of these patterns, clay contents above 2 wt% were found to be ineffective.

4.1.2.3 Effects of Clay Type

Effects of different clay types were investigated in the last part of the study. XRD patterns of the nanocomposites, which were prepared with Nanofill® 5 and Nanofill® 8, were compared. In this part of the study, the clay content was limited up to 2 wt% and the compatibilizer content was limited up to 6 wt% since additive content higher than these were found to be nonproductive in the previous experiments.

In Figure 4.14, XRD diagram of binary nanocomposites of Nanofill® 8 and EP300L polymer matrix are shown exhibiting three distinct diffraction peaks, and it was observed that the characteristic peak of Nanofill® 8 was shifted to lower angles at low clay loadings even in the absence of the compatibilizer. All of the XRD data with N8 are shown in Table 4.3. At high clay loadings a decrease in d-spacing values were observed compared to pure clay powder, which could be a consequence of collapsed clay layers due to displacement of ammonium compounds during thermal and mechanical treatment [86]. In the diagrams, three distinct diffraction peaks were observable.

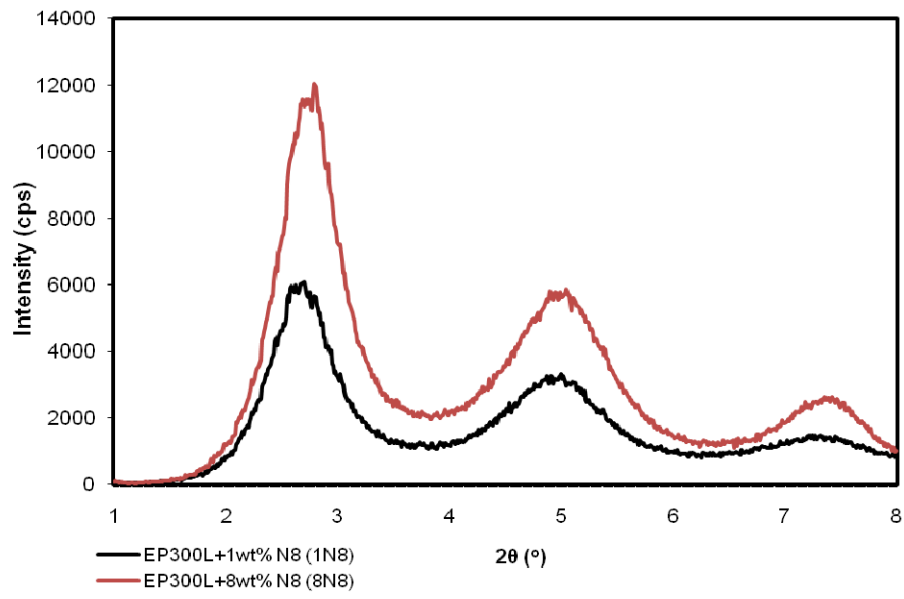


Figure 4.14 XRD patterns of binary composites prepared with Nanofill® 8.

Table 4.3 XRD results, effects of clay type with N8.

Sample	Peak-I		Peak-II		Peak-III	
	2 θ (°)	d ₁ (Å)	2 θ (°)	d ₂ (Å)	2 θ (°)	d ₃ (Å)
Organoclay						
N8	2.59	34.1	4.9	18.1	7.36	12.0
Binary nanocomposites						
1N8	2.58	34.20	5.0	17.65	7.32	12.06
8N8	2.79	31.63	5.05	17.48	7.36	12.0
Ternary nanocomposites						
2M1N8	2.34	37.71	4.44	19.88	6.54	13.50
2M2N8	2.44	36.16	4.64	19.02	6.88	12.83
3M1N8	2.32	38.04	4.42	19.97	6.50	13.58
3M2N8	2.46	35.87	4.58	19.27	6.62	13.34
4M1N8	2.34	37.71	4.50	19.61	6.36	13.88
4M2N8	2.44	36.16	4.64	19.02	6.68	13.22
6M1N8	2.36	37.39	4.54	19.44	6.50	13.58
6M2N8	2.33	37.87	4.52	19.53	6.63	13.32

Figures 4.15 and 4.16 show the XRD pattern of the ternary composites with N8 and the results are already given in Table 4.3. XRD diagrams of ternary composites prepared with Nanofill® 8 and compatibilizer M reveal that the characteristic peak of the organoclay was shifted to lower angles indicating intercalated structure. However, partial delamination was not observed since, the peak intensities did not decrease or the peaks did not broaden.

When the two organoclays are compared it is observed that, Nanofill® 5 based nanocomposites exhibit mostly intercalated-delaminated structure, while Nanofill® 8 based nanocomposites are mostly intercalated. Nanofill® 8 has a higher initial d-spacing than Nanofill® 5, and when the structures are compared it is observed that, Nanofill® 8 and Nanofill® 5 both contain two long tallow chains. These two aliphatic chains in the organoclay structure would be limiting the entrance of PP macromolecules to the silicate surface. Two long tails create a shielding effect

between MMT and polymer resulting in mostly intercalated structures rather than delaminated [87].

The modifier content of Nanofill® 5 and Nanofill® 8 are given as, 93 meq/100 g clay and 125 meq/100 g clay respectively. The long aliphatic chains may also act as a shield for the polar groups on the silicate surface, covering the oxygen and hydroxyl groups on the silicates. As the modifier content increases, polar groups which may interact with the MAH group on the compatibilizer would be covered, thus the interactions between MMT and MAH would be decreased. This could be the reason for obtaining intercalated-delaminated structure with N5 and intercalated structure with N8.

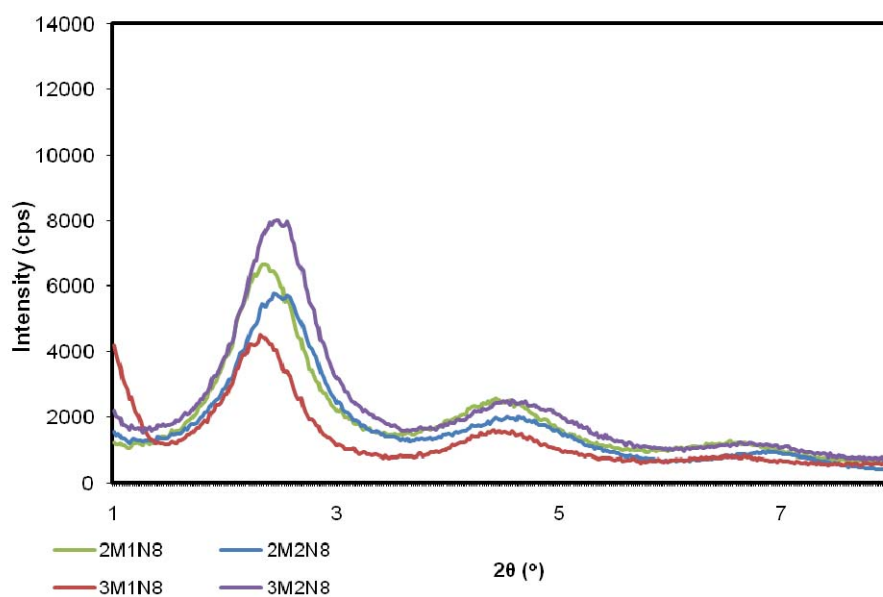


Figure 4.15 XRD patterns of ternary nanocomposites with different Nanofill® 8 and low compatibilizer loadings.

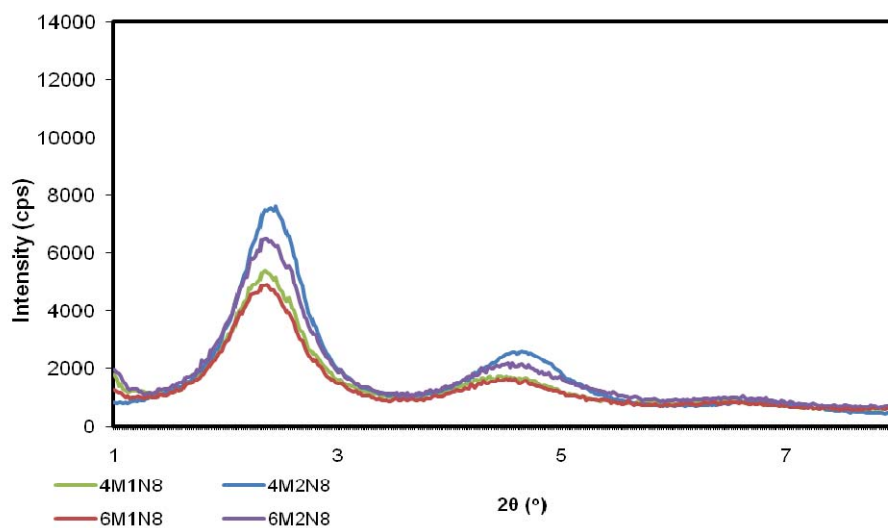


Figure 4.16 XRD patterns of ternary nanocomposites with different Nanofill® 8 and high compatibilizer loadings.

In conclusion, excess amount of clay loading (above 2wt % in this case), diminished the intercalation mechanism even in the presence of compatibilizer. High affinity of maleic anhydride content enhanced possible reactions between organoclay and compatibilizer and favored intercalation up to a certain content (6 wt% for this case). In addition to these, it was observed that the structure and accommodation of alkyl chains are more important than polarity or initial d spacing of an organoclay.

The method of production of the nanocomposites could be a reason for improved intercalation mechanism in nearly all of the compositions, since with masterbatch (MB) method expansion of silicate layers is achieved before the addition of polymer. In the MB mixing process, compatibilizer M chains penetrate into organoclay layer and react with silicate surfaces. Then, the matrix polymer can easily penetrate into these thick layers and form a broad interphase, thus polymer molecules can easily penetrate between the silicate layers [88].

4.1.3 Scanning Electron Microscopy Analysis (SEM)

In order to investigate the morphology of the composites and examine the dispersion of the organoclays and compatibilizers, SEM analysis was conducted. Dispersion of the organoclays and compatibilizers are important factors in toughening mechanisms. The base polymer EP300L is a heterophasic PP with elastomeric phase (elastomeric domains). Using Equation 4.1-4.2 and Image J program, average sizes of the elastomeric phase (size of the domains) in EP300L were calculated. For each calculation 100 to 200 domains were selected. The calculated number average area values were converted to number average diameters. In the Equation 4.1 N_i is the number of the domains selected with calculated area of A_i .

$$\bar{A} = \frac{\sum N_i A_i}{\sum N_i} \quad [4.1]$$

$$\bar{d} = \sqrt{\frac{4\bar{A}}{\pi}} \quad [4.2]$$

The morphological structure of once extruded EP300L polypropylene matrix was porous owing to its heterophasic copolymer structure, which is also confirmed by its producer. Figure 4.17 shows the SEM images EP300L that was extruded once. The surface morphologies of the nanocomposites are shown in Figures 4.17 to 4.22 and the domain sizes calculated are given in Table 4.4. The ternary composites analyzed by SEM were the ones having the most intercalated-delaminated structures according to XRD analysis. The samples analyzed were not etched since there was no significant change expected with etching.

Table 4.4 SEM results and the domain sizes of the heterophasic EP300L.

Components	\bar{d} (μ)
EP300L (extruded once)	1.14
Polymer Matrix- Compatibilizer Blends	
EP300L+ 2 wt% M (2M)	1.09
EP300L+ 6 wt% M (6M)	1.0
Polymer Matrix- Organoclay Blends	
EP300L+1 wt% N5 (1N5)	1.11
EP300L+8 wt% N5 (8N5)	1.05
EP300L+1 wt% N8 (1N8)	1.10
EP300L+8 wt% N8 (8N8)	1.01
Ternary Nanocomposites	
EP300L+ 1wt% N5+ 6wt% M (6M1N5)	0.99
EP300L+ 2wt% N5+ 6wt% M (6M2N5)	0.96
EP300L+ 4wt% N5+ 6wt% M (6M4N5)	0.98
EP300L+ 1wt% N8+ 3wt% M (3M1N8)	0.98

The mechanism of the formation of the domains can be explained as the stretching of the dispersed phases and then breaking down of the stretched fibers into the smaller droplets during blending. Finally, these droplets coalesce and form larger particles [89]. Due to the forced collisions of the dispersed domains with an input of energy, coalescence and recombination of the domains occur and new surfaces and interfaces form [90, 91].

The optimum domain size is achieved when the number of coalescence of the droplets and breakdown of the stretched fibers are balanced [92]. Domain sizes are controlled by the viscosity and melt elasticity of the components, shear stresses and rates, mobility of the interface and surface tension [89].

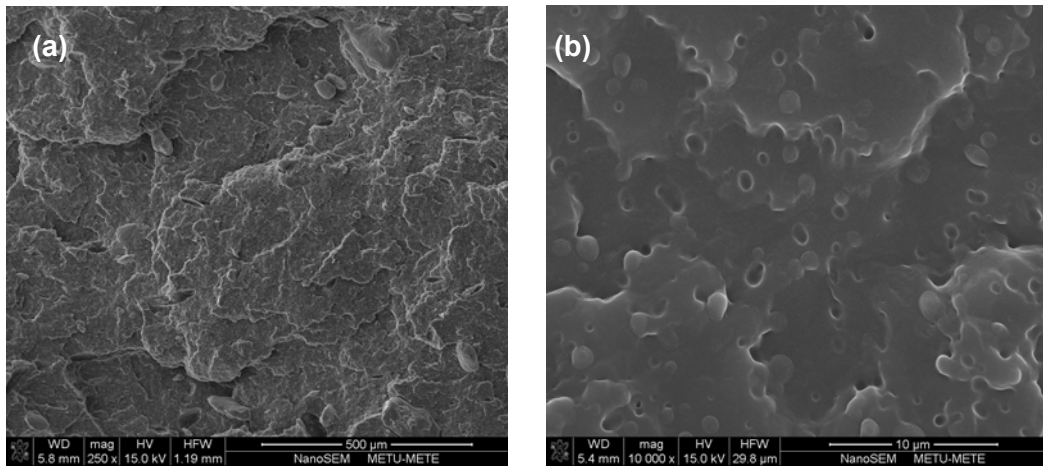


Figure 4.17 SEM micrographs of EP300L extruded once a) x250 b) x3000.

4.1.3.1 Effects of Clay Content

Figure 4.18 shows the binary mixtures of Nanofill® 5 and EP300L at different clay contents. The figures indicate that, increasing clay loading from 1 wt% to 8 wt% caused reduction in the size of the EP300L domains. During extrusion the breakage of domains into smaller sizes occurred, and on the other hand, by the barrier effect of the organoclay, recombination of the domains could be suppressed [42]. As the organoclay loading was increased the coalescence of the domains became more difficult and the domain sizes were smaller.

It is also observed in Figure 4.18 that, the crack lines go through the surface structure. The fracture surface of neat EP300L (Figure 4.17a) is more tortuous than the fracture surface of binary composites (Figure 4.18a and 4.18c). The roughness of the surface indicates that, in the binary composites cracks progressed along a less tortuous path which decreases the fracture surface area, toughness and tensile strength with respect to neat EP300L. SEM observations also show that, in binary composites clay particles were dispersed in the polymer matrix in the form of aggregates indicating the incompatibility of the matrix and the clay without the compatibilizer.

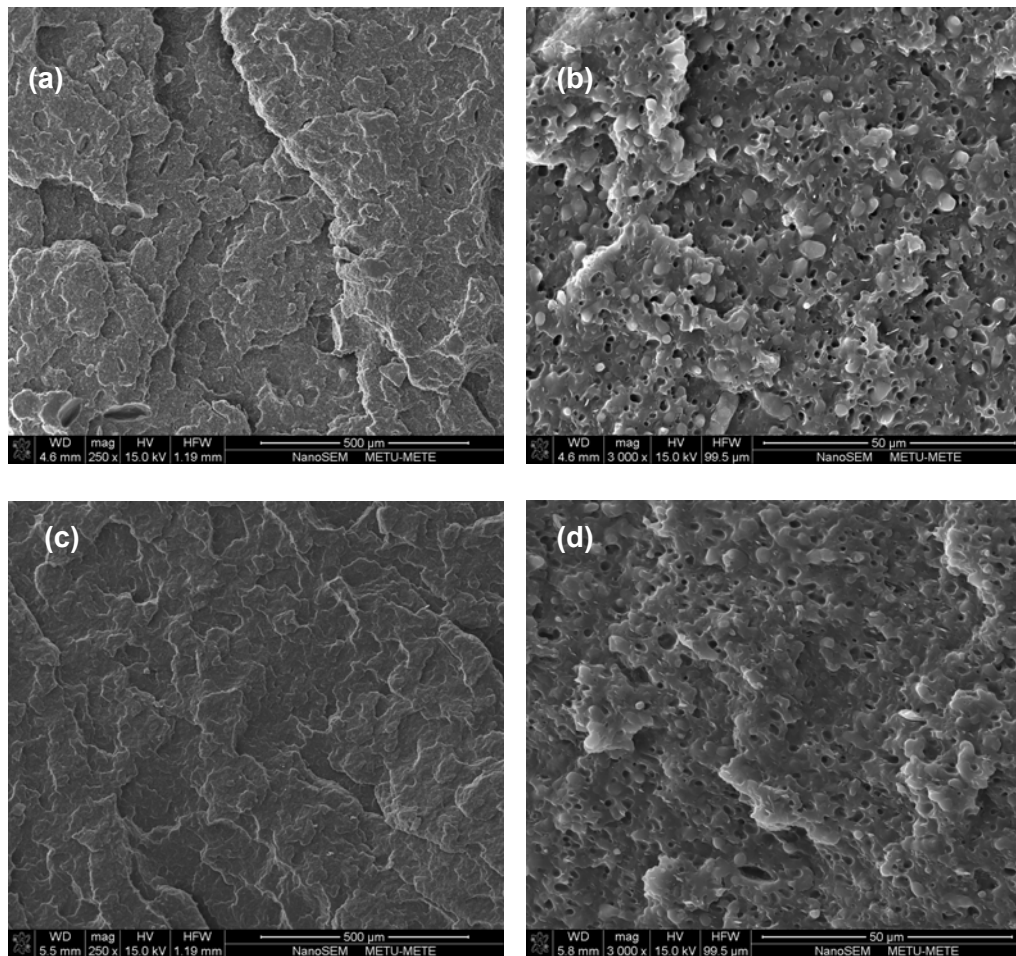


Figure 4.18 SEM micrographs of binary composites with organoclay N5 a) 1wt% N5 (x250) b) 1wt% N5 (x3000) c) 8 wt% of N5 (x250) d) 8 wt% of N5 (x3000)

4.1.3.2 Effects of Compatibilizer Content

Figure 4.19 shows the SEM images of binary blends prepared with compatibilizer M and EP300L. It is observed that as the compatibilizer content increased the domain size of the dispersed phase decreased, average interdomain spacing increased and the crack lines became more significant. Toughness values measured are also consistent with these observations as discussed later. These results are also similar in the ternary composites with compatibilizer M.

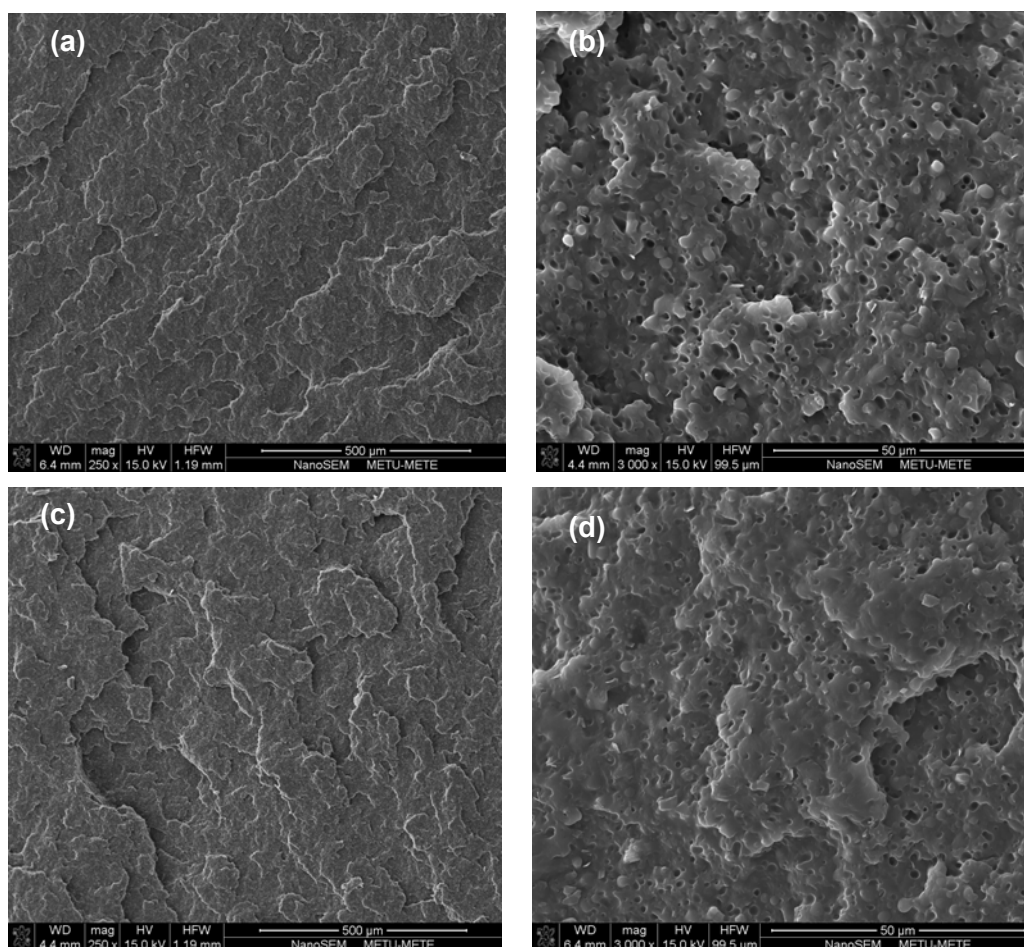


Figure 4.19 SEM micrographs of binary blends with compatibilizer a) 2wt% M (x250) b) 2 wt% M (x3000) c) 6 wt% of M (x250) d) 6 wt% of M (x3000)

Due to stabilizing effect which is a result of reduced interfacial tension and the settlement of the compatibilizer at the interface forming a protecting layer which hinders the coalescence, the presence of an interfacial agent or a compatibilizer can stabilize the morphology in blends and hinder coarsening [43, 44]. In addition to these, size and dispersion of the domains are also affected by resultant compatibility of the polymer and M [93]. Compatibilizer M has a lower viscosity which promotes compatibilizer chains to diffuse between the dispersed phase and PP. By diffusing between the dispersed phase domains, compatibilizer chains would strengthen and immobilize the interface, preventing coagulation of dispersed phase and providing smaller domains.

The presence of the functional groups in the structure of the compatibilizer M would also promote the interaction of composite components and reduce the interfacial tension due to chemical bonding of the polar groups, strengthening the effect of the Van Der Waals attraction. This mechanism may also provide sufficient adhesion for toughening [94, 95].

4.1.3.3 Ternary Nanocomposites

In Figure 4.20, the SEM micrographs of nanocomposites prepared with 6 wt% compatibilizer and different Nanofill® 5 loadings are shown. When these micrographs are compared, it is seen that the reduction of the domain size and increase in the interdomain spacings are most significant in the nanocomposite containing 2 wt% organoclay loading. This result is in accordance with the XRD results and mechanical results discussed later. Owing to the enhanced adhesion due to the high amount of compatibilizer M and well dispersion of organoclay layers in the matrix, possible coagulation of the dispersed phase is inhibited, the average domain size is reduced.

Figure 4.20 shows that, as the clay content is increased above 2wt%, the average domain size increased slightly and the organoclay agglomerates became more visible. It is also observed that crack lines became more significant and went through a more tortuous path in the 6M2N5 nanocomposite which indicates that the toughness and mechanical properties of the composite could be improved.

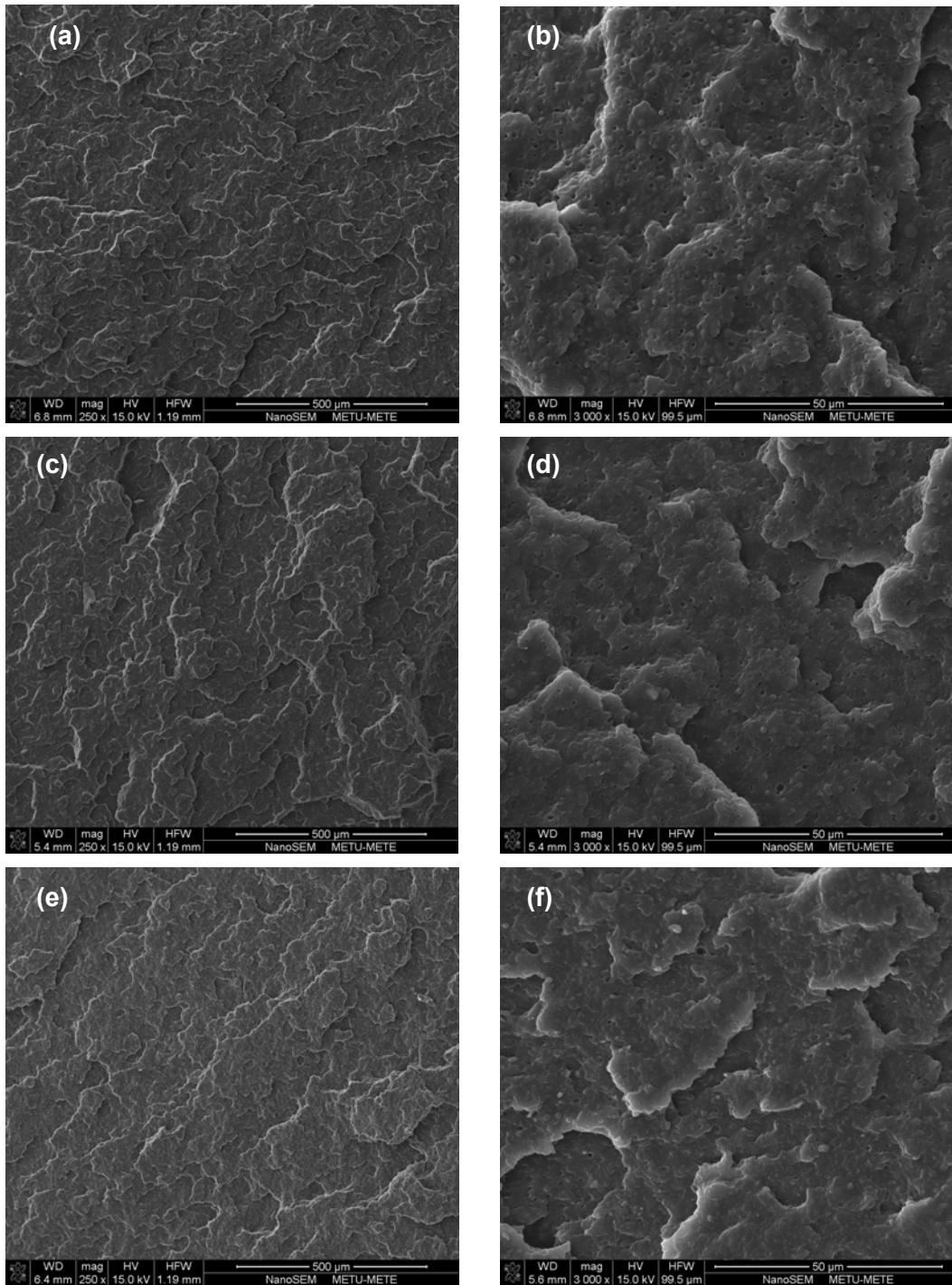


Figure 4.20 SEM micrographs of ternary composites a) 6M1N5 (x250) b) 6M1N5 (x3000) c) 6M2N5 (x250) d) 6M2N5 (x3000) e) 6M4N5 (x250) f) 6M4N5 (x3000)

These results could also be related to the processing conditions of the nanocomposites at high screw speed and low temperature. At low temperatures the matrix viscosity is higher, hence the exerted the shear rate and shear stresses would be higher. In the literature, the effects of shear rate and shear stresses on the homogeneous dispersion of the domains are mentioned to be significant [23, 89].

4.1.3.4 Effects of Clay Type

In the final part of the study, the effects of clay type were investigated. Figures 4.21 and 4.22 show the SEM micrographs of binary and ternary composites prepared with organoclay N8 respectively. Increasing clay loading from 1 wt% to 8 wt% caused reduction in the size of the domains regardless of the type of organoclay. As the organoclay loading was increased the coalescence of domains became more difficult and the domain sizes remained smaller. However, in addition to the well dispersion of the domains, the increase in the interdomain spacings was more significant in the nanocomposites prepared with N5 type of organoclay. Also, the fracture surface is more tortuous in N5 nanocomposites in comparison to N8 nanocomposites, indicating higher toughness, which could be due to the enhanced interactions between compatibilizer M and the N5. In the ternary blend, which is shown in Figure 4.22, the reduction in the domain size is significant. However, crack propagation path is less tortuous than the corresponding N5 nanocomposite and the clay agglomerates are more significantly observed. Due to the agglomeration of the clay, non-homogeneous coalescence of the domains was observed altering the barrier effect of the clay, which decreases the impact strength of the nanocomposite with N8.

To conclude, the domain sizes are reduced and well dispersion of the dispersed phase is obtained with organoclay and compatibilizer additions owing to the barrier effect of organoclay and enhanced adhesion between matrix and the domains by incorporation of the compatibilizer. Finally, a significant difference on the morphology is not observed by the addition of different types of organoclay.

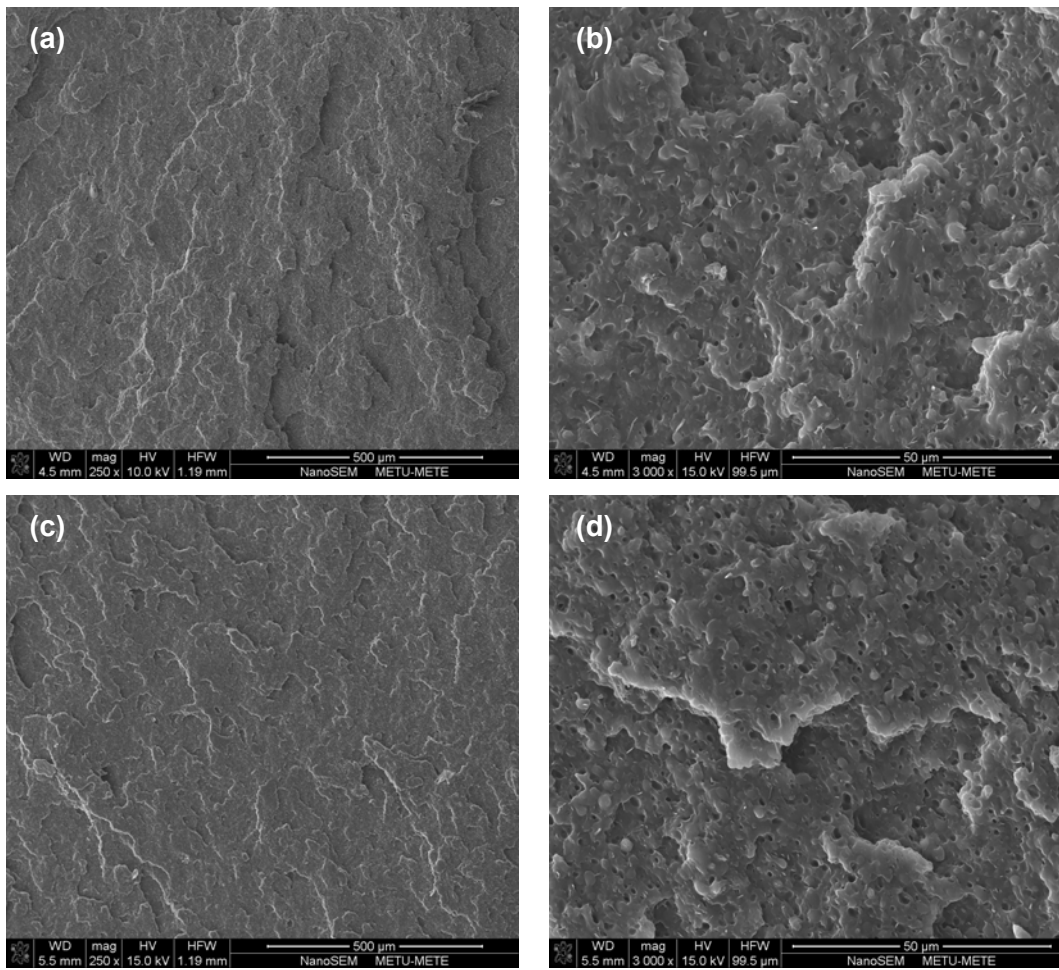


Figure 4.21 SEM micrographs of binary composites with organoclay N8 a) 1wt% N8 (x250) b) 1wt% N8 (x3000) c) 8 wt% of N8 (x250) d) 8 wt% of N8 (x3000)

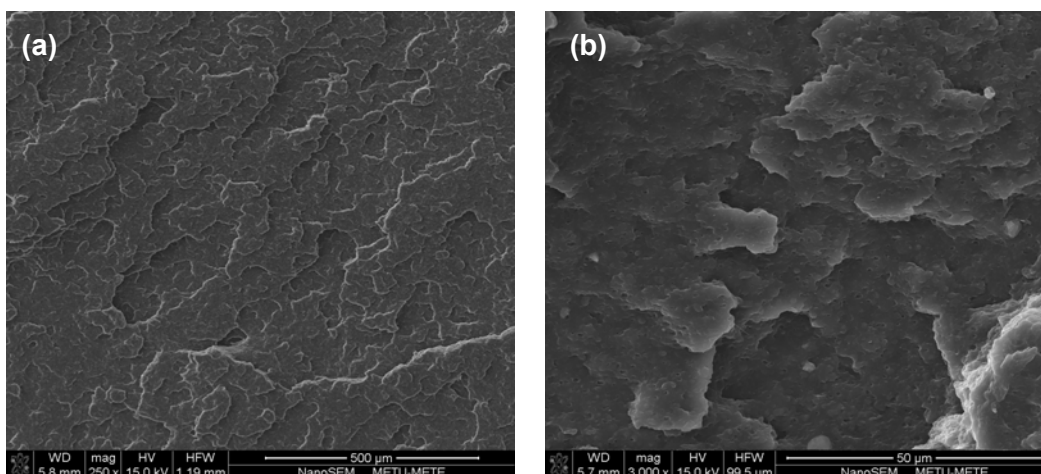


Figure 4.22 SEM micrographs of ternary composites with organoclay N8 a) 3M1N8 (x250) b) 3M1N8 (x3000)

4.2 Mechanical Properties

In this study, tensile and Charpy impact tests were done in order to determine the degree of changes in stiffness and toughness of the matrix material owing to modifications.

4.2.1 Tensile Tests

Stress-strain curves were obtained during the tensile tests of the materials and Young's Modulus, tensile stress at yield, tensile strength and elongation at break (%) values were determined from these curves. The tensile test results of the EP300L and the nanocomposites are given in Figures 4.24 to 4.43 and the numerical values are given in Appendix A for all the composites. The given results of stress and strain are all engineering stress and engineering strain values.

Typical stress strain curves of polypropylene matrix (EP300L) used in this study are shown in Figure 4.23. EP300L is a ductile material, displaying linear elastic behavior up to a specific strain which is the yield strain. After yielding, polymer matrix undergoes strain hardening period due to stretched polymer chains in the direction of

load. Young's Modulus, tensile stress at yield, tensile strength and elongation at break values of the EP300L were 1434 MPa, 36.5 MPa, 51.4 MPa and 812.3%, respectively.

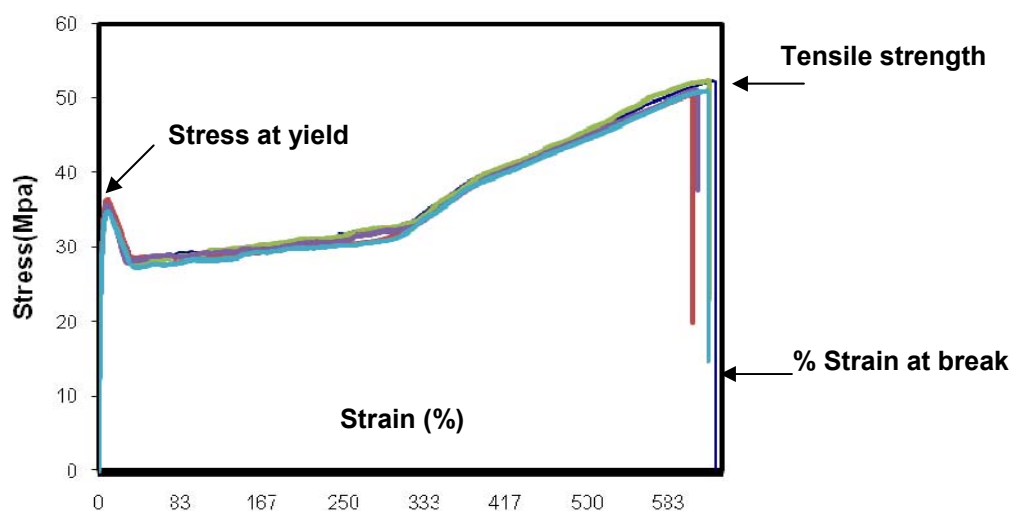


Figure 4.23 Typical engineering stress-strain curve of EP300L polymer matrix.

In Figures 4.24 to 4.39 the tensile properties of the binary blends and ternary nanocomposites prepared with compatibilizer M, organoclay N5 and EP300L with several compositions are shown.

4.2.1.1 Effects of Compatibilizer

Figures 4.24 to 4.27 show the tensile test results of the binary blends and ternary nanocomposites prepared with compatibilizer M at different compatibilizer and clay loadings. In binary blends with 2 wt% and 6 wt% M content, all of the tensile properties except % elongation at break values are reduced. Since M has a lower tensile modulus than polymer matrix (for the compatibilizer M Young's Modulus is 991 MPa and tensile strength is 32 MPa), EP300L+M binary blends have lower

Young's Modulus, yield stress and tensile strength values when compared to neat EP300L due to the addition of the compatibilizer. Compatibilizer phase is added to improve organoclay dispersion and to compensate for the decrease in the tensile properties in the presence of the silicate layers. Young's Modulus and tensile stress at yield values of the ternary nanocomposites are also lower and the reductions in these values are more significant as the compatibilizer content was increased.

The reduction in the tensile strength values of the ternary composites is more significant when the clay content is above 2 wt%. Especially, at high concentrations of organoclay, aggregates of clay platelets may act as defects and stress concentrators in the matrix and promote the failure mechanism [96]. In addition to aggregation of clay platelets, increase in the number of micro voids in the matrix would be increased with further addition of organoclay. Micro voids may form due to high organoclay content in the matrix and then combine causing tearing and failure in the matrix. Increase in % elongation at break values when compared to the neat EP300L, especially at low clay loadings, could be due to good adhesion between clay layers and matrix which is enhanced with the compatibilizer, leading to reduction of the number of micro voids in the matrix. At low clay loadings, especially at 2 wt%, as the compatibilizer content is increased, tensile properties are improved except for the composites having 8 wt% compatibilizer loading.

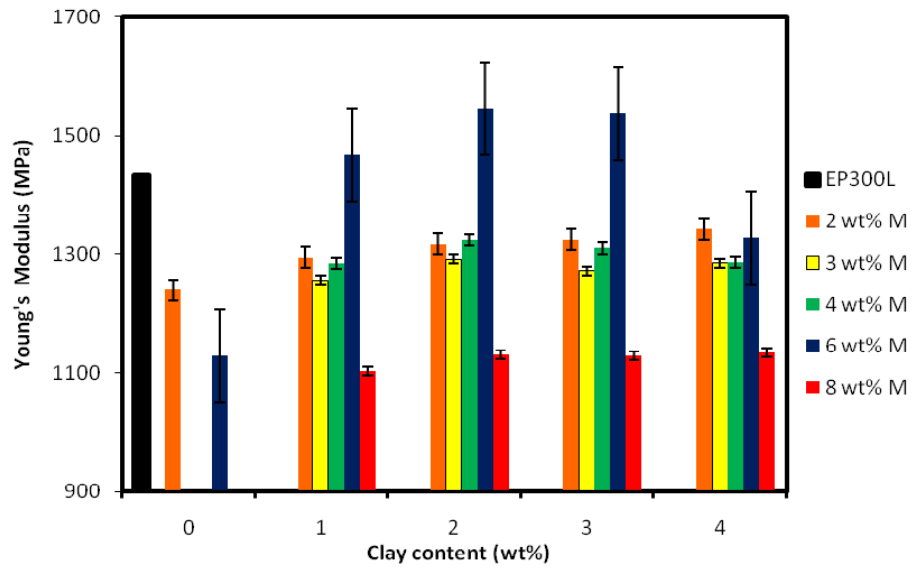


Figure 4.24 Young's Modulus of binary blends and ternary nanocomposites prepared with compatibilizer M and N5 clay at different loadings.

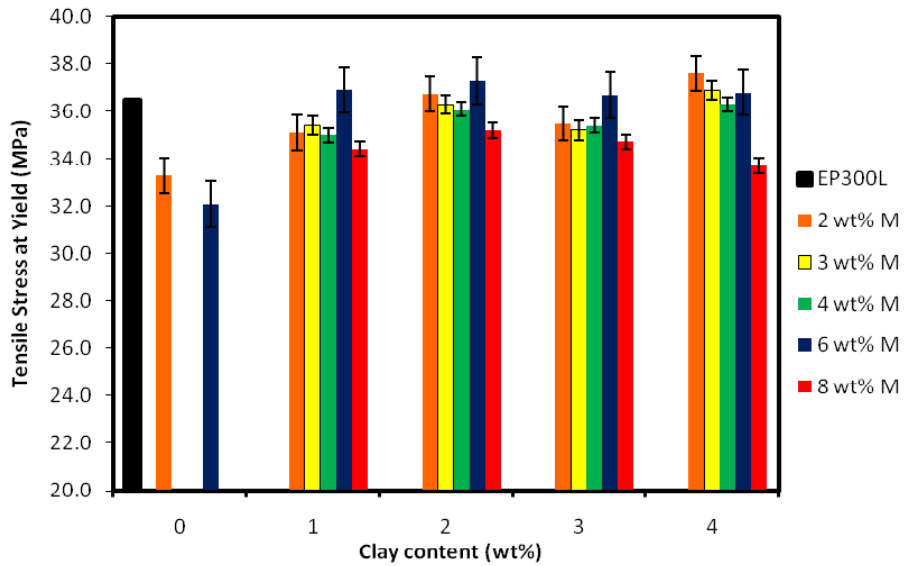


Figure 4.25 Tensile stress at yield values of binary blends and ternary nanocomposites prepared with compatibilizer M and N5 clay at different loadings.

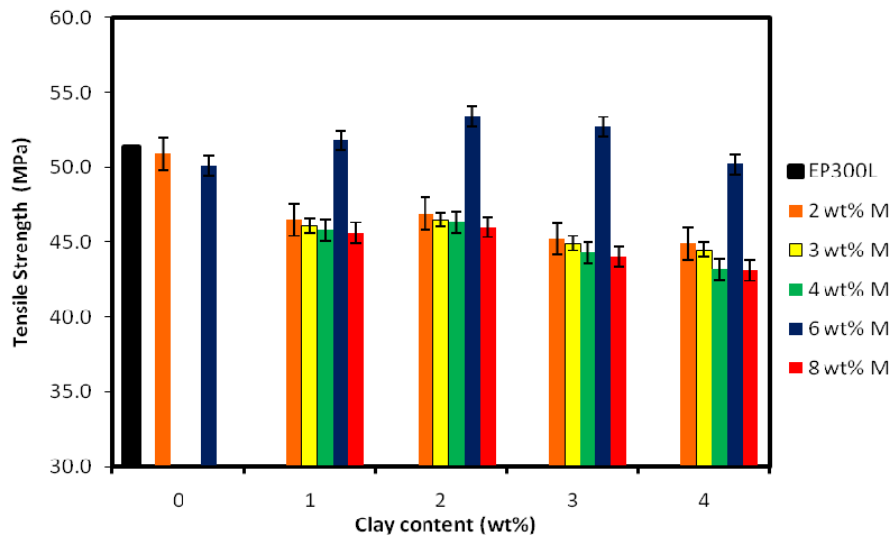


Figure 4.26 Tensile strength values of binary blends and ternary nanocomposites prepared with compatibilizer M and N5 clay at different loadings.

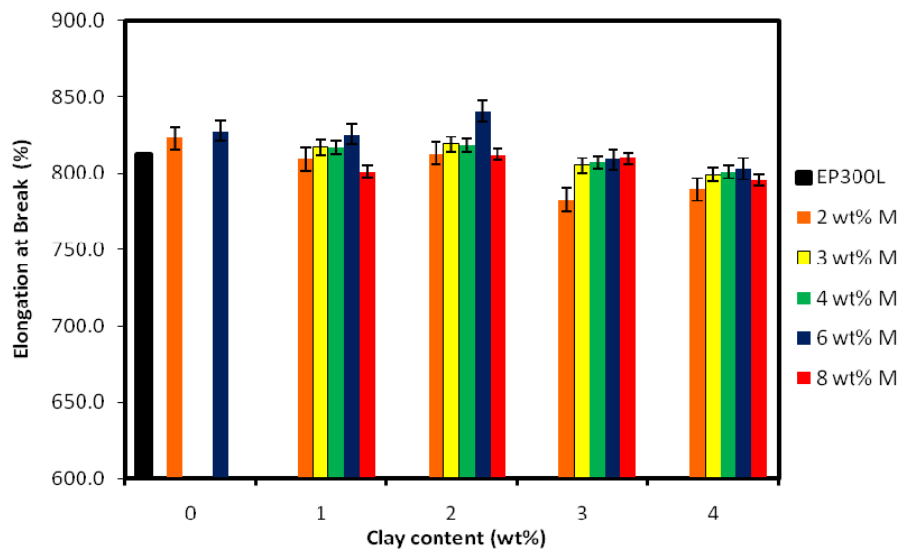


Figure 4.27 Elongation at break (%) values of binary blends and ternary nanocomposites prepared with compatibilizer M and N5 clay at different loadings.

In Figures 4.24 to 4.27, the most significant improvement is observed in the nanocomposites which have 6 wt% compatibilizer loading. This result is expected since, these are the only composites exhibiting both intercalated and partially delaminated structure in the XRD analysis, and increased amount of compatibilizer results in better intercalation owing to higher affinity and hydrogen bonding with the compatibilizer M. It can be concluded that the organoclay particles are dispersed more uniformly as M content increases. This is also stated in the literature and desired nanoscale dispersion of organoclay is achieved with M through strong hydrogen bonding between hydroxyl group of silicate structures and the maleic anhydride group, while relying on chemical similarity of isotactic PP and grafted PP in the M structure [15, 97].

Mechanical properties, especially elongation at break, are very sensitive to adhesion strength between the components or partial miscibility at the interface of blend components in phase separated systems [98]. Thus, increase in the elongation at break values together with the stiffness properties can be attributed to possible increased adhesion provided by both compatibilizer and organoclay system in the nanocomposites containing 6 wt% M.

4.2.1.2 Effects of Clay Content

Figures 4.28 to 4.31 show that in binary composites prepared with organoclay N5, addition of organoclay increases Young's Modulus and tensile stress at yield and decreases the % elongation at break and tensile strength values. The effect of clay is observed more significantly as the content of the N5 increases. Improvement in modulus and yield stress indicates the reinforcing effect of organoclay due to clay's high aspect ratio, platelet structure and large contact area with the polymer matrix [42, 99]. At constant compatibilizer loading, the same increasing trend in tensile modulus and yield stress is also observed in the ternary composites as the N5 content is increased. In Figures 4.28 to 4.30, the effect of increasing clay content in ternary nanocomposites is clearly observed. According to these figures, Young's Modulus and tensile strength values are generally reduced due to compatibilizer phase addition, but significantly less reduction occurs at 2 wt% clay loading.

Figure 4.28 and 4.29 show that tensile modulus and yield stress of the composites with 6 wt% compatibilizer loading are significantly higher than the corresponding properties of the other materials. Results indicate that clay is well dispersed in the matrix and delamination is observed in these composites as mentioned before. This result is expected considering the XRD results, since these composites have both intercalated and delaminated structures with increased d-spacing values, decreased intensity and broadening of the peaks. Since insertion of the polymer chain inside clay galleries leads to an increase in contact area between clay and polymer, the increase in modulus value for these compositions are expected.

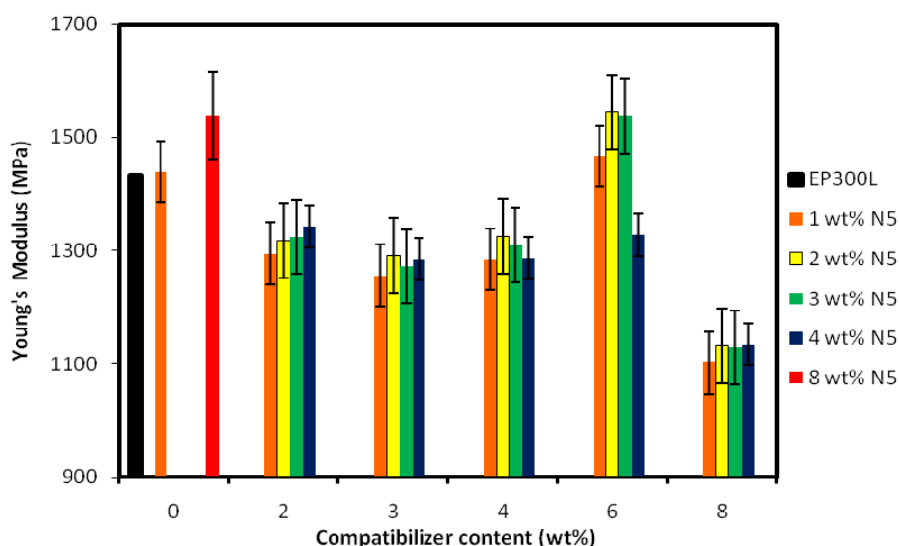


Figure 4.28 Young's Modulus of binary and ternary nanocomposites prepared with compatibilizer M and N5 at different loadings.

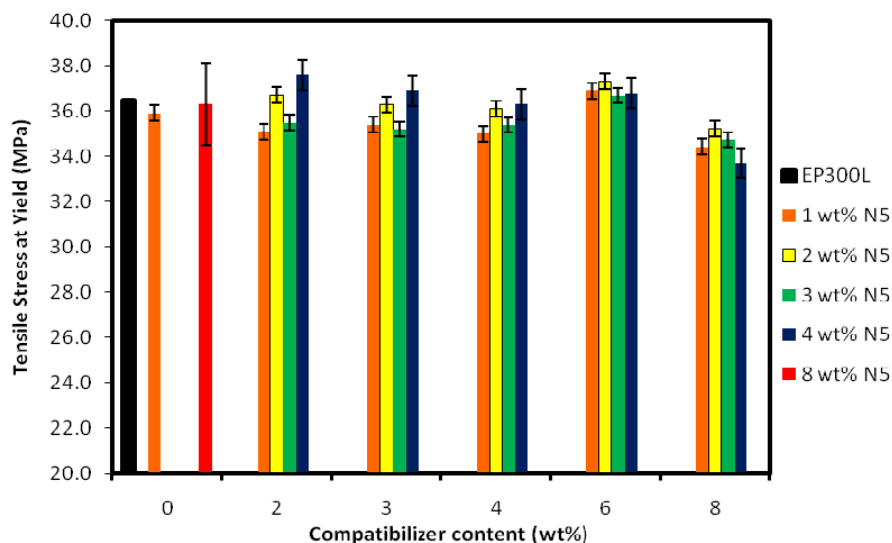


Figure 4.29 Tensile stress at yield values of binary and ternary nanocomposites prepared with compatibilizer M and N5 at different loadings.

Elongation at break values decreases (Figures 4.30) as the clay content increases, except for the 6 wt% compatibilizer content, at 1wt% and 2 wt% clay loadings. The improvement of % elongation values of the mentioned nanocomposites could be due to good dispersion as observed in the XRD pattern. This structure allows for chain mobility under extension. In the other nanocomposites which exhibit decrease in % elongation at break values, it is believed that presence of clay platelets reduce the mobility of the polymer chains [100]. It is a known fact that silicate layers cannot undergo elongation under applied external stresses due to their rigidity [89]. Because of the possible decrease in the amount of the tie chains between crystalline domains, the stress applied cannot be transferred through the composite and an early rupture might occur [101]. Figures 4.26 and 4.30 also reveal that due to early rupture, the tensile strength at break values decreased as the clay content increases.

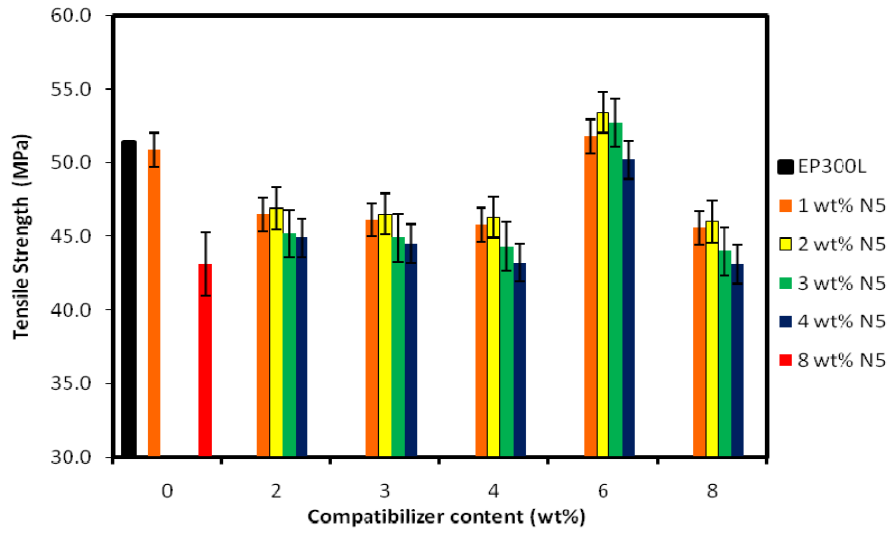


Figure 4.30 Tensile strength values of binary and ternary nanocomposites prepared with compatibilizer M and N5 at different loadings.

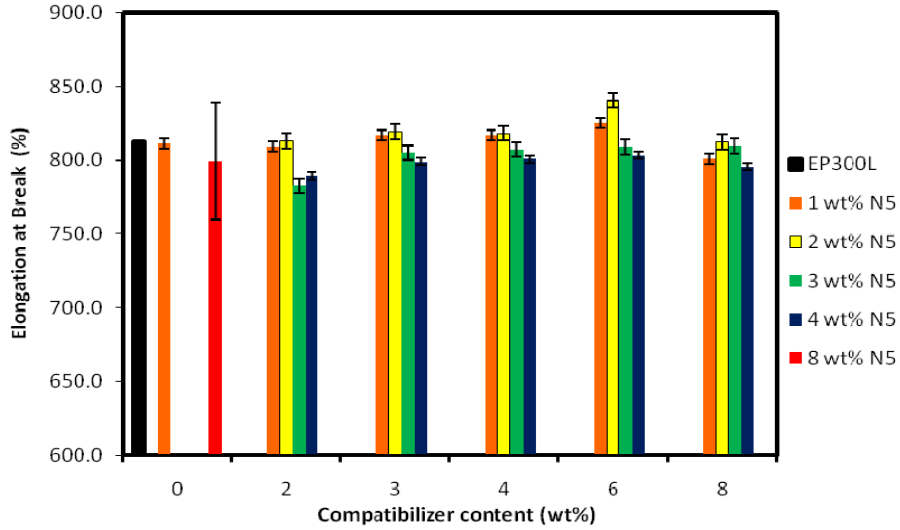


Figure 4.31 Elongation at break (%) values of binary and ternary nanocomposites prepared with compatibilizer M and N5 at different loadings.

The only reduction in d-spacing value is observed in 8M4N5 nanocomposite which contains 8 wt% compatibilizer and 4 wt% N5 organoclay. XRD results indicate that when compared with pure N5 powder; d-spacing value of 8M4N5 nanocomposite is lower. As a result of this, all tensile properties of this nanocomposite are low as expected. This could be a consequence of the collapsed clay layers owing to displacement of ammonium compounds during thermal and mechanical treatment.

4.2.1.3 Improved Nanocomposites

In Figures 4.32 to 4.35 the tensile test results of the ternary composites having 6 wt% compatibilizer loading are shown in detail since the highest improvements in all the tensile properties are observed in these nanocomposites. XRD patterns of these composites indicate the best dispersion and delamination of clay layers enhancing the stiffness properties of these composites. According to the figures, 6M4N5 composite which has the highest clay content showed reduction in the tensile properties, since XRD analysis of this composite showed less intercalation in comparison to the d-spacing values of the others.

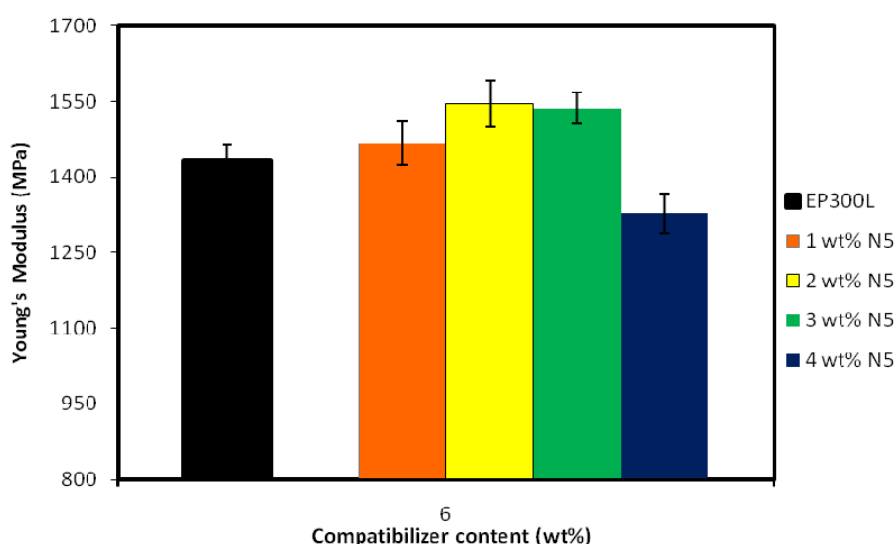


Figure 4.32 Young's Modulus of ternary nanocomposites prepared with 6 wt% compatibilizer M and N5 at different loadings of clay.

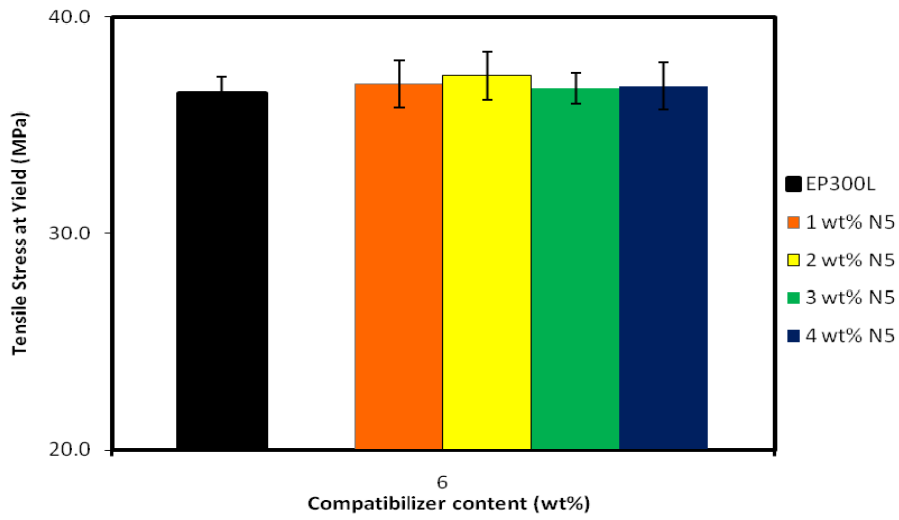


Figure 4.33 Tensile stress at yield values of ternary nanocomposites prepared with 6 wt% compatibilizer M and N5 at different loadings of clay.

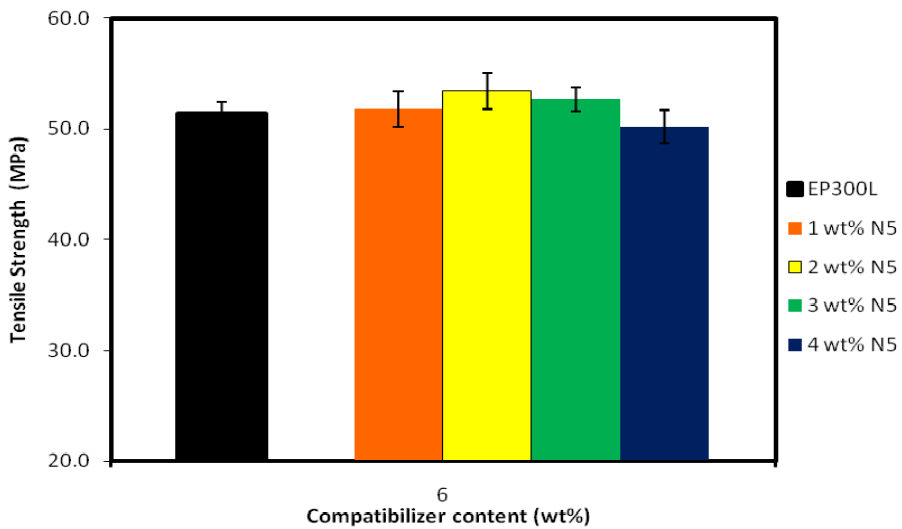


Figure 4.34 Tensile strength values of ternary nanocomposites prepared with 6 wt% compatibilizer M and N5 at different loadings of clay.

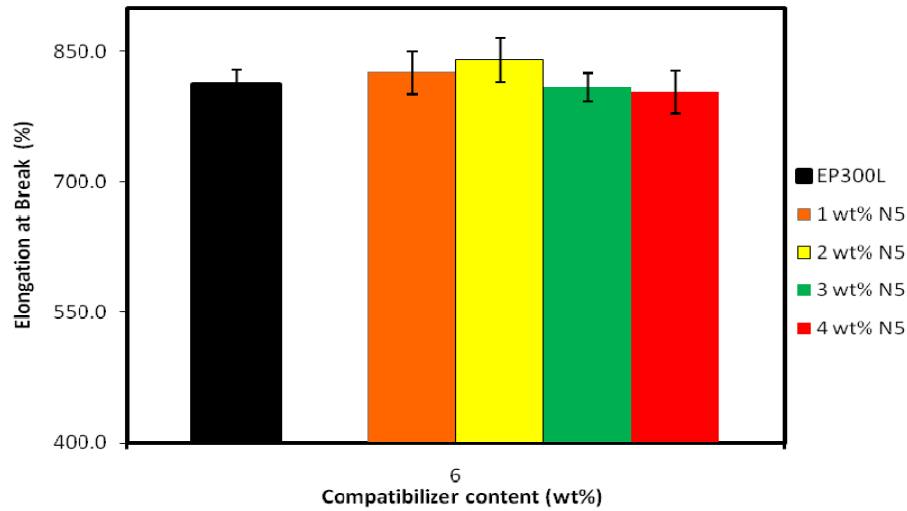


Figure 4.35 Elongation at break (%) values of ternary nanocomposites prepared with 6 wt% compatibilizer M and N5 at different loadings of clay.

Tensile modulus, yield stress, tensile strength and the % elongation at break values significantly increased for the composites having 1 wt% and 2 wt % clay loading, but the best improvement is observed in the 6M2N5 composite. This improvement could be due to the good dispersion as observed in the XRD pattern. Results show that the lower the amount of the clay, the smaller is the degree of agglomeration due to cohesive forces resulting in better dispersion.

Mentioning the blend morphology, location of the organoclay particles at the interface during compounding, can lead to a significant decrease in interfacial tension and reduction in domain size. In this case, organoclay acts both as a reinforcing agent and a compatibilizer in the immiscible blend systems [11]. SEM analysis indicate that the domain sizes are reduced in the ternary composites with 6 wt% compatibilizer content leading to a general increase in the % elongation at break values. In a previous study, it was found that the enhancement in Young's Modulus with the addition of organoclay and M could be attributed to the increase in the crystallinity of the PP phase and increased adhesion between the phases [23].

Mechanical properties, especially elongation at break, are very sensitive to adhesion strength between components or partial miscibility at the interface of blend

components in phase separated systems [98]. Thus, increase in the elongation at break values together with the stiffness properties can be attributed to possible increased adhesion provided by both the compatibilizer and the organoclay in the nanocomposites containing 6 wt% M.

Moreover, according the DSC results shown later, an increase in the crystallinity of these composites is observed, indicating that the compatibilizer M strengthens the matrix at 6 wt % compatibilizer loading; increases crystallinity and consequently the mechanical properties are enhanced. Nanocomposite containing 6 wt% M and 2 wt% N5 exhibited 7.7% increase in Young's Modulus which is the highest improvement in the modulus obtained in this study.

4.2.1.4 Effects of Clay Type

In the last part of the study, effects of different clay types on mechanical properties were investigated at low organoclay content and different compatibilizer loadings. Figures 4.40 to 4.43 show the results of the nanocomposites prepared with N8 type of organoclay. XRD patterns of N8 nanocomposites indicated that these composites have intercalated structure but delamination did not occur.

In the binary composites' tensile test results, as well as the ternary ones, a general decreasing trend is observed. Young's modulus and tensile stress at yield values of 3M1N8 composite are improved with respect to other ternary nanocomposites, while tensile strength and % elongation at break values are reduced. These results are consistent with the SEM and XRD results of this composite, since the dispersion of the domains is not uniform and clay agglomeration is present. XRD patterns of the composite indicate that, higher intercalation is observed which is consistent with the low reduction observed in elastic modulus and yield strength values of this composite. With the effect of higher filler-compatibilizer interactions, and more effective clay dispersion with N5, less reduction in tensile properties is observed and with appropriate load of compatibilizer and at low clay content, improvements are observed. However, even in the presence of the intercalated structures, N8 organoclay addition significantly decreases the tensile properties.

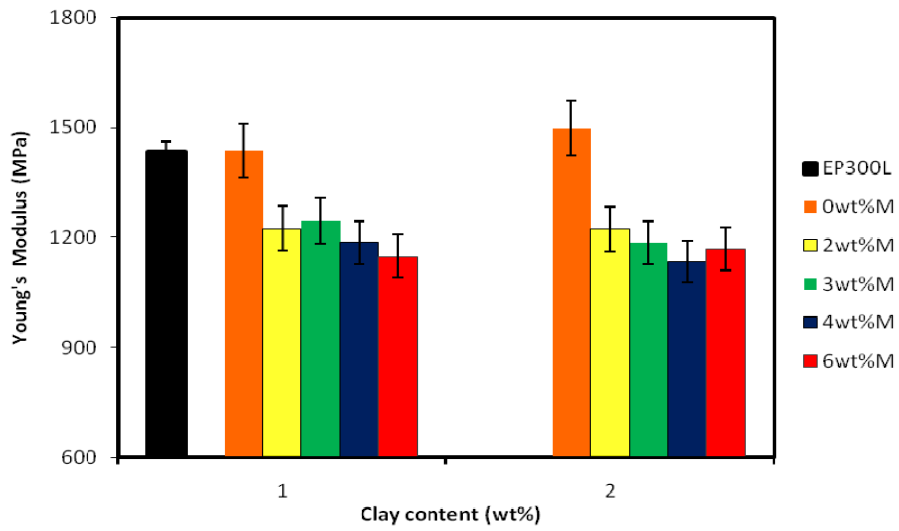


Figure 4.36 Young's Modulus of binary and ternary nanocomposites prepared with N8 at low content and compatibilizer M at different loadings.

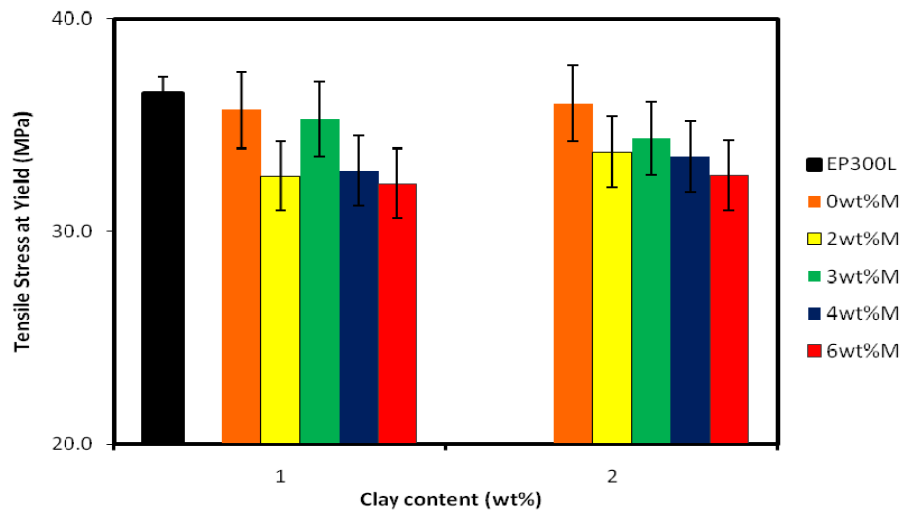


Figure 4.37 Tensile stress at yield values of binary and ternary nanocomposites prepared with N8 at low content and compatibilizer M at different loadings.

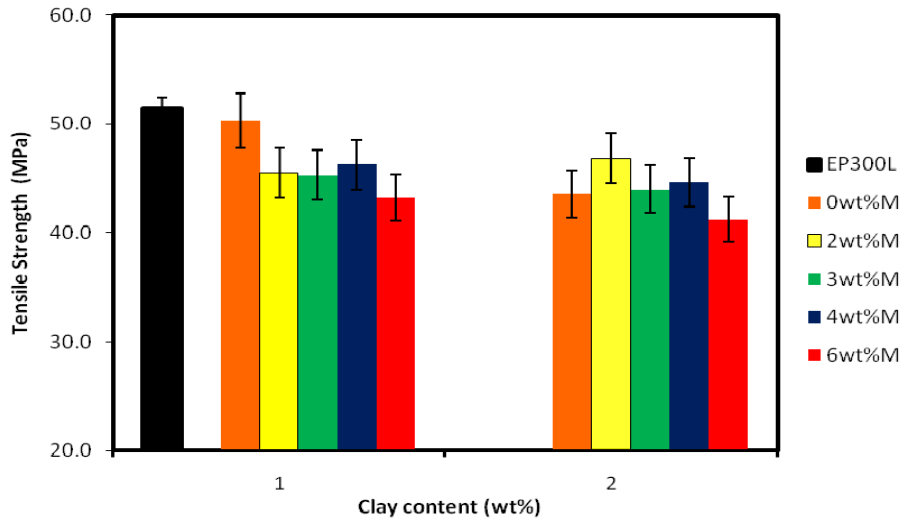


Figure 4.38 Tensile strength values of binary and ternary nanocomposites prepared with N8 at low content and compatibilizer M at different loadings.

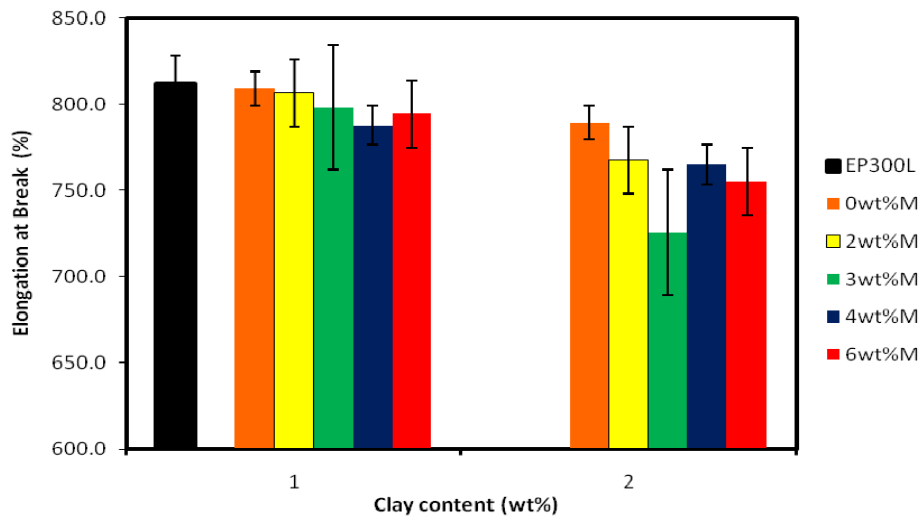


Figure 4.39 % Elongation at break values of binary and ternary nanocomposites prepared with N8 at low content and compatibilizer M at different loadings.

4.2.2 Impact Tests

Notched Charpy impact tests were carried out for determination of impact strength of the blends and nanocomposites. The polymer matrix of the study is a semi-crystalline polymer. Polypropylene exhibits ductile behavior at low strain rates and brittle behavior at high strain rates [66]. In order to increase the impact resistance and toughness of the PP, PP's are blended with modifiers [88].

Initiation of the crack due to impact stress begins by stress concentrators which are sharp points, voids and notches in the matrix. Impact stress is concentrated in inhomogeneities and creates micro cracks followed by the tearing of the matrix in a single direction.

Toughening of the thermoplastic materials is attributed to the conversion of the high impact strength in one direction into small multidirectional stresses. The absorption of the impact stress is also possible, preventing the crack formation.

Toughness of the PP is affected by the size and dispersion of the domains, adhesion at the interface of the modifier and the continuous phase, interdomain distances and modulus ratio of the polymer matrix and dispersed phase [89]. Interfacial adhesion, modulus of the matrix and ratio between the modulus of the matrix and compatibilizer domains are intrinsic parameters which affect interdomain distances. On the other hand, domain size is also affected by the stability of the surface mobility and interfacial tension reduction [89]. Extrinsic parameters such as impact speed, test temperature and deformation mode were kept constant during the study.

4.2.2.1 Effects of Clay Content

Figure 4.40 shows the effects of clay content on the impact strength in binary and ternary nanocomposites. Organoclay particles have a large surface area decreasing the chain mobility. This reduction in the chain mobility is inversely proportional with the stiffness of the polymer [103]. Thus, impact strength of the EP300L decreases and the material experiences more brittle fracture as the organoclay content is increased. The decrease in the impact strength of the matrix was much more significant at high clay contents in both the binary and ternary nanocomposites.

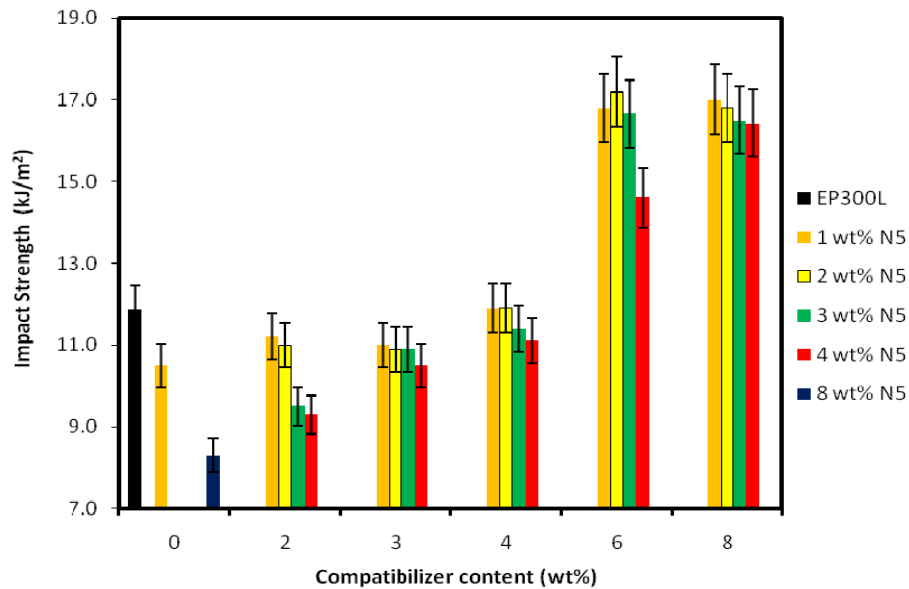


Figure 4.40 Impact strength values of binary and ternary nanocomposites prepared with N5 and compatibilizer M at different loadings.

To prevent crack propagation, the domain sizes which are observed by SEM analysis should be optimum. Also, in the literature it is mentioned that, cavitation formation may become easier in the presence of larger domains [104]. When the fracture ligament size is larger than the dispersed phase size, existence of the domains cannot influence the crack propagation [93]. Thus, there should be an optimum domain size to prevent crack formation. Due to the barrier effect of the organoclays preventing the coalescence of the domains, the domain sizes in the binary composites were reduced and failed in preventing crack formation. This result was also observed in the SEM images of the binary nanocomposites. The agglomeration of the organoclay particles which is more significant and expected at high clay loadings due to incompatibility of the clay and the matrix, also promotes crack formation.

Figure 4.40 shows that at any compatibilizer content the impact strength decreases with increasing clay content. The XRD data show that agglomeration increases with the clay content. The agglomerated clay particles, acting as very sensitive crack tips, initiate crack propagation, decrease impact strength of the matrix and inhibit the toughening mechanism.

4.2.2.2 Effects of Compatibilizer Content

Figure 4.41 shows the impact resistance of binary blends and ternary nanocomposites prepared with EP300L, N5 and compatibilizer M. In the binary blends with compatibilizer M, a significant improvement in impact toughness behavior is observed with the addition of 2 wt% compatibilizer, and the toughness is further enhanced with 6 wt% compatibilizer addition. In ternary nanocomposites, impact strength values of the materials increase as higher amount of M is added; resulting in more effectively absorbed and dissipated impact energy by increased compatibilizer content. Since the modulus of the compatibilizer used is lower than the matrix material, the energy absorption capacity of the compatibilizer is higher than the matrix. In addition to this, the critical interdomain spacings increases as the modulus of the modifier decreases, and it decreases as the modulus of the matrix increases [46, 105].

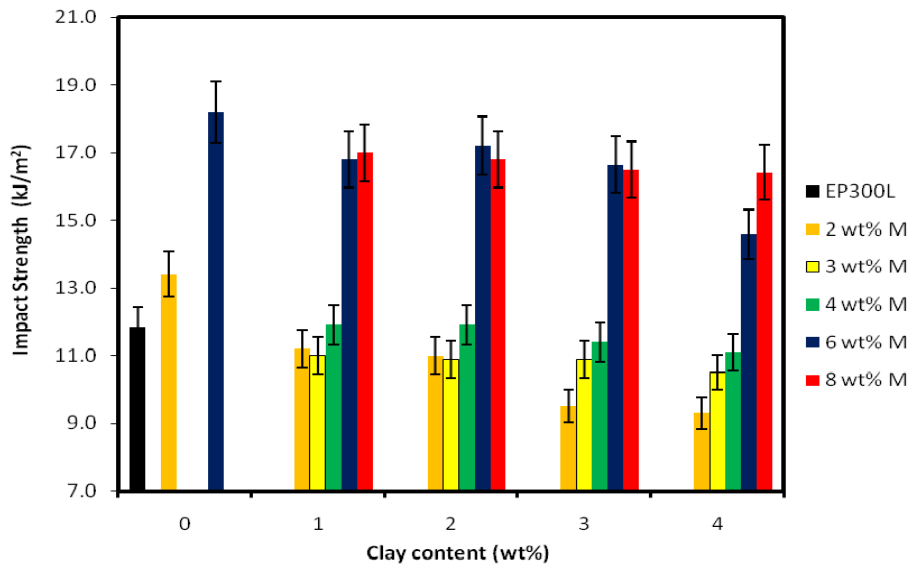


Figure 4.41 Impact strength values of binary blends and ternary nanocomposites prepared with N5 and compatibilizer M at different loadings.

There are no improvements in toughness values observed in the nanocomposites having less than 6 wt% compatibilizer loading. For the 6 and 8 wt% compatibilizer loadings, due to increased energy absorption capacity of the nanocomposite, the toughness reduction effect of organoclay addition is compensated. More than 6 wt % compatibilizer addition does not significantly further improve the toughness values. In addition to this, since the interaction between the clay and the compatibilizer M increases as the M content increases, more homogeneous organoclay dispersion is observed at 6 wt% compatibilizer content.

6 wt% M and 2 wt% N5 type of organoclay containing nanocomposite (6M2N5), which has the highest improvement in toughness values, exhibits a more significant increase in interdomain distances in the SEM analysis. In this nanocomposite, decrease in the domain size and a well dispersion of the domains are also observed. Moreover, in the XRD patterns of 6 wt % M containing nanocomposites, more delaminated structures are observed. Better dispersion of organoclay, i.e. delamination of the clay, decreases the domain size by its barrier effect [42]. Since the impact strength of the nanocomposites is also improved, the optimum domain

size to prevent crack propagation may have been obtained. On the other hand, as the organoclay content increases, the improvements in toughness values are reduced due to possible agglomeration of the organoclay. Thus, clay content and dispersion are the controlling factors for the toughness properties since partial delamination of the organoclay was seen only at 6 wt % M loading based on XRD results.

4.2.2.3 Effects of Clay Type

Binary nanocomposites prepared with N8 type of organoclay, exhibit the same behavior as N5 type of organoclay as it is seen in Figure 4.42. Due to decrease in chain mobility and the stiffness of the matrix, impact strength of the binary nanocomposites decreases as the clay content increases. There are no significant improvements in the toughness of the materials up to 6 wt% compatibilizer loading. Considering the same compatibilizer loading, the composites with N8 type of organoclay, have less improvement than the ones with N5 type of organoclay. In the XRD, it is observed that nanocomposites having N8 have mostly intercalated structures. High intercalation of the polymer chains decreases the chain mobility and prevents coalescence of the heterophasic domains. Thus, the domain sizes remain smaller than the optimum size needed to prevent crack propagation. On the other hand delaminated structures and improved adhesion properties of the N5 type of organoclay improve the impact strength in nanocomposites with N5. Moreover, in the N8 type of organoclay containing nanocomposites, there are clay agglomerates as observed in SEM analysis, acting as stress concentrators and promoting crack formation.

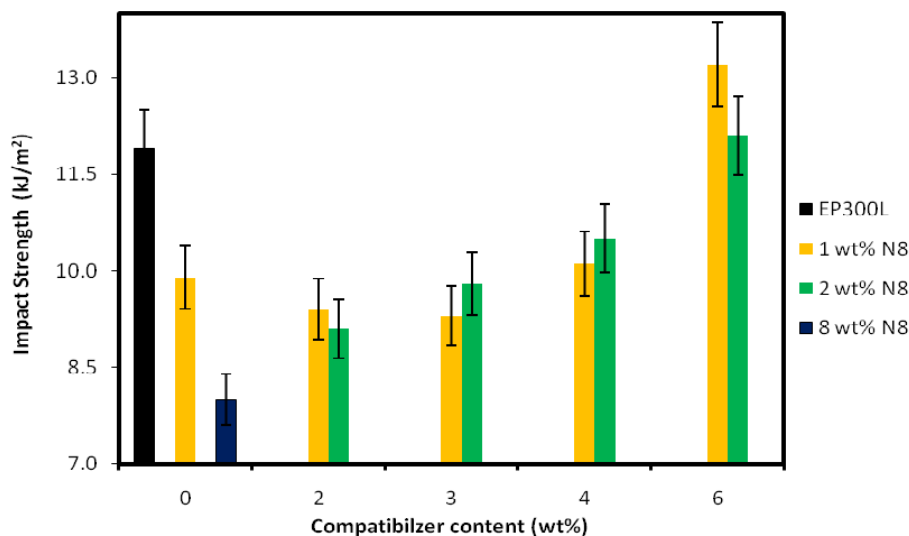


Figure 4.42 Impact strength values of binary and ternary nanocomposites prepared with N8 and compatibilizer M at different loadings.

4.3 Differential Scanning Calorimetry (DSC) Analysis

In order to determine the crystallization behavior of the nanocomposites, DSC analyses are done. DSC thermogram of polypropylene is shown in Figure 4.43 which exhibits a peak at 163.77 °C, indicating to a single crystalline phase in the polypropylene. Compatibilizer M also exhibits one peak at 164 °C and its DSC thermogram is shown in Figure 4.44. Related representative DSC thermographs of the samples are given in Appendix B. The glass transition temperatures of the samples are not detected in the thermograms, since they are below the room temperature.

The percent crystallinity values of each nanocomposite are calculated by dividing the heat of fusion of the sample (ΔH_f) with the weight fraction of the polymer matrix in the nanocomposite and the heat of fusion of the pure crystalline form of the polypropylene which is 209 J/g [78]. Crystallinity of pure EP300L is calculated as 37.6 % under a low crystallization rate of 5 °C/min.

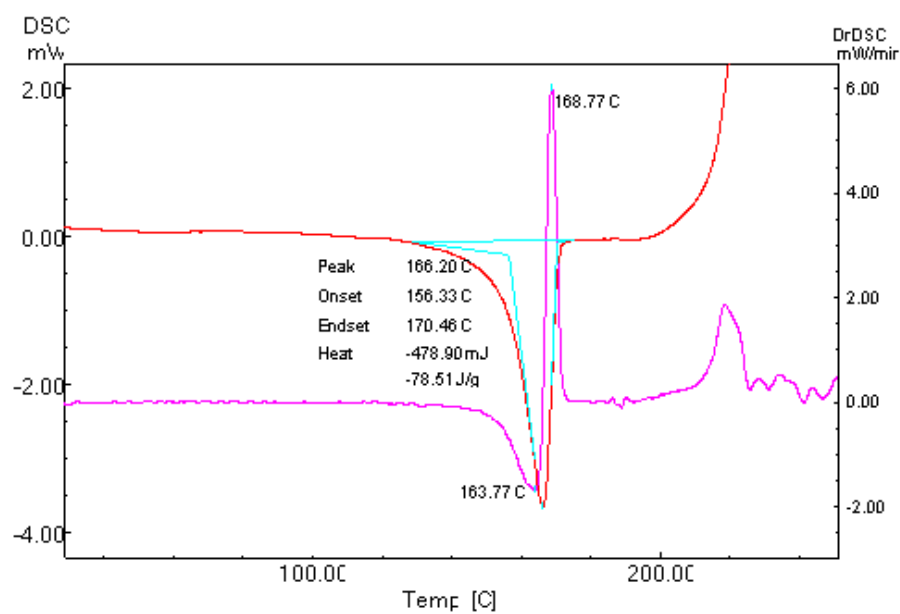


Figure 4.43 DSC thermogram of EP300L.

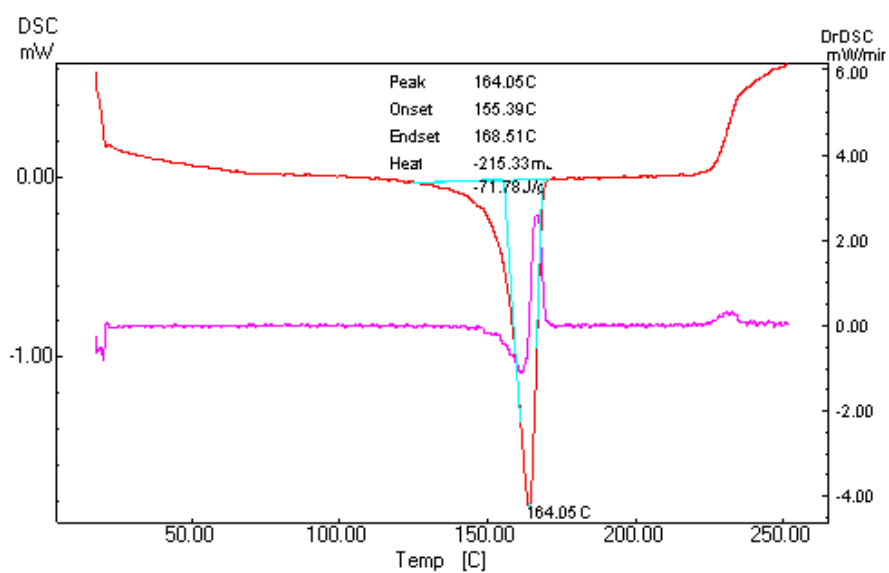


Figure 4.44 DSC thermogram of compatibilizer M.

The heat of fusion, melting temperature and the calculated % crystallinity values of the samples are given in Table 4.5. The melting temperatures of the samples decreases with respect to increasing clay and compatibilizer content, but this decrease is not considerable in all the compositions.

Table 4.5 DSC results

Sample	Peak-II		
	T _m , (°C)	ΔH, (J/g)	X _c , (%)
Polymer Matrix			
Polypropylene (EP300L)	166.2	78.5	37.6
Compatibilizer			
M	164.0	71.8	34.4
Binary blends			
2M	165.1	73.7	36.0
6M	166.2	68.2	34.7
Binary nanocomposites			
1N5	165.2	81.9	39.6
8N5	165.5	89.9	46.8
1N8	165.0	77.4	37.4
8N8	165.3	73.6	38.3

Table 4.5 (cont'd) DSC results

Sample	Peak-II		
	T _m , (°C)	ΔH, (J/g)	X _c , (%)
Polymer Matrix			
Polypropylene (EP300L)	166.2	78.5	37.6
Compatibilizer			
M	164.0	71.8	34.4
Binary blends			
2M	165.1	73.7	36.0
6M	166.2	68.2	34.7
Binary nanocomposites			
1N5	165.2	81.9	39.6
8N5	165.5	89.9	46.8
1N8	165.0	77.4	37.4
8N8	165.3	73.6	38.3
Ternary nanocomposites			
2M2N5	165.9	72.9	36.3
3M2N5	165.5	71.0	35.8
4M2N5	165.1	70.8	36.0
6M1N5	165.8	74.5	38.3
6M2N5	164.8	87.7	45.6
6M3N5	165.5	74.1	39.0
6M4N5	165.5	76.1	40.4
8M2N5	166.8	66.5	35.3
2M2N8	165.4	78.2	39.0
3M2N8	165.5	74.1	37.3
4M2N8	166.0	73.8	37.6
6M2N8	166.4	67.0	34.9

In the binary composites containing N5 type of organoclay, % crystallinity values are increased significantly as the content of the clay increases. It is mentioned in the literature that, in the presence of dispersed clay platelets in the matrix, heterogeneous nucleation is enhanced. Thus, crystallization rate and the crystallinity of the polymer matrix would increase [70]. Addition of organoclay also decreases the crystallization temperature and increases the number of crystallite sizes [106]. The increasing trend in crystallinity values, which is observed as the organoclay content increases, is also seen in the ternary nanocomposites at same compatibilizer loading.

In the binary blends of the polymer matrix and the compatibilizer, crystallinity values of the samples are reduced as the M content increases. Since compatibilizer M is a less crystalline material than EP300L, the reduction in crystallinity values are expected.

The increase in crystallinity values of the N5 type organoclay loaded nanocomposites is observed only in the ones with 6 wt% compatibilizer content. As expected, as the organoclay content increases, the % crystallinity also increases. The results are attributed to the well dispersion of the organoclay platelets owing to high interaction with the compatibilizer M and N5 at this compatibilizer loading. XRD results of these nanocomposites have revealed that, these specimens are partially delaminated. Relatively better dispersion of organoclays in the presence of compatibilizer M affects the rate of heterogeneous nucleation and increases the crystallinity. 6M2N5 nanocomposite shows the most significant increase in crystallinity values which is expected, since the most delaminated structure and the best dispersion is observed in this sample. Since the best dispersion is obtained with N5 type of organoclay addition as it is shown in XRD and SEM results, the increase in % crystallinity is negligible with N8 type of organoclay containing nanocomposites.

CHAPTER 5

CONCLUSIONS

In order to improve the mechanical properties of a heterophasic polypropylene copolymer, binary blends and binary and ternary nanocomposites were prepared by melt compounding method with a twin screw extruder. Effects of organoclay types and concentrations, as well as the effects of compatibilizer content on the morphology, mechanical and thermal properties of the nanocomposites were investigated.

XRD results revealed that, as the compatibilizer content increased, intercalation of the polymer chains was enhanced due to high interaction between the polymer matrix and the compatibilizer. Increase in the d-spacing values and decrease in the intensity of the peaks were observed indicating more effective dispersion of the clay platelets. The driving forces of the interaction between the clay and the polymer matrix were the high affinity of the compatibilizer M, hydrogen bonding between the maleic anhydride group and the silicate surfaces and also the chemical compatibility between the polypropylene matrix and polypropylene present in the compatibilizer structure. Since compatibilizer M had lower crystallinity than the polymer matrix, with the increasing compatibilizer content, the % crystallinity values of the ternary composites and binary blends were reduced in general, except for 6 wt% compatibilizer loaded nanocomposites. This was an expected result based on XRD analysis, since these composites were partially delaminated with better dispersion of the organoclay.

Nanocomposites with two different types of organoclay, Nanofill® 5 (N5) and Nanofill® 8 (N8), were prepared in order to investigate the effects of organoclay types. N8 loaded nanocomposites showed mostly intercalated structures while N5

loaded ones showed both intercalated-delaminated structures with better dispersion of the clay platelets. At low organoclay contents, the dispersive forces easily overcame the cohesive forces between the clay platelets for both of the nanoclay types. In addition, the % crystallinity was increased and domain sizes observed in the SEM images were reduced regardless of the clay type at low clay contents. Tensile properties and the impact strength of the N5 loaded nanocomposites were improved more than those of the nanocomposites with N8, due to better dispersion of the clay platelets and the increased interdomain distances observed by XRD and SEM analysis respectively.

Intercalated structures were observed nearly in all of the composites. However, when the organoclay content exceeded 2 wt%, increase in the d-spacing values was diminished in both binary and ternary nanocomposites. In the presence of the organoclay, % crystallinity and stiffness were increased due to the nucleating effect and stiffness of the organoclay at high clay loadings. On the other hand, in the SEM analysis, a significant reduction in the domain size and clay agglomeration was observed in N8 type of organoclay loaded nanocomposites. The barrier effect of the organoclay prevented the coalescence of the heterophasic domains, hence the domain size was decreased. Moreover, clay agglomerates present in the matrix, acted as stress concentrators and initiated the crack propagation; both effects decreased the impact strength of the nanocomposites at high clay loadings. Introduction of the compatibilizer M to the polymer increased the toughness owing to its higher energy absorbing capacity in the absence of the clay. Addition of organoclay, decreased the toughness values, however increased the tensile properties of the ternary nanocomposites at low clay loadings (1 wt % and 2 wt %).

Finally, the best improvement in mechanical properties were obtained for the nanocomposites containing 6 wt% M and 2 wt% N5 with %7.7 increase in Young's Modulus, %2.2 increase in tensile stress at yield, %3.9 in tensile strength, % 3.5 in elongation at break and % 44.5 in impact strength.

REFERENCES

1. Lubin G., "Handbook of Composites", Van Nostrand Reinhold, New York, 1982.
2. Kaw A.K., "Mechanics of Composite Materials", 2nd Edition, CRS Press, Boca Raton, Fla., 2006.
3. Matthews F.L., Rowlings R.D., "Composite Materials, Engineering & Science", Chapman & Hall, London, New York, 1994.
4. Fischer H., Materials Science and Engineering, C 23, 763–772, 2003.
5. Chawla K., "Composite Materials Science and Engineering", 2nd Ed., Springer -Verlag, New York, 1998.
6. Callister W., "Materials Science and Engineering: An Introduction", 4th Edition, John-Wiley & Sons, USA, 1997.
7. Giannelis E.P., 1996. Polymer Layered Silicate Nanocomposites, Review, Advanced. Materials, 8, 29-35.
8. Isik I., Yilmazer U. and Bayram G., 2003., Polymer, 44, 6371-6377.
9. Huang X., Lewis S., Brittain W. J. and Vaia R. A., 2000., Macromolecules, 33, 2000-2004.
10. Vaia R.A., Ishii H., Giannelis E.P., Chemistry of Materials, 5, 1694-6, 1993.
11. Ray S.S., Okamoto M., Progress in Polymer Science, 28, 1539-1641, 2003.
12. Manias E., Touny A., Wu L., Strawhecker K., Lu B., Chung T.C., Chemistry of Materials, 13, 3516-3523, 2001.
13. Lertwimolnun W., Vergnes B., Polymer Engineering Science, 46, 314-323, 2006.

14. Karian H.G., "Handbook of Polypropylene and Polypropylene Composites", Marcel Dekker Incorporated, New York, 1999.
15. 16. Kim D.H., Fasulo P.D., Rodgers W.R., Paul D.R., Polymer, 48, 5308-5323, 2007.
16. Starr F.L., "Composites: A Profile of the Worldwide Reinforced Plastics Industry, Markets and Suppliers", 3rd Edition, Elsevier, Kidlington, Oxford, UK, 1999.
17. Ajayan P.M., Schadler L.S., Braun P.V., "Nanocomposite Science and Technology", Wiley-VCH, Weinheim, Great Britain, 2003.
18. Mai Y.W., Yu Z.Z., "Polymer Nanocomposites", CRS Press, Boca Raton, Fla., Woodhead, Cambridge, England, 2006.
19. Alexandre M., Dubois P., Materials Science and Engineering, 28, 1-63, 2000.
20. Zanetti M., Lomakin S. and Camino G., Macromolecular Materials and Engineering, 279, 1-9, 2000.
21. Giannelis E.P., Krishnamoorti R., Manias E., Advances in Polymer Science, 138, 107-147, 1999.
22. Gilman J.W., Jackson C.L., Morgan A.B., Harris R., Chemistry of Materials, 12, 1866-1873, 2000.
23. Cengiz, F., (2008). Ms. Thesis "Preparation and Characterization of Recycled Polypropylene Based Nanocomposites", Graduate School of Natural and Applied Sciences of Middle East Technical University
24. Kornmann, X., PhD Thesis, "Synthesis and Characterization of Thermoset-clay Nanocomposites", Division of Polymer Engineering, Luleå University of Technology: Luleå, Sweden, 2001.
25. Beyer G., Polymer Additives and Compounding, 22-28, 2002.
26. Cho J.W., Paul D.R., Polymer, 42, 1083-1094, 2001.

27. Vasile C., "Handbook of Polyolefins", 2nd Edition, CRC Press, 2000.
28. Kroschwitz J.I., Mark H.F., "Encyclopedia of Polymer Science and Technology", 3rd Ed., Wiley Interscience, 2003.
29. Van der Vegt A.K., "From Polymers to Plastics", Delft University Press, Delft, The Netherlands, 2002.
30. Tripathi D., "Practical Guide to Polypropylene", 1st Edition, Rapra Technology Ltd., UK, 2002.
31. Long Y., Shanks R.A., Journal of Applied Polymer Science, 62, 639-646, 1996.
32. Li Y., Wei G.X., Sue H.J., Journal of Material Science, 37, 2447-2459, 2002.
33. Kim D.H., Fasulo P.D., Rodgers W.R., Paul D.R., Polymer, 48, 5960-5978, 2007.
34. Lei S.G., Hoa S.V., Ton-That, M.T, Composites Science and Technology, 66, 1274-1279, 2006.
35. Modesti M., Lorenzetti A., Bon D., Besco S., Polymer, 46, 10237-10245, 2005.
36. Mehrabzadeh M., Hossein N.K., Journal of Applied Polymer Science, 72, 1257-1265, 1999.
37. Zhao R.F., Dai G., Journal of Applied Polymer Science, 86, 2486-2491, 2002.
38. Utracki L. A., "Clay-Containing Polymeric Nanocomposites", first edition, Rapra Technology Ltd., Shawbury, UK, 2004.
39. Kawasumi M., Hasegawa N., Kato M., Usuki A., Okada A., Macromolecules, 30, 6333, 1997.
40. Garcia Lopez D., Gobernado Mitre I., Merino J.C., Pastor J.M., Polymer Bulletin, 59, 667-676, 2007.

41. Hasegawa N., Usuki A., Journal of Applied Polymer Science, 93, 464-470, 2004.
42. Hassan A., Othman N., Wahit M.U., Wei L.J., Rahmat A.R., Ishak Z.A.M., Macromolecular Symposia, 239, 182-191, 2006.
43. Baker W.E., Scott C.E., Hu G.H., "Reactive Polymer Blending", Hanser, Munich, Germany, 2001.
44. Macosko C.W., Guegan P., Khandpur A.K, Macromolecules, 29, 5590-5598, 1996.
45. Kato M., Usuki A., Okada, A., Kurauchi T., Journal of Applied Polymer Science, 63, 137-139, 1997.
46. Liu X., Wu Q., Polymer, 42, 10013-10019, 2001.
47. Yayla, S., (2007). "Production and Characterization of Polypropylene/Organoclay Nanocomposites", Graduate School of Natural And Applied Sciences of Middle East Technical University
48. Hasegawa N., Okamoto H., Kawasumi M., Kato M., Tsukigase A., Usuki A., Macromolecular. Materials and Engineering, 280/281, 76-79, 2000.
49. Middleman S., "Fundamentals of Polymer Processing", McGraw-Hill, New York, 1997.
50. Harper, C.A., "Modern Plastics Handbook", McGraw-Hill Professional Publishing, Blacklick, OH, USA, 2000.
51. Tadmor Z., Gogos C.G., "Principles of Polymer Processing", Wiley, New York, 1979.
52. Crawford R. J., "Plastics Engineering", third edition, BH., Oxford, 1998.
53. Todd D.B., "Plastics Compounding-Equipment and Processing", Hanser Publishers, Munich, 1998.
54. Ram A., "Fundamentals of Polymer Engineering", Plenum Press, New York, 1997.

55. Margolis J.M., "Engineering Plastics Handbook", McGraw-Hill, New York, 2006.
56. Shigley J.E., Mischke C.R., Brown T.H., "Standard Handbook of Machine Design", McGraw-Hill, New York, 2004.
57. Seymour R.B., "Polymer Chemistry: An Introduction", 4th Edition, Marrel Dekker, New York, 1996.
58. Fried J. R., "Polymer Science and Technology", 2nd Edition, Prentice Hall Publications, USA, 2003.
59. Sandler S.R., "Polymer Synthesis and Characterization: A Laboratory Manual", Academic Press, San Diego, 1998.
60. Billmeyer F.W., "Textbook of Polymer Science", John Wiley & Sons, New York, 1984.
61. Rosen S.L., "Fundamental Principles of Polymeric Materials", Wiley, New York, 1982.
62. Cao G., "Nanostructures and Nanomaterials: Synthesis, Properties and Applications", Imperial College Press, 2004.
63. Ramakrishna, S., "An Introduction to Electrospinning and Nanofibers", River Edge, NJ, USA: World Scientific Publishing Company, 2005.
64. Sperling, L.H., "Introduction to Physical Polymer Science", 4th Edition, Wiley, 2006.
65. Goodhew P.J., Humphreys F.J., Beanland R., "Electron Microscopy and Analysis", 3rd Edition, Taylor & Francis, 1975.
66. Deshmane C., Yuan Q., Perkins R.S., Misra R.D.K, Materials Science and Engineering, A458, 150-157, 2007.
67. Zhang Q., Fu Q., Jiang L., Lei Y., Polymer International, 49, 1561-1564, 2000.

68. Ton-That M. T., Perrin-Sarazin F., Cole K. C., Bureau M. N., Denault J., *Polymer Engineering and Science*, 44, 1212-1219, 2004.
69. Lertwimolnun W., Vergnes B., *Polymer*, 46, 3462-3471, 2005.
70. Modesti M., Lorenzetti A., Bon D., Besco S., *Polymer Degradation and Stability*, 91, 672-680, 2006.
71. Zhu L., Xanthos M., *Journal of Applied Polymer Science*, 93, 1891-1899, 2004.
72. Southern Clay Products, "<http://www.scprod.com>", last accessed; on 5th of June, 2010.
73. Polyram, "<http://www.polyram.co.il>", last accessed; on 7th June, 2010.
74. Kim S.W., Jo W.H., Lee M.S., Ko M.B., Jho J.Y., *Polymer Journal*, 34, 103-111, 2002.
75. Yilmazer U, Cansever M., *Polymer Composites*, 23, 61-71, 2002.
76. ISO 527, International Organization for Standardization - Plastics, "Determination of Tensile Properties" & "Test Conditions for Molding and Extrusion Plastics".
77. ISO 179, International Organization for Standardization - Plastics, "Determination of Charpy Impact Properties".
78. Chen J.H., Zhong J.C., Cai Y.H., Su W.B., Yang Y.B., *Polymer*, 48, 2946-2957, 2007.
79. Xu W., Liang G., Wang W., Tang S., He P., Pan W.P., *Journal of Applied Polymer Science*, 88, 3225-3231, 2003.
80. Park K.W., Chowdhury S.R., Park C.C, Kim G.H., *Journal of Applied Polymer Science*, 104, 3879-3885, 2007.
81. Mirzadeh A., Kokabi M., *European Polymer Journal*, 43, 3757-3765, 2007.

82. González I., Eguiazábal J.I., Nazábal J., *Composites Science and Technology*, 66, 1833-1843, 2006.
83. Marchant D., Jayaraman K., *Industrial and Engineering Chemistry Research*, 41, 6402-6408, 2002.
84. Chang Y.W., Lee D., Bae S.Y., *Polymer International*, 55, 184-189, 2006.
85. Chung Y.C., Cho T.K., and Chun B.C., *Fibers and Polymers*, 9, 7-14, 2008.
86. Pozsgay A., Frater T., Papp L., Sajo I., Pukanszky B., *Journal of Macromolecular Science, Part B*, 41, 1249, 2002.
87. Fornes T.D., Yoon P.J., Hunter D.L., Keskkula H., Paul D.R., *Polymer*, 43, 5915-5933, 2002.
88. Lim J.W., Hassan A., Rahmat A.R., Wahit M.U., *Journal of Applied Polymer Science*, 99, 3441-3450, 2006.
89. Contreras V., Cafiero M., Da Silva S., Rosales C., Perera R. and Matos M., *Polymer Engineering and Science*, 46, 1111-1120, 2006.
90. Plochocki A.P., Dagli S.S., Andrews R.D., *Polymer Engineering Science*, 30, 741, 1990.
91. Pukanszky B., Tudos F., Kolarik J., Lednicky F., *Polymer Composites*, 11, 98, 1990.
92. Tokita N., *Rubber Chem. Technology*, 50, 292, 1977.
93. Liang J. Z., Li R. K. Y., *Journal of Applied Polymer Science*, 77, 409-417, 2000.
94. Wu S., *Polymer Engineering Science*, 27, 335, 1987.
95. Arcana I.M., Bundjali B., Yudistra I., Jariah B., Sukria L., *Polymer Journal*, 39, 1337-1344, 2007.

96. Solomon M.J., Somwangthanaroj A, "Intercalated Polypropylene Nanocomposites," Dekker Encyclopedia of Nanoscience and Nanotechnology, Marcel Dekker, 1483-1490, 2004.
97. Hasegawa N., Okamoto H., Kawasumi M., Usuki A., Journal of Applied Polymer Science, 74, 3359, 1999.
98. Nielsen L.E., Landel R.F., "Mechanical Properties of Polymers and Composites", 2nd Edition, Marcel Dekker Inc., USA, 1994.
99. Chow, W. S., Mohd Ishak Z. A., Karger-Kocsis J., Apostolov A. A., Ishiaku U. S., Polymer, 44, 7427, 2003.
100. Saminathan K., Selvakumar P., Bhatnagar N., Polymer Testing, 27, 296-307, 2008.
101. Vlasveld D.P.N, Vaidya S.G., Bersee H.E.N, Picken S.J, Polymer, 46, 3452-3461, 2005.
102. Galgali G., Agarwal S., Lele A., Polymer, 45, 6059-6069, 2004.
103. Tjong S.C., Bao S.P., Journal of Polymer Science, Part B, Polymer Physics, 43, 585-595, 2005.
104. Van der Wal, A., Gaymans, R., Journal of Polymer, 40, 6067, 1999.
105. Jiang W., Liu C. H., Wang Z. G., An L. J., Liang H. J., Jiang B.Z., Wang X. H. And Zhang H. X., Polymer, 39, 3285-3288, 1998.
106. Qin H., Su Q., Zhang S., Zhao B., Yang M., Polymer, 44, 7533-7538, 2003
107. Deenadayalan E., Vidhate S., Lele A., Polymer International, 55, 1270-1276, 2006.

APPENDIX A

MECHANICAL TEST RESULTS

Table A.1 Calculated tensile properties and standard deviations for all compositions.

	Tensile at Yield	Stress	Tensile Strength	Elongation Break	at Young's Modulus
	MPa		MPa	%	MPa
Polymer Matrix					
EP300L	36.5		51.4	812	1434
St.dev	0.61		0.9	32.1	34.1
Binary Composites					
1N5	35.9		50.9	811	1439
St.dev	0.7		0.5	22.1	23.0
8N5	36.3		43.1	799	1538
St.dev	0.3		0.4	19.2	35.0
1N8	35.7		50.3	809	1436
St.dev	0.3		0.1	12.1	22.0
8N8	36.0		43.6	789	1498
St.dev	0.2		0.4	13.2	28.0

Table A.1 Calculated tensile properties and standard deviations for all compositions (Cont'd).

	Tensile Stress at Yield	Tensile Strength	Elongation at Break	Young's Modulus
	MPa	MPa	%	MPa
Binary Blends				
2M	33.3	50.9	822	1240
St.dev	1.2	0.2	1.7	29.0
6M	32.1	50.1	827	1129
St.dev	0.9	0.3	3.2	36.0
Ternary Composites				
8M1N5	34.4	45.6	801	1102
St.dev	0.77	1.3	11.4	25.9
8M2N5	35.2	46.0	812	1131
St.dev	1.05	0.9	7.4	35.1
8M3N5	34.7	44.0	810	1129
St.dev	0.88	1.4	23.6	24.0
8M4N5	33.7	43.1	795	1134
St.dev	3.89	1.7	22.1	11.1
6M1N5	36.9	51.8	825	1467
St.dev	0.56	2.6	5.2	21.0
6M2N5	37.3	53.4	841	1545
St.dev	0.7	1.6	3.7	17.5

Table A.1 Calculated tensile properties and standard deviations for all compositions (Cont'd).

	Tensile Stress at Yield	Tensile Strength	Elongation at Break	Young's Modulus
	MPa	MPa	%	MPa
Ternary Composites				
6M3N5	36.7	52.7	809	1537
St.dev	1.19	2.7	8.6	23.1
6M4N5	36.8	50.2	803	1327
St.dev	1.12	1.4	9.6	39.9
6M1N8	32.3	43.2	794	1149
St.dev	0.93	1.7	24.9	43.1
6M2N8	32.6	41.2	755	1169
St.dev	1.1	0.9	26.2	43.1
4M1N5	35.0	45.8	817	1285
St.dev	1.2	1.2	15.6	32.9
4M2N5	36.1	46.3	818	1324
St.dev	0.7	0.6	6.4	43.7
4M3N5	35.4	44.3	807	1310
St.dev	1.14	3.8	17.6	36.8
4M4N5	36.3	43.2	801	1287
St.dev	0.8	1.7	25.2	27.6
4M1N8	32.8	46.3	788	1186
St.dev	0.9	1.8	35.7	16.9
4M2N8	33.5	44.6	765	1135
St.dev	0.5	1.4	30.3	15.1

Table A.2 Impact strength data and standard deviations for all compositions.

Sample	Impact Strength (kJ/m²)	St.dev
Polymer Matrix		
<i>EP300L</i>	11.9	0.9
Binary Composites		
1N5	10.5	<i>1.8</i>
8N5	8.3	<i>0.3</i>
1N8	9.9	<i>0.9</i>
8N8	8	<i>1.9</i>
Binary Blends		
2M	13.4	<i>0.7</i>
6M	18.2	<i>1.3</i>
Ternary Nanocomposites		
8M1N5	17.0	<i>0.4</i>
8M2N5	16.8	<i>0.8</i>
8M3N5	16.5	<i>1.0</i>
8M4N5	16.4	<i>1.1</i>
6M1N5	16.8	<i>0.5</i>
6M2N5	17.2	<i>0.7</i>
6M3N5	16.7	<i>1.3</i>
6M4N5	14.6	<i>1.1</i>
4M1N5	11.9	<i>0.7</i>
4M2N5	11.9	<i>0.9</i>
4M3N5	11.4	<i>1.9</i>
4M4N5	11.1	<i>0.7</i>
3M1N5	11.0	<i>1.3</i>
3M2N5	10.9	<i>1.1</i>
3M3N5	10.9	<i>2.8</i>
3M4N5	10.5	<i>0.3</i>
2M1N5	11.2	<i>1.1</i>
2M2N5	11.0	<i>0.9</i>
2M3N5	9.5	<i>1.3</i>
2M4N5	9.3	<i>2.6</i>

Table A.2 Impact strength data and standard deviations for all compositions (Cont'd).

Impact		
Sample	Strength	St.dev
(kJ/m²)		
Ternary Nanocomposites		
6M1N8	13.2	<i>0.5</i>
6M2N8	12.1	<i>1.2</i>
4M1N8	10.1	<i>1.1</i>
4M2N8	10.5	<i>0.9</i>
3M1N8	9.3	<i>1.3</i>
3M2N8	9.8	<i>0.4</i>
2M1N8	9.4	<i>2.8</i>
2M2N8	9.1	<i>2.7</i>

APPENDIX B

DSC ANALYSIS

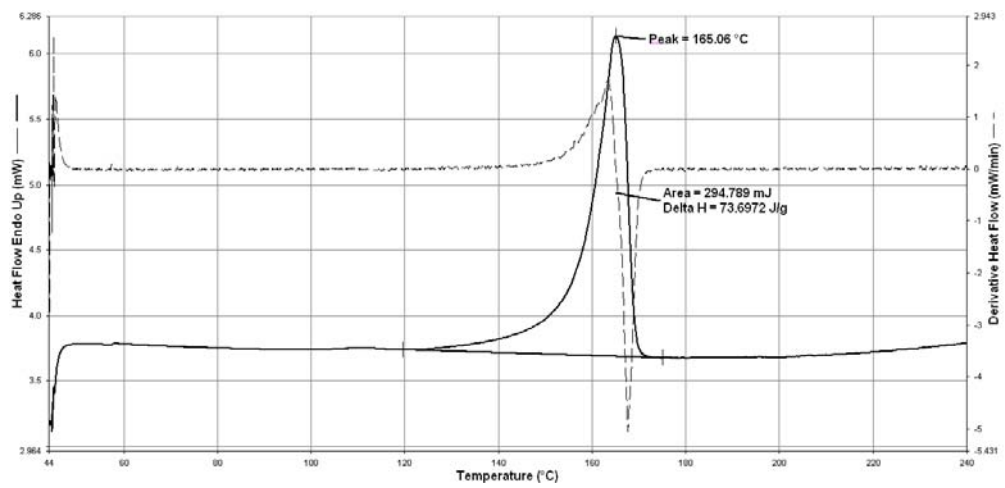


Figure B.1 DSC thermogram of binary blend containing 2 wt% M.

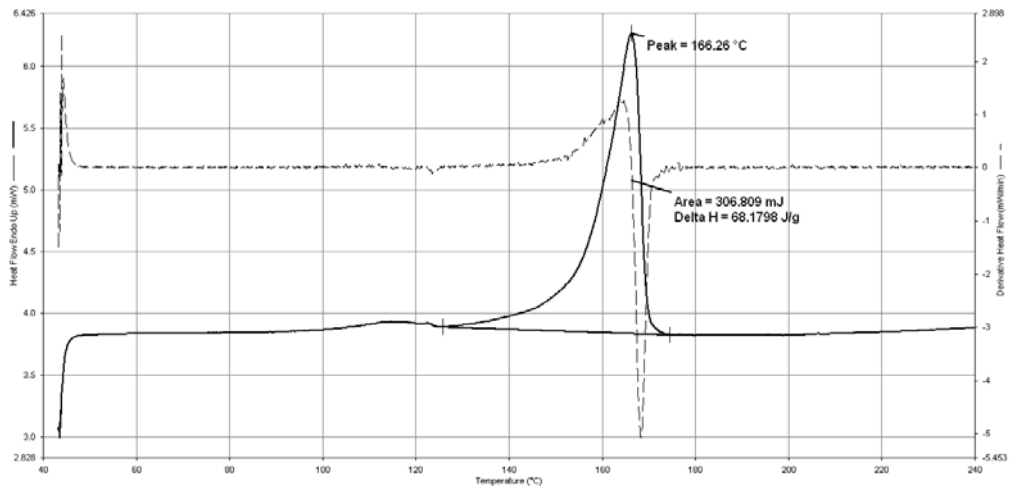


Figure B.2 DSC thermogram of binary blend containing 6 wt% M.

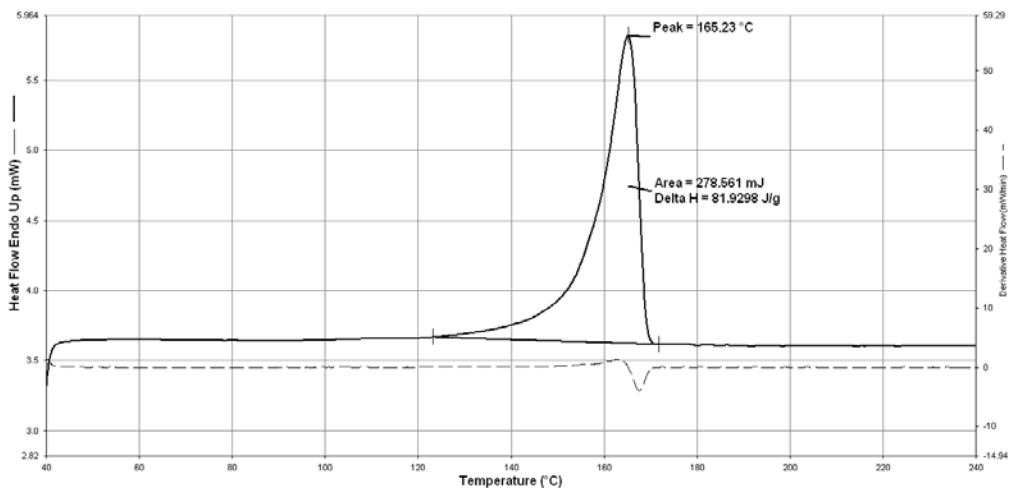


Figure B.3 DSC thermogram of binary nanocomposite containing 1 wt% Nanofill® 5.

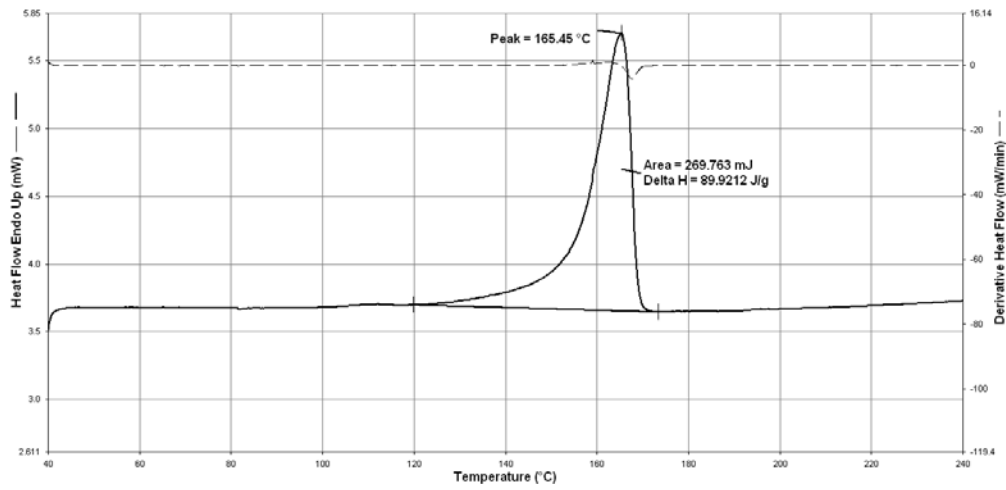


Figure B.4 DSC thermogram of binary nanocomposite containing 8 wt% Nanofill® 5.

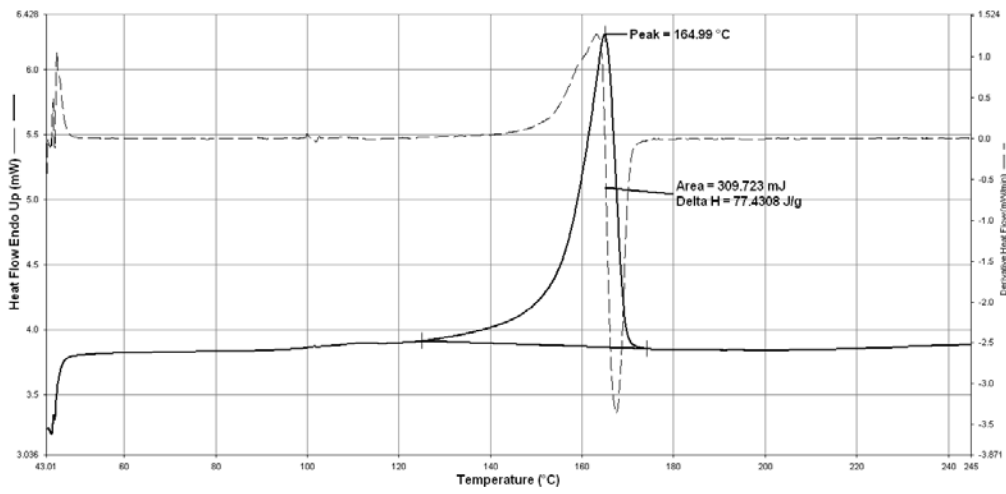


Figure B.5 DSC thermogram of binary nanocomposite containing 1 wt% Nanofill® 8.

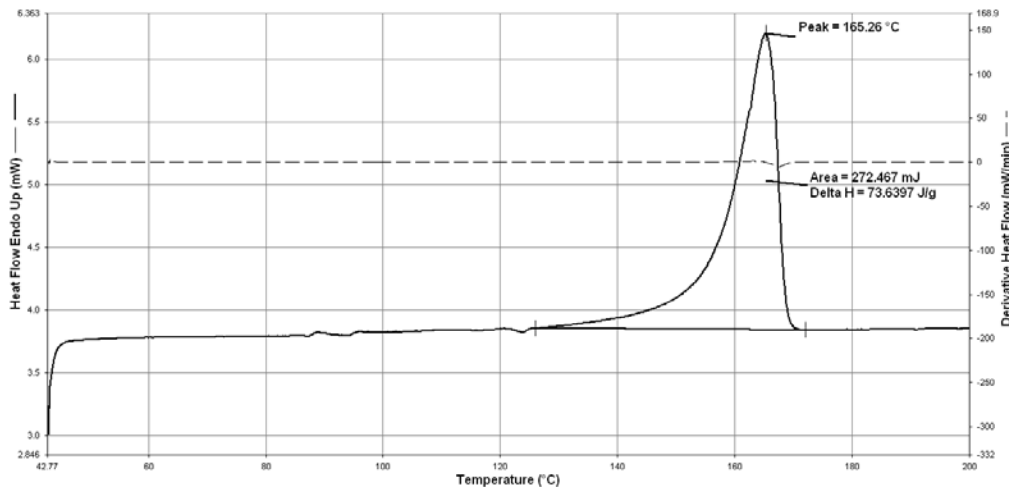


Figure B.6 DSC thermogram of binary nanocomposite containing 8 wt% Nanofill® 8.

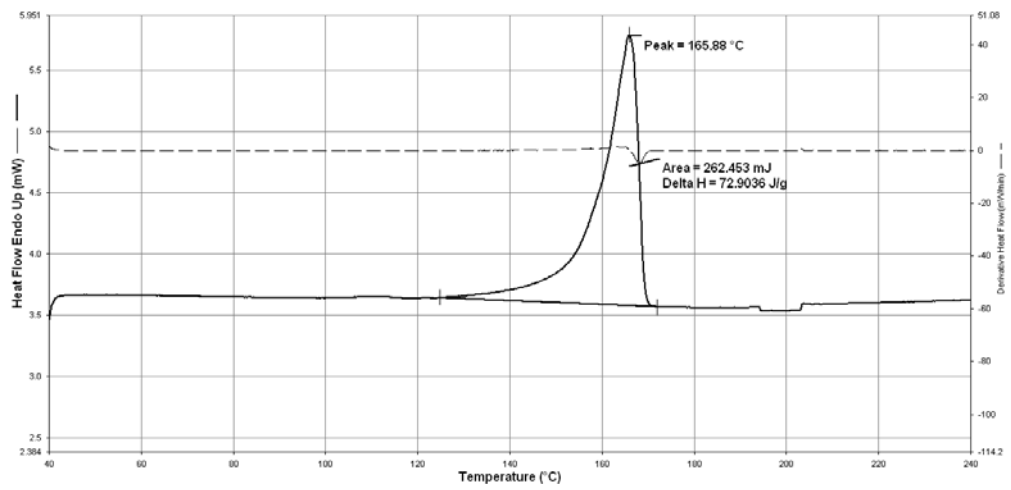


Figure B.7 DSC thermogram of ternary nanocomposite containing 2 wt% Nanofill® 5 and 2 wt% M.

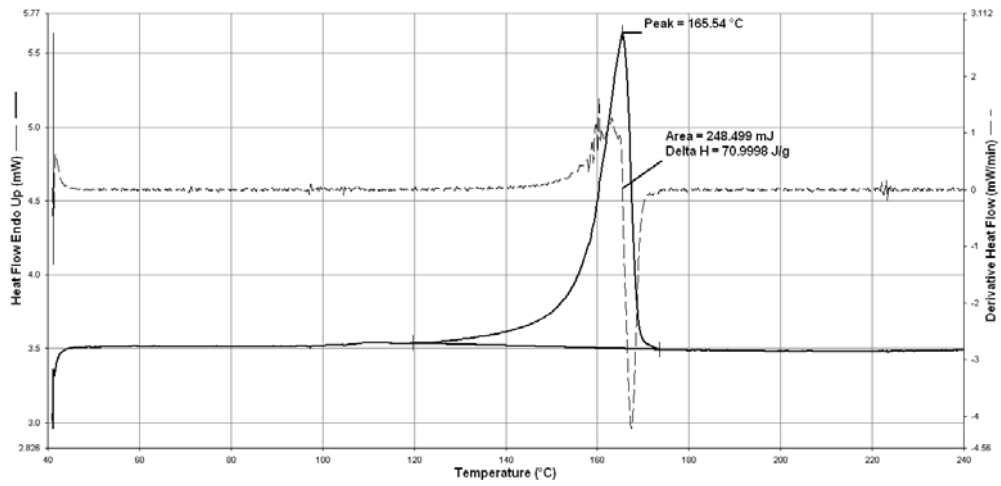


Figure B.8 DSC thermogram of ternary nanocomposite containing 2 wt% Nanofill ® 5 and 3 wt% M.

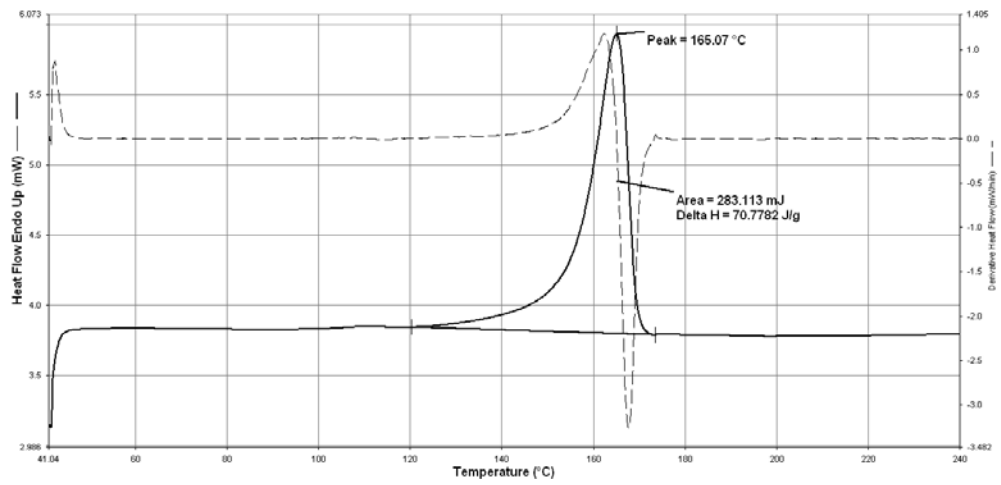


Figure B.9 DSC thermogram of ternary nanocomposite containing 2 wt% Nanofill ® 5 and 4 wt% M.

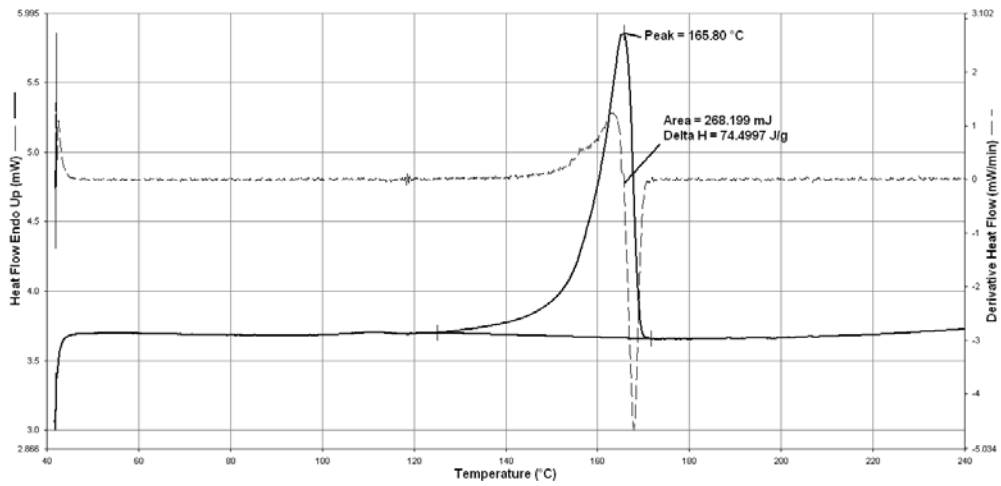


Figure B.10 DSC thermogram of ternary nanocomposite containing 1 wt% Nanofill[®] 5 and 6 wt% M.

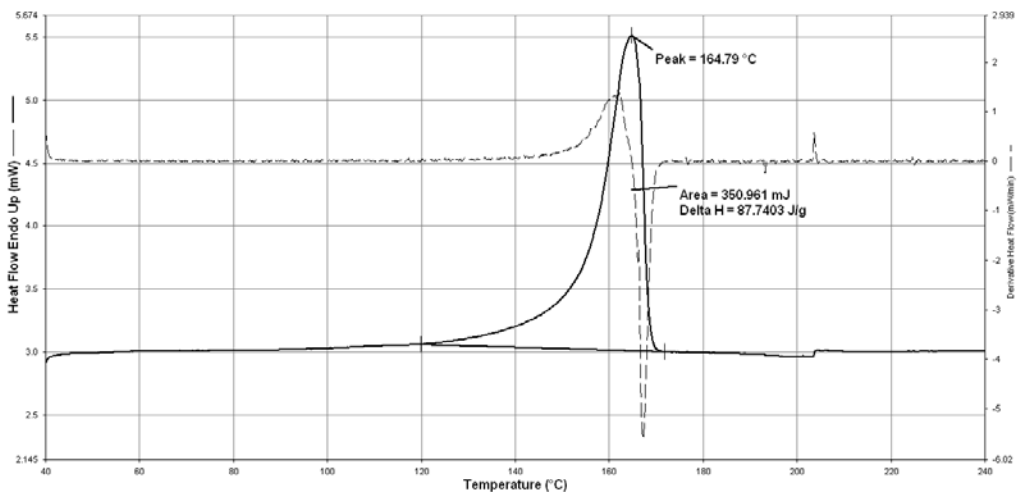


Figure B.11 DSC thermogram of ternary nanocomposite containing 2 wt% Nanofill[®] 5 and 6 wt% M.

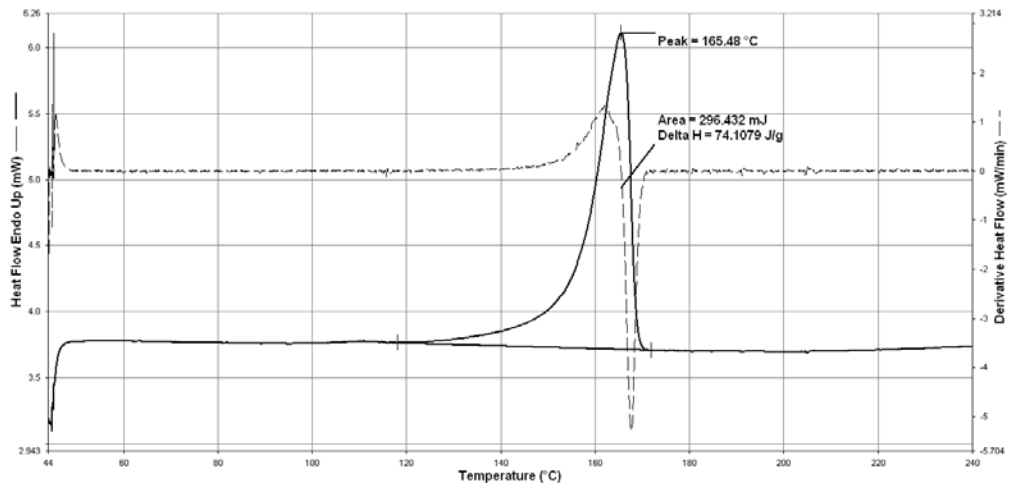


Figure B.12 DSC thermogram of ternary nanocomposite containing 3 wt% Nanofill[®] 5 and 6 wt% M.

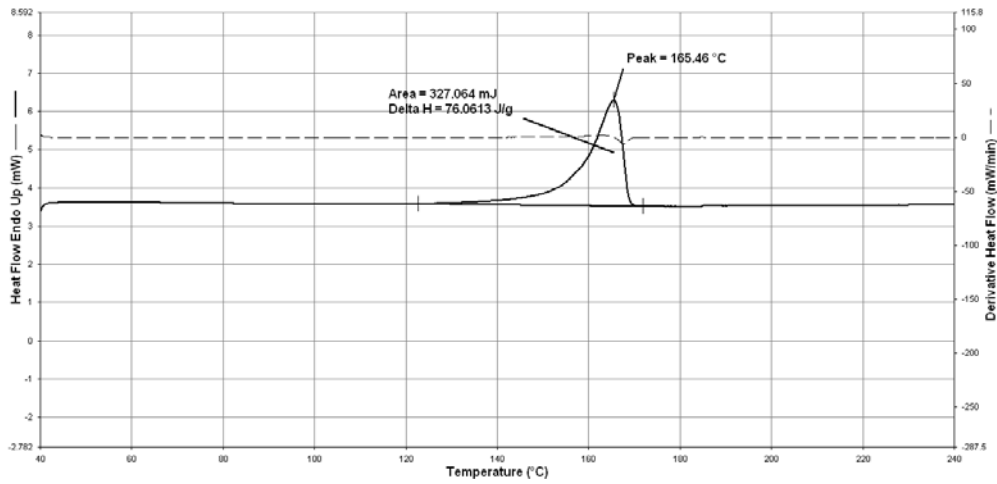


Figure B.13 DSC thermogram of ternary nanocomposite containing 4 wt% Nanofill[®] 5 and 6 wt% M.

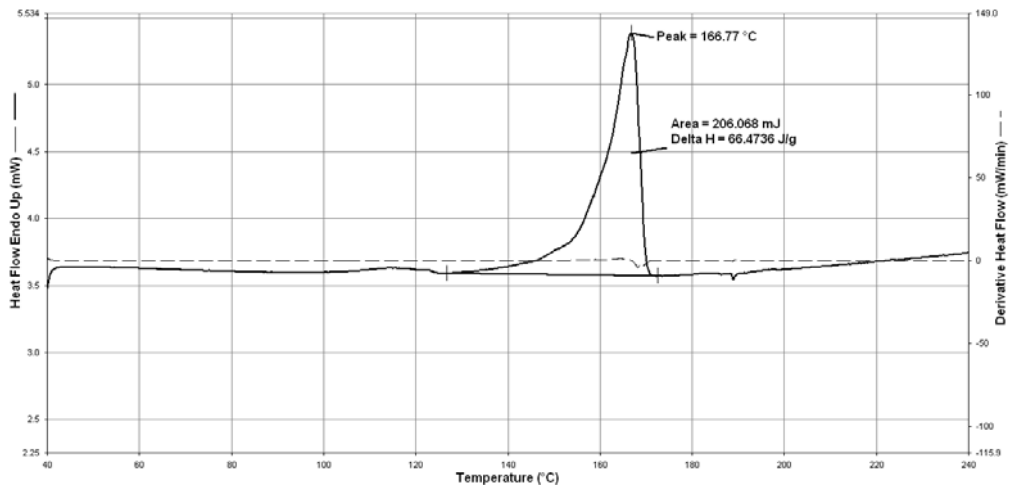


Figure B.14 DSC thermogram of ternary nanocomposite containing 2 wt% Nanofill[®] 5 and 8 wt% M.

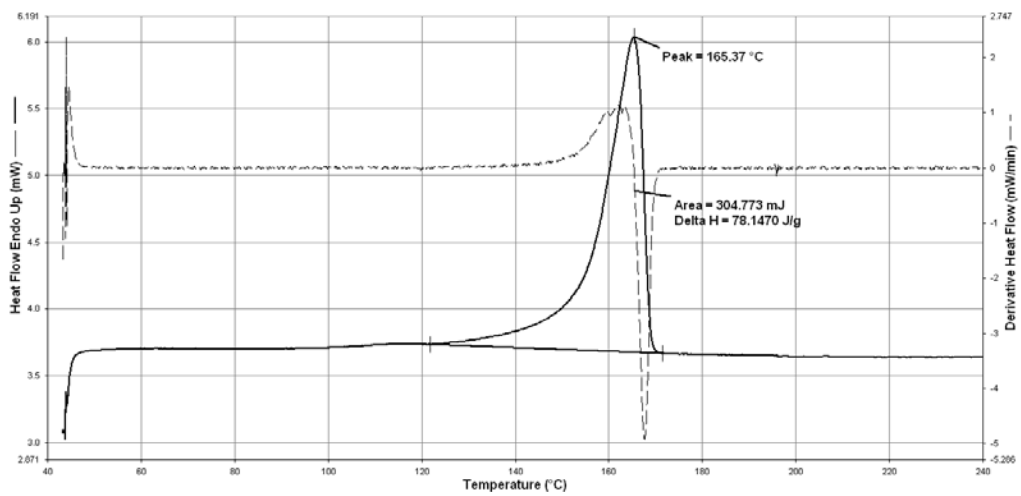


Figure B.15 DSC thermogram of ternary nanocomposite containing 2 wt% Nanofill[®] 8 and 2 wt% M.

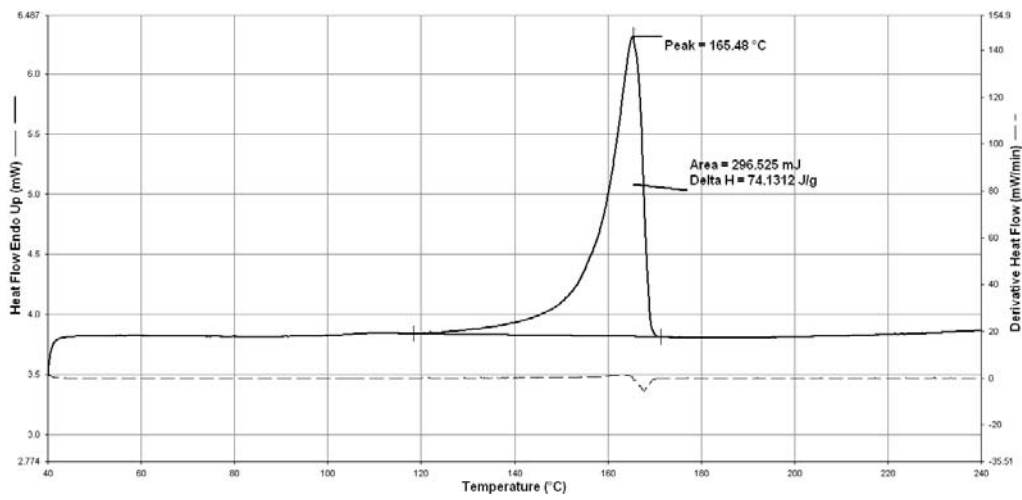


Figure B.16 DSC thermogram of ternary nanocomposite containing 2 wt% Nanofill[®] 8 and 3 wt% M.

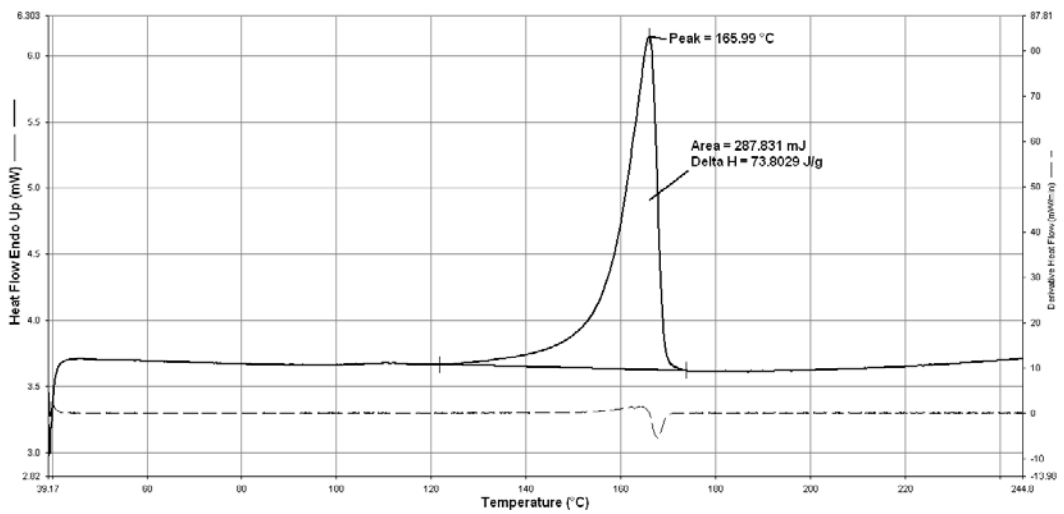


Figure B.17 DSC thermogram of ternary nanocomposite containing 2 wt% Nanofill[®] 8 and 4 wt% M.

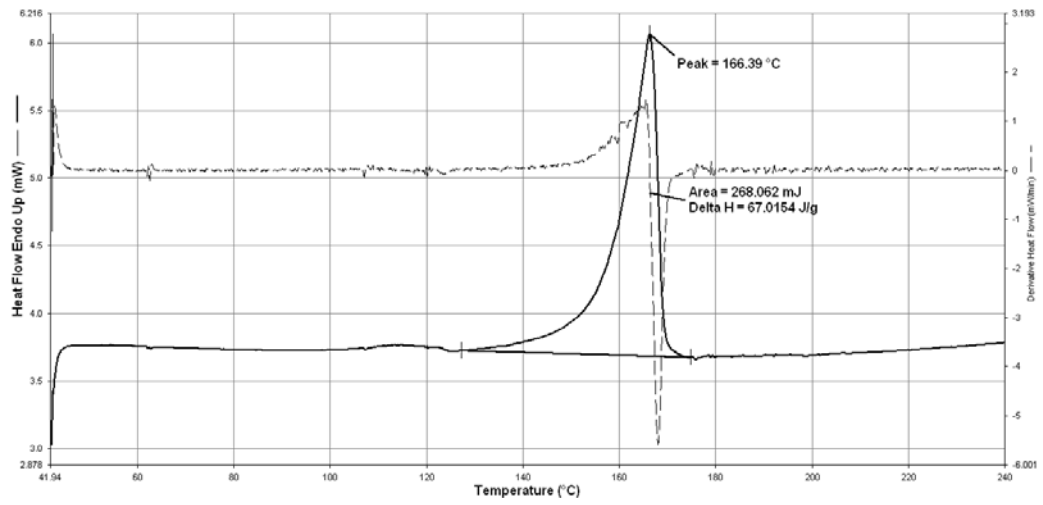


Figure B.18 DSC thermogram of ternary nanocomposite containing 2 wt% Nanofill[®] 8 and 6 wt% M.